SELENOLOGY TODAY

Selenology Today #9

Selenology Today is devoted to the publication of contributions in the field of lunar studies.

Manuscripts reporting the results of new research concerning the astronomy, geology, physics, chemistry and other scientific aspects of Earth's Moon are welcome.

Selenology Today publishes papers devoted exclusively to the Moon.

Reviews, historical papers and manuscripts describing observing or spacecraft instrumentation are considered.

The Selenology Today

Editorial Office

selenology_today@christian-woehler.de

SELENOLOGY TODAY #9
February 2008

Geological Lunar Researches Group

Cover : Image taken by KC Pau

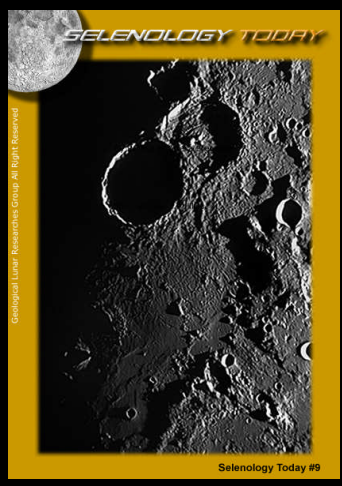

Selenology Today websites

http://digilander.libero.it/glrgroup/

Profiles Of Features In the J. Herschel Crater, Fontenelle Crater, and La Condamine Crater Area

by Steve Boint

Vice President of American Lunar Society (ALS) and publisher of the journal Selenology

Abstract

Using LTVT, vertical displacements for a number of far-northern features were calculated and profiles were graphed. In spite of the limitations imposed by mediocre photographs and the dearth of readily-available, high-quality maps of this area, results were remarkably good. The depth of J. Herschel Crater along its eastern wall varied between 380m and 1570m. La Condamine Crater's eastern wall rose between 820m and 1800m above its interior. The partial rim south of J. Herschel F (longitude -35.29°, latitude 57.55° for the northernmost point measured) varied between 320m and 470m. The old rim north of Fontenelle Crater (longitude -22.15°, latitude 68.41° for the northernmost point measured), once it attained full height, varied between 810m and 1330m. Low hills to the west of the old rim run for 33,000m and rise to a maximum height of 210m. The depth of Fontenelle Crater along its eastern wall was measured in two locations. The northern point gave a value of 1690m. The southern measurement gave a value of 1050m. Individual measurements were made of several features.

The outside west rim of J. Herschel F was between 650m and 720m tall. The outside west rim of La Condamine B was between 740m and 940m tall.

The outside west rim of Fontenelle A was between 650m and 780m tall. The west side of Fontenelle Epsilon rose between 540m and 640m above the mare. And, the west side of a peak just north of Fontenelle Epsilon rose between 280m and 360m above its surroundings

.

Introduction

Until the recent interest in the polar regions of the moon, mapping of these areas was often neglected. The LAC maps available on-line barely touch the northern regions and in these areas they contain few measurements other than crater depths (U.S. Air Force, NASA and Aeronautical Chart and Information Center 1967). The Topographic Lunar Map put out by the Army Corp of Engineers is low resolution and difficult to read (Army Map Service 1964). Rukl's Atlas Of The Moon gives only crater diameters for this region (Rukl, 2004). Westfall's Atlas Of The Lunar Terminator does contain a table listing depths of craters, but these are single values and the exact position measured is not indicated (Westfall, 2000). The-Moon Wiki contains many entries of crater depths but these are also single values with no precise location of measurement. It does contain values for the height of elevated lunar features unconnected to craters, but none that were measurable in the photos used for this study (The-Moon Wiki). As a contribution toward filling this gap in our knowledge of the moon, low-resolution, amateur photographs of the region bounded by the craters J. Herschel, Fontenelle, and La Condamine were

coupled with LTVT to measure several vertical displacements.

Method

Four photographs were used. All were taken from Sioux Falls, SD: 96.73133° W. longitude, 43.5293° N latitude, 435 m above sea level. The area around J. Herschel was imaged using a Newtonian telescope with a ten inch primary, f/4.5, 2x Barlow lens, and an SBIG 237a CCD camera. The area around Fontenelle was imaged with the same telescope but a 5x Barlow lens and the Toucam Pro II camera. Each area was photographed twice. Photos of the J. Herschel area were taken on 6/11/03 at 2:06 UT and 7/10/03 at 2:40 UT. Photos of the Fontenelle area were taken on 4/27/07 at 1:33 and 1:51 UT. In order to determine the precision of the measurements, comparisons were made between data gathered from each photo of an area.

LTVT (Mosher and Bondo, 2006) was used to determine the vertical displacement of various features. When using LTVT, it is preferable to calibrate the measurements against a known vertical displacement. This is due to difficulties in determining the exact beginning or ending of a shadow. If a known vertical displacement is available, it can be used to determine the extent to which a measurement should extend into the penumbral areas of the shadow. Experience has shown that this can vary considerably between photos (probably largely due to changes in shadow length due to processing). Since no suitable vertical displacements were available as references for features measurable on the photographs, the method found most common in past experience was used: the shadow tip was measured at the outer end of the penumbra and the shadow base (against the lunar feature casting the shadow) was measured in the middle of the penumbral area when a sharp edge was not available (Boint 2006; 2007; 2008, publication pending).

Ideally, the reference values for calibrating LTVT would come from a detailed contour map like the Lunar Topographic Orthophoto maps (U.S. Defense Mapping Agency, 1975). Unfortunately, none exist for this region of the moon. Their usefulness for calibrating LTVT is that a specific point can be tied to various shadow lengths in order to show what the correct value should be for the shadow being used for calibration. The LAC maps provide the next best option by giving the vertical displacement of a specific point and indicating the shadow length and the direction it fell in the photo used by the LAC researchers to determine the height or depth of the feature. Unfortunately, few values of this kind are available for the northern polar regions. LAC 11 provides three possible values, two of an unnamed hill east of J. Herschel crater and one of the southwestern wall of La Condamine. Unfortunately, the photo measured for this study lacked sufficiently clear shadows in these areas. LAC 12 also had candidate locations. Unfortunately, the only values calculated near enough to the target area were for Fontenelle crater's eastern outer rim. The shadow in the photo measured for this study fell on the inside of the rim. There is sufficient difference in rim height above the lunar surface inside and outside a crater that these measurements could not be used for calibration. A few other options are available. Using LTVT, Mosher has measured the height of La Condamine from the Lunar Orbiter photo

LO-IV-152H (Mosher, The-Moon Wiki). He has found the height to vary between 1100m to 1700m. Unfortunately, he does not indicate the exact positions that were measured—limiting the usefulness of this data for calibration. It does, however, provide ballpark values within which data from lower resolution images should fall. Non-reporting of the exact position from which a measurement was taken plagues data on crater depth. Often one value is given for a crater's depth and no indication is made of the position on the rim from which the measurement was made. Crater rims are not perfectly smooth. While less of a problem on smaller craters, large crater rims can vary by hundreds of meters. Using craters for calibration of LTVT is also difficult because the depth given in tables or maps is assumed to be the deepest value. On a single photo, there is no guarantee that the shadow tip falls exactly at the deepest point. While this is somewhat easier to determine on a large crater, these are the very craterswhose rims show the most variation. Still, they can be used to determine a maximum depth and in this way provide a vague calibration guide or at least a check on results. Unfortunately, the depths provided for smaller craters in these areas were rendered unusable by the shadows in the photographs used in this study—none of them appeared to fall near the center of the craters.

Results

Measurements inside the eastern rim of J. Herschel Crater were graphed as a profile. They show how the rim would look when standing inside the crater and looking eastward.

Uncertainties in both the vertical and horizontal values make presentation as a profile preferable. Absolute height values will undoubtedly become available with the lunar orbiters currently or soon to be circling the moon. Once a solid height is established, the profile can be adjusted up or down and still be valuable. LAC 11 was used for horizontal positioning. While usable, it does not provide an ideal level of precision.

The two photos were measured on separate days (over a week apart) without reference to each other and then the results were compared. This minimized any carryover. As the comparison of the two profiles shows, the measurements are solid once difficulties in horizontal positioning are taken into account.

Westfall's depth for J. Herschel at 900m (Westfall, 2000) and Arthur's depth of 0.74km (Arthur, 1974) are significantly below the heights calculated here. The value of 1.7km from Cherrington (Cherrington, 1969) agrees well with the profile. However, with such a large crater and no indication of the location on the rim which was measured in their studies, it is not clear how to compare the data from these sources with that of this study. Various other features in this area were measured. A profile was secured for the inside, eastern rim of La Condamine. LAC 11 lists a depth for La Condamine of 2000m. The profile's maximum value of 1800m agrees well with this ballpark figure. While the highest point falls above and the lowest point falls below that suggested by Mosher (Mosher, The-Moon Wiki), only the lowest point falls outside of a plus or minus value of ten percent-which touches the limit of accuracy traditionally ascribed to the shadow method (Davis, 1997). It also approaches

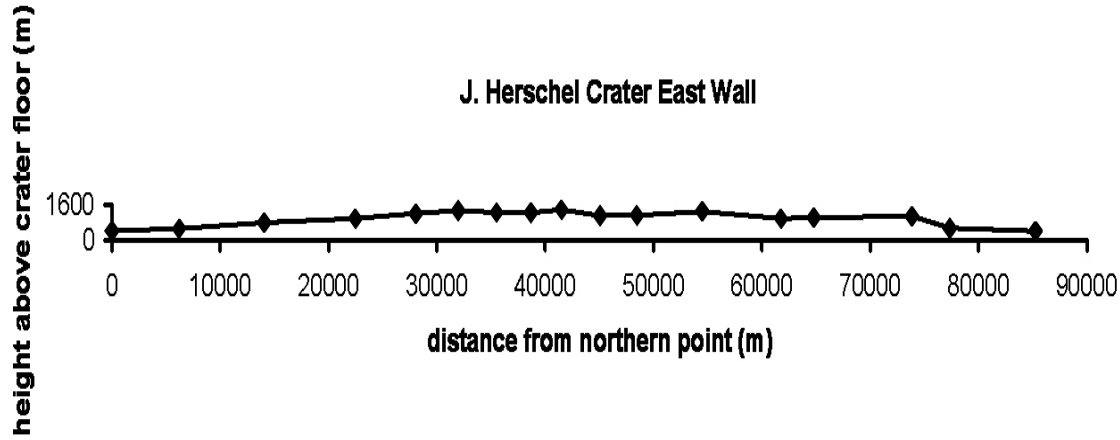

Figure 1 – Inside profile of J.Herschel Crater's eastern wall from an image taken on 6/11/03 at 2:06 UT.

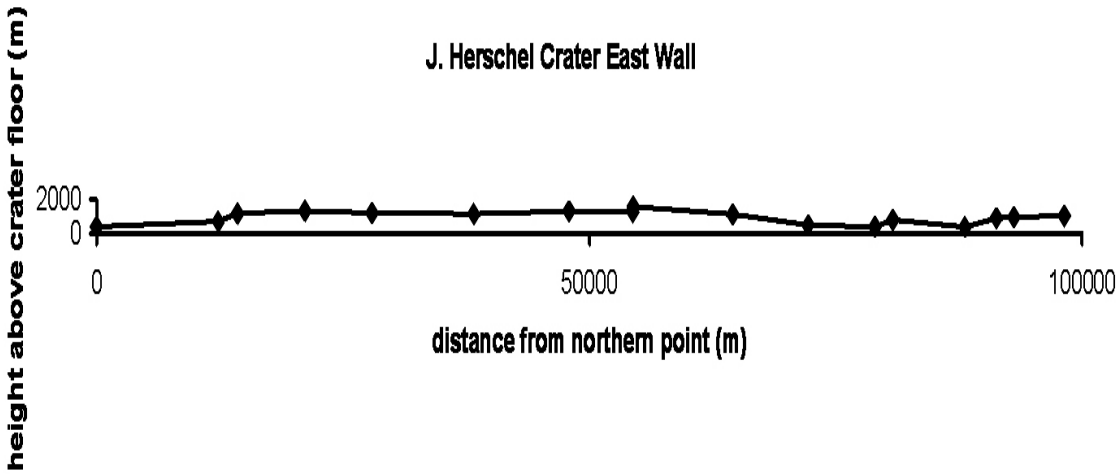

Figure 2 – Inside profile of J.Herschel Crater's eastern wall from an image taken on 7/10/03 at 2:40 UT.

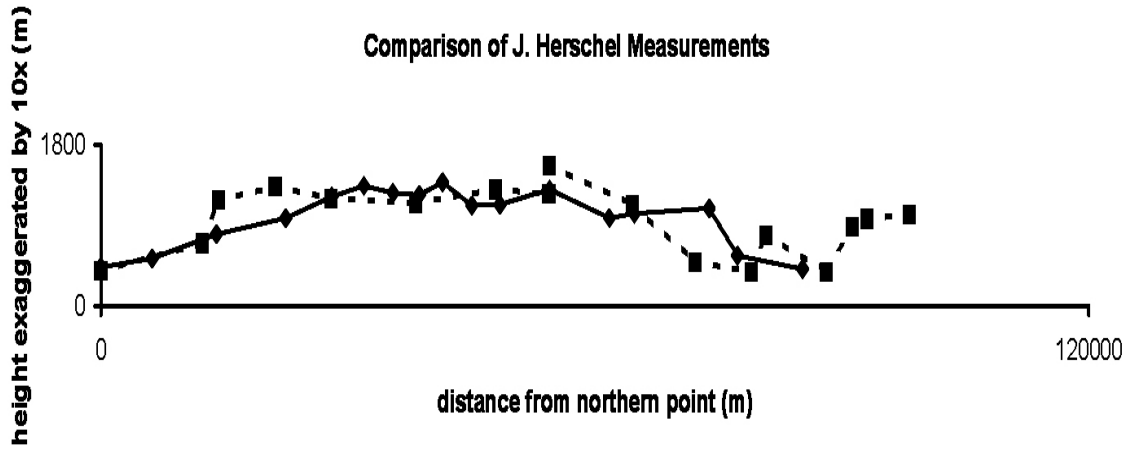

Figure 3 – Comparison of the measurements of J. Herschel Crater's eastern rim.

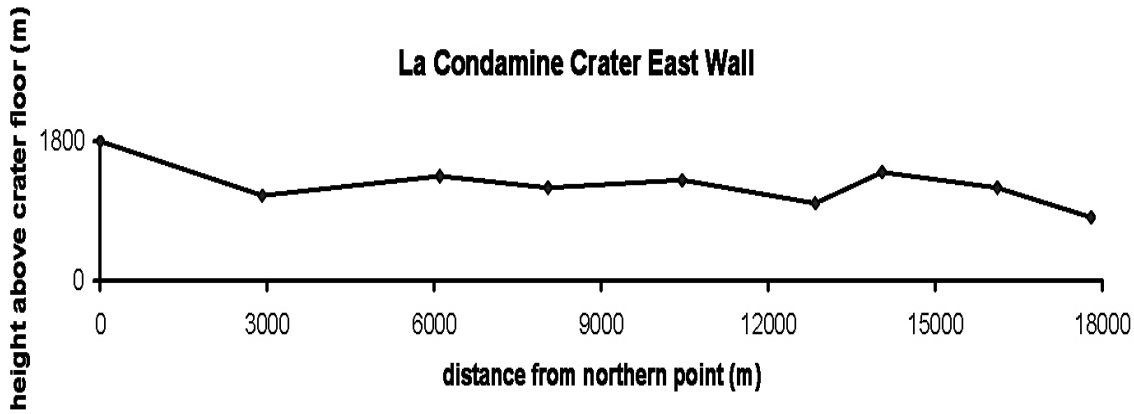

Figure 4 - Inside profile of La Condamine Crater's eastern wall.

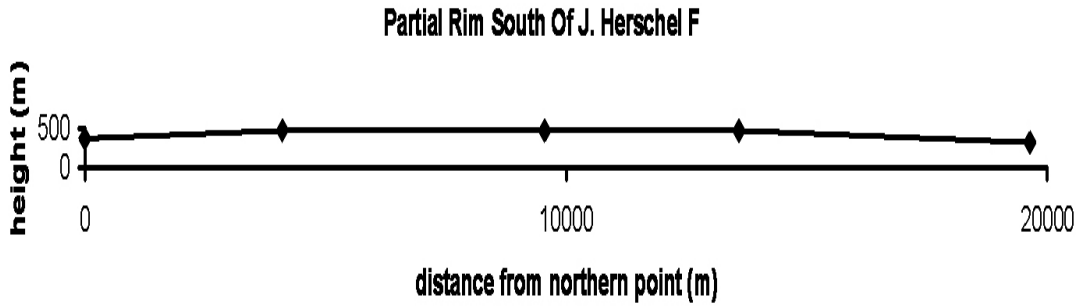

Figure 5 – Profile of the partial rim south of crater J. Herschel F as seen looking east. LTVT lists the most northerly measured point as -35.29° longitude and 57.55° latitude. The most southern point is listed as -35.2° longitude and 56.93° latitude.

the vertical accuracy attainable by the best LTVT measurements (Wood, 2006) The southernmost point is the least certain. The relative profile should stand although it may need to be adjusted upward or downward. Westfall's value of 1510m for La Condamine (Westfall, 2000) falls comfortably within the range of the profile generated in this study. Elger's value of 4000ft also fits the profile unless it is meant as the deepest point (Elger, The-Moon Wiki). The ruined crater wall below J. Herschel F was also measured and a profile determined. Single measurements were made of other features (Table 1). The partial rim north of Fontenelle Crater was measured on its eastern terminus. This feature, also, was measured twice and profiles generated. A comparison of the two profiles reveals a remarkable degree of similarity once difficulties in horizontal positioning are considered. This was undoubtedly helped by the greater resolution of the photographs.

In addition to the difficulties of horizontal positioning encountered with the J. Herschel area photographs, an added wrinkle came from using the Toucam. In order to stack enough frames to limit noise, the images produced were narrow strips which needed to be mosaiced (Adobe Photoshop) in order to provide a useful final image. Enough care was taken that no more distortion occurred than would be produced by the Earth's atmosphere in any but the most fortunate images. However, the image from 1:51 on 4/27/07 was too northerly for the LAC map to be helpful. It was calibrated horizontally using coordinates provided by LTVT from the previously calibrated photo of the same area at 1:33. This magnified the imprecision in the measurements.

A profile was also produced of a set of hills west of the old rim.

Although a profile could not be produced for Fontenelle Crater because its shadow in the photograph was interrupted by the crater's central peak, Fontenelle was measured on two points along its eastern rim. On the south (longitude -18.27°, latitude 63.02°) it rose 1050m above the interior floor. On the north (longitude -17.98°, latitude 63.73°) it had a height of 1690m. These values agree well with those measured by Mosher (Mosher, The-Moon Wiki) from the Lunar Orbiter photo LO-IV-128H where he estimated the height at between 1100m and 1500m. Westfall gives a depth of 1500m (Westfall, 2000, 274), Viscardy gives a depth of 1.75km (Viscardy, 1985) and Cherrington gives a depth of 2.8km (Cherrington, 1969).

Single values were also determined for a number of other features in this area (Table 2).

The locations of the features measured in the J. Herschel Crater area are presented on the image from 6/11/03 (Fig.10).

The locations of the features measured in the Fontenelle Crater area are presented on the image from 4/27/07 at 1:33 (Fig.11).

References

[1] Arthur. 1974. URL: http://digilander.libero.it/glrgroup/addmaterial.htm. (last date accessed: 12 January 2008).

[2] Army Map Services, Corp Of Engineers. 1964 (2nd Ed.). Topographic Lunar Map. URL: http://www.lpi.usra.edu/resources/mapcatalog/LTM/sheet_1/. (last date accessed: 12 January 2008).

Various Features South Of J. Herschel

Name	Lowest Height (m)	Highest Height (m)	Longitude	Variation	Latitude	Variation
outside west rim of J. Herschel F	650	720	-35.77	-35.83	58.48	58.52
outside west rim of La Condamine B	740	940	-31.99	-32.09	58.63	58.66

Table 1 – Single measurements of features in the J. Herschel Crater area. Both the lowest and highest possible heights determined by LTVT are given. Under "longitude variation", measurements are given for the most easterly and westerly values for each feature's location as determined using LTVT. Under "latitude variation", measurements are given for the most southerly and most northerly values determined using LTVT.

Various Features

Name	Lowest Height (m)	Highest Height (m)	Longitude	Variation	Latitude	Variation
Fontenelle Epsilon bottom triple peak	540	640	-16.53	-16.48	62.52	62.55
north of Fontenelle Epsilon	280	360	-16.18	-16.16	63.5	63.53
outside west rim of Fontenelle A	650	780	-17.81	-17.68	68.14	68.2

Table 2 – Single measurements of features in the Fontenelle Crater area. Both the lowest and highest possible heights determined by LTVT are given. Under "longitude variation", measurements are given for the most easterly and westerly values for each feature's location as determined using LTVT. Under "latitude variation", measurements are given for the most southerly and most northerly values determined using LTVT.

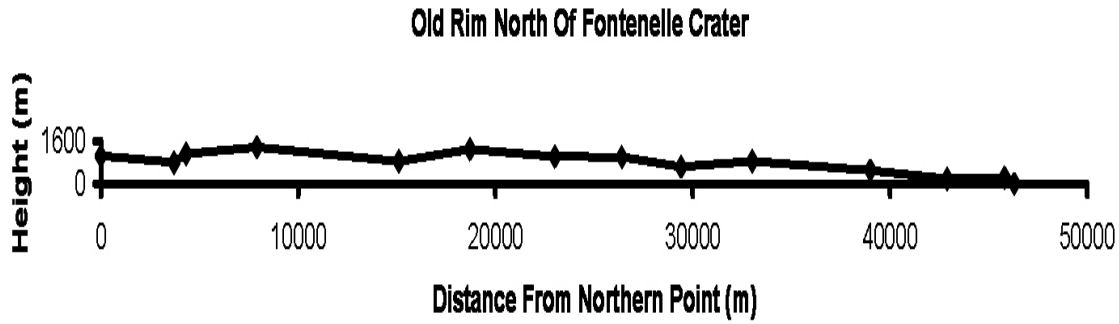

Figure 6 – Profile of the old rim north of Fontenelle Crater as seen looking eastward. The measurements were generated from a photo taken on 4/27/07 1:33 UT. LTVT gives the longitude and latitude of the southernmost measured point as -21.67° and 66.96°, respectively. The northernmost measured point has the coordinates of -22.15° longitude and 68.41° latitude

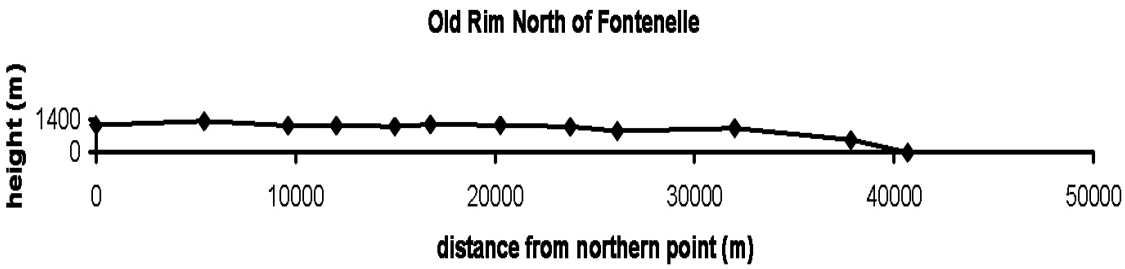

Figure 7 – Profile of the old rim north of Fontenelle Crater as seen looking eastward. The measurements were generated from a photo taken on 4/27/07 1:51 UT. LTVT gives the longitude and latitude of the southernmost measured point as -22.03° and 66.94°, respectively. The northernmost measured point has the coordinates of -22.6° longitude and 68.31° latitude.

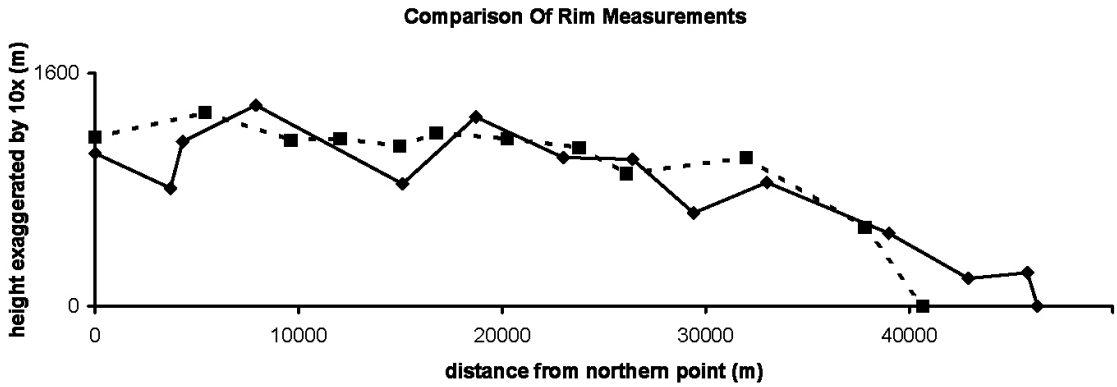

Figure 8 – Comparison of the profiles of the old rim north of Fontenelle Crater.

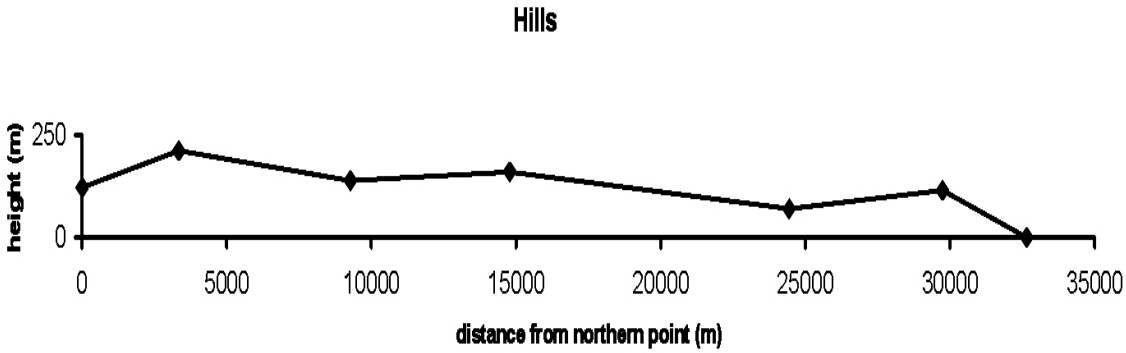

Figure 9 – Profile of the hills to the west of the old rim north of Fontenelle Crater as seen looking eastward. Height is exaggerated by 10x.

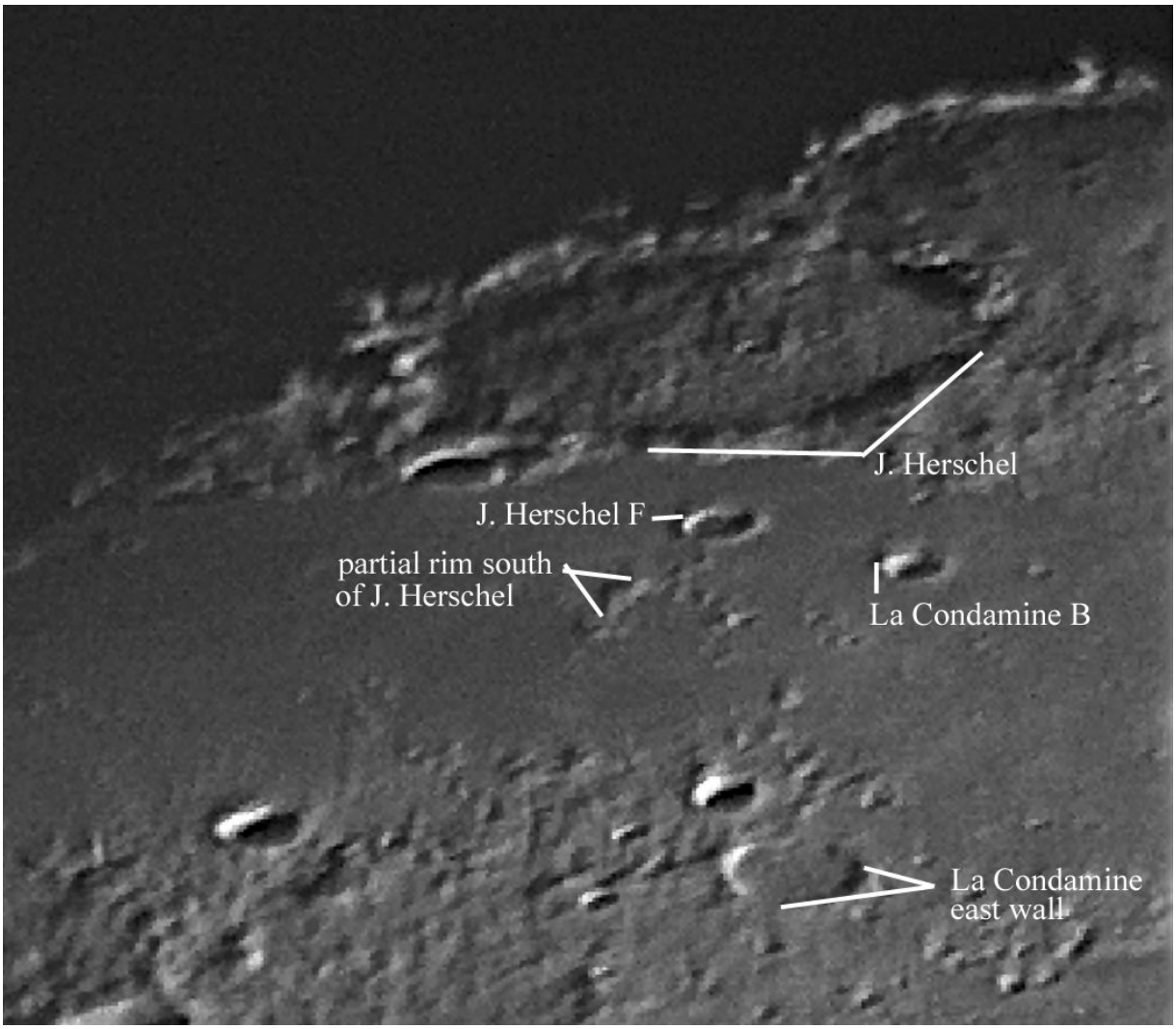

Figure 10 – Location of measurements in the J. Herschel Crater area.

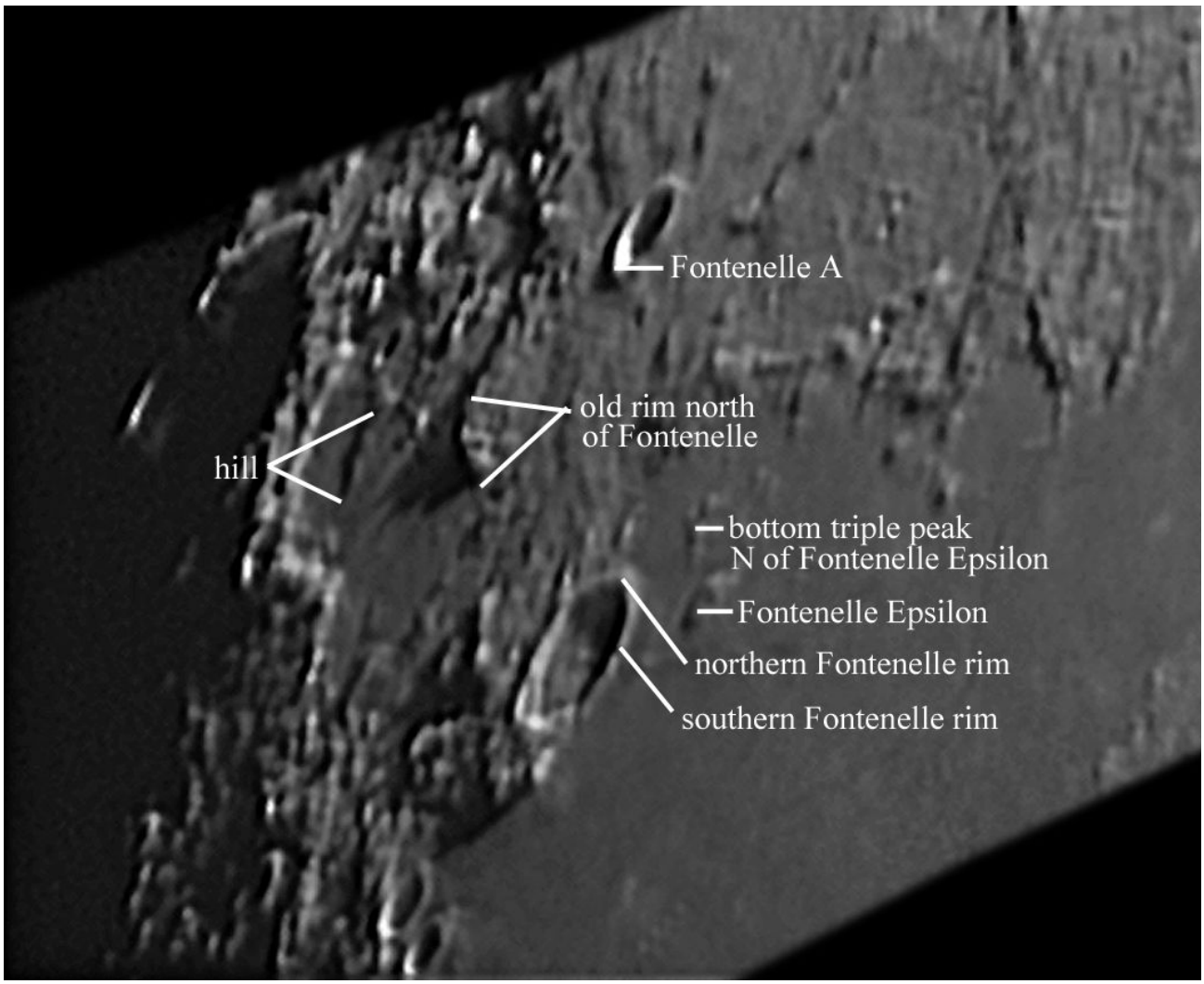

Figure 11 – Location of measurements made in the Fontenelle Crater area.

[3] Boint, S. 2006. LTVT Evaluated At Gassendi. Selenology: The Journal Of The American Lunar Society. Vol. 25. No. 3. Fall, 2006. 8-12.

[4] Boint, S. 2007. A Study Of Mountain Ranges And Isolated Peaks In Northwestern Mare Imbrium. Selenology: The Journal Of The American Lunar Society. Vol. 26. No. 1. Spring, 2007. 9-13.

[5] Boint, S. 2007. How High The Moon—Or At Least A Few Peaks: Lunar Photo Of The Day, March 29, 2007. URL: http://www.lpod.org/?cat=10&paged=3. (last date accessed: 12 January 2008).

[6] Boint, S. Publication Pending. Profile of the Apennines. The Lunar Observer: The Official Newsletter Of The Lunar Section Of The Association Of Lunar And Planetary Observers. URL: http://www.zone-vx.com/. (last date accessed: 12 January 2008).

[7] Cherrington, E. H. 1969. (2nd Ed. 1984). Exploring the Moon Through Binoculars and Small Telescopes. Dover. ISBN: 0486244911. URL: http://the-moon.wikispaces.com/Kurt+Fisher+crater+depths. (last date accessed: 12 January 2008).

[8] Davis III, W.F. 1997. Determination of Lunar Elevations by the Shadow Method: Analysis and Improvements. URL:

http://www.zone-vs.com/vertical-studies.pdf. (last date accessed: 12 January 2008).

[9] Elger The-Moon Wiki. URL: http://the-moon.wikispaces.com/La+Condamine. (last date accessed: 12 January 2008).

[10] Fisher, K.A. 2007. The Third Dimension: Crater Depths From The Apollo Era To The Present. Selenology Today. 5:17-61. URL: http://digilander.libero.it/glrgroup/journal.htm. (last date accessed: 12 January 2008).

[11] Mosher, J. LTVT. Jim's Lunar Terminator Visualization Tool. URL: http://inet.uni2.dk/~d120588/henrik/jim_ltvt.html. (last date accessed: 3 January 2008).

[12] Mosher. J. The-Moon Wiki. URL: http://the-moon.wikispaces.com/Introduction. (last date accessed: 12 January 2008). For Fontenelle Crater: http://the-moon.wikispaces.com/Fontenelle. For La Condamine Crater: http://the-moon.wikispaces.com/La+Condamine.

[13] Rukl, A. 2004. Atlas Of The Moon. Sky Publishing Corp.

[14] The-Moon Wiki. URL: http://the-moon.wikispaces.com/Introduction. (last date accessed: 12 January 2008).

[15] U.S. Air Force, NASA and Aeronautical Chart and Information Center. 1967. (1st Ed.) Lunar Aeronautical Chart (LAC) 11: Herschel. URL:

http://www.lpi.usra.edu/resources/mapcatalog/LAC/lac11/. (last date accessed: 12 January 2008).

[16] U.S. Air Force, NASA and Aeronautical Chart and Information Center. 1967. (1st Ed.) Lunar Aeronautical Chart (LAC) 12: Plato. URL: http://www.lpi.usra.edu/resources/mapcatalog/LAC/lac12/. (last date accessed: 12 January 2008).

[17] U.S. Defense Mapping Agency. 1975. NASA Lunar Topographic Orthophotomap (LTO). URL: http://www.lpi.usra.edu/resources/mapcatalog/LTO/. (last date accessed: 12 January 2008).

[18] Viscardy, G. 1985. *Atlas-guide photographique de la lune: ouvrage de référence à haute résolution*. Masson. ISBN/ISSN/EAN : 2-225-81090-7. URL: http://the-moon.wikispaces.com/Fontenelle. (last date accessed: 12 January 2008).

[19] Westfall, J.E. 2000. Atlas of the Lunar Terminator. Cambridge University Press.

[20] Wood, C. 2006. Mosher, personal communication in Fisher, K.A. 2007.

A Workflow for Sharpening Lunar Images

By Bob Pilz

Syzygy Observatory, Asheville, N.C., USA

Abstract

Sharpening is a key aspect of post-processing AVIs recorded by a web-cam/video camera. In this article sharpening criteria are discussed and a detailed workflow is described and illustrated with screen prints and comparison images. The relationship of image stack size to sharpness is also explored. Compared to previous sharpening workflows I have used, this one provides greater detail, less noise and a more natural appearance due to less exaggeration of topographical details.

Introduction

The most common methodology for obtaining high-resolution lunar images uses a webcam/video camera to record an AVI containing thousands of frames. Post-processing this AVI generally involves the following steps:

1. Raw AVI Processing- Finding the sharpest frames, aligning them and stacking a sufficient number to produce an image with low noise.

2.Sharpening– Using various deconvolution and edge contrast enhancing tools to reveal all details inherent in the stacked image without bringing out objectionable noise, creating artifacts, blowing out highlights or otherwise creating an over-sharpened look.

3.Tonal Adjustment – Selectively adjusting contrast and brightness to produce a natural and aesthetically pleasing image.

The purpose of this article is to describe a workflow for the sharpening part of post-processing – specifically for sharpening lunar images created from processed AVIs. Clearly this is only one of many factors that contribute to the final sharpness of an image. Seeing conditions, equipment, image acquisition skills and procedures and even the raw AVI processing contribute enormously to the final sharpness of an image. Here I'm focusing very narrowly just on the sharpening workflow, but it is still a critical factor in a long chain of critical factors where the ultimate image quality is only as good as the weakest link. There are probably as many workflows for sharpening lunar images as there are lunar imagers. So what makes this one any better than any other? Well, maybe nothing! Unfortunately it's hard to compare with others, because very few people document their entire sharpening workflow in sufficient detail for anyone else to replicate it. The best I can do is to judge any new sharpening workflow relative to ones I have used previously on the same images, and also compare my images to those taken by others with comparable sized scopes. I hope this article will motivate people to document their sharpening workflows in detail so that comparisons can be made. This would help everyone in the amateur community to identify optimal sharpening practices. To evaluate a new sharpening workflow I use the following criteria. Of course all these things are inter-dependent, but I still find it useful to think

about them as distinct criteria.

- *Detail* – Are small details such as craterlets and rilles more visible or better defined?
- *Noise* – For the same number of stacked frames is less noise visible? Can I now stack fewer frames or apply stronger sharpening and still have acceptable noise?
- *Tonality* – Has sharpening caused any highlights to become blown-out (i.e. in 8-bit images having a pixel value of 255)? Has the contrast increased such that topographical details appear over-exaggerated?
- *Artifacts* – Have details in the image been introduced that are not real? Are they obviously false or do they effectively masquerade as real data?

It would be desirable to be rigorous and have quantitative measurements for each of these criteria, but for the most part I just make a subjective judgment. Since I can compare images sharpened different ways side-by-side on the computer monitor, this actually suffices quite well.

In the next section I will describe in detail the programs and parameters that make up this sharpening workflow. At the end I'll discuss how well this workflow meets the above criteria.

Sharpening Workflow

Overview

I use two tools which work together synergistically:

1. Registax Wavelets
2. FocusMagic™

Registax V4 (http://www.astronomie.be/registax/) is a very powerful tool in general for post-processing AVIs. Cor Berrevoets of the Netherlands has done an incredible service to the amateur community by developing this software and making it freely available. An excellent manual can be downloaded from the Registax website which gives a short tutorial and discusses the individual functions and features.

Registax Wavelets is part of Registax V4 and is an excellent sharpening tool. Previously I used it to get an image about 90% of the way to final sharpened state. I then used a variety of other tools either before or after Registax Wavelets for additional sharpening. However, about six months ago, by chance, I ran across a commercial software package called FocusMagic™ (hereafter called FM) (http://www.focusmagic.com/, $45.00 US). This software has been around for a few years, but I had never heard of anyone using it in astronomical image processing.

After much experimentation, I found that splitting the sharpening processing between Registax Wavelets and FM and using both in very specific ways enables me to get more detail out of my images generally with less visibility of noise and less exaggeration of topographical details. One consequence is that I can use smaller stack sizes which for a given number of recorded frames means using frames with a higher average quality. I have had success with stack sizes as low as 16 frames using this method when camera gain is sufficiently low (see Figure 1).

To illustrate this workflow in detail I am using a b/w AVI of the lunar crater Tycho taken September 3, 2007, in very good seeing conditions. I took this with a 200mm f/6 Newtonian at a focal length of 4500mm using a TIS DMK 21BF04 camera with an IR-block filter. The AVI has 7,000 frames and was recorded using a

Figure 1 – Image of Orontius – Stacksize of 16 Frames

LEAD MCMP/MJPEG CODEC. Typically I capture as many as 9,000 frames, but from the real-time view on the monitor, I could tell seeing was very good and fewer frames would be sufficient. This AVI was processed in Registax V4 using Multiple Alignment Point (MAP) processing consisting of 63, 64 x 64 pixel alignment boxes.

Stacked images were created with stack sizes of 200, 100, 75, 50, 40, 30 and 20 frames, since I wasn't sure how small a stack size would be viable. After sharpening each image I was able to determine that a stack size of 50 provided the best tradeoff between noise and detail, and it is the image I will use in the workflow description. The stacked images were saved in a lossless format supporting 16 bits (i.e. PNG).

Registax Wavelets

The goal here is to provide just sufficient sharpening so that the next program, FM, can finish the job of extracting the most detail. These are the settings that I've found work the best for me (see Figure 2):

-Under "Wavelet filter" specify "Gaussian". "Gaussian" produces a much milder effect than "Default".

-For "Layer 1" specify ".2" in the up/down arrow box. Why ".2"? It's a value that I found by much trial and error as allowing a sufficient sharpening effect while minimizing noise in the image.

-For "Layer 1" the slider has to be adjusted appropriately to the inherent noise in the stack. The only way to determine this is by trial and error for your images. The goal is to produce a visible sharpening effect but not by too much. A value too large will, when all sharpening steps are completed, end up making the inherent noise too visible and also result in an over-sharpened look. For this image with the chosen stack size of 50, a slider value of 5 is all that can be used. Figure 3 shows a part of this image before and after wavelets has been applied. As you can see, the effect is not large but is clearly noticeable. Values I typically find useful range from 5 to 10 with larger values being useful as stack sizes increase. Typically I will use 5 for stack sizes smaller than 100 and might use a value of 8 or 10 with a stack size of 400 to 600. Just experiment and keep records and you will soon zero in on appropriate values for your images.

-For the remaining layers I set all sliders to a value of "-5". Why a negative value? Higher number wavelet layers affect coarser and coarser features in an image. I've found that specifying a negative value helps prevent these larger scale features from developing an over-exaggerated or over-sharpened look.

-Lastly, I save the resulting image in a lossless 16-bit format such as PNG.

The image at this point has a thin, light border (see Figure 4). This is an artifact that has been introduced by Registax Wavelets. I crop this off in Photoshop and typically rotate the image to the desired orientation prior to proceeding to the next step.

FocusMagic™

I complete final sharpening of the image with FM (see Figure 5). This product can work as a standalone program or as a Photoshop™ plug-in (see the FM website for other programs that it can work with).

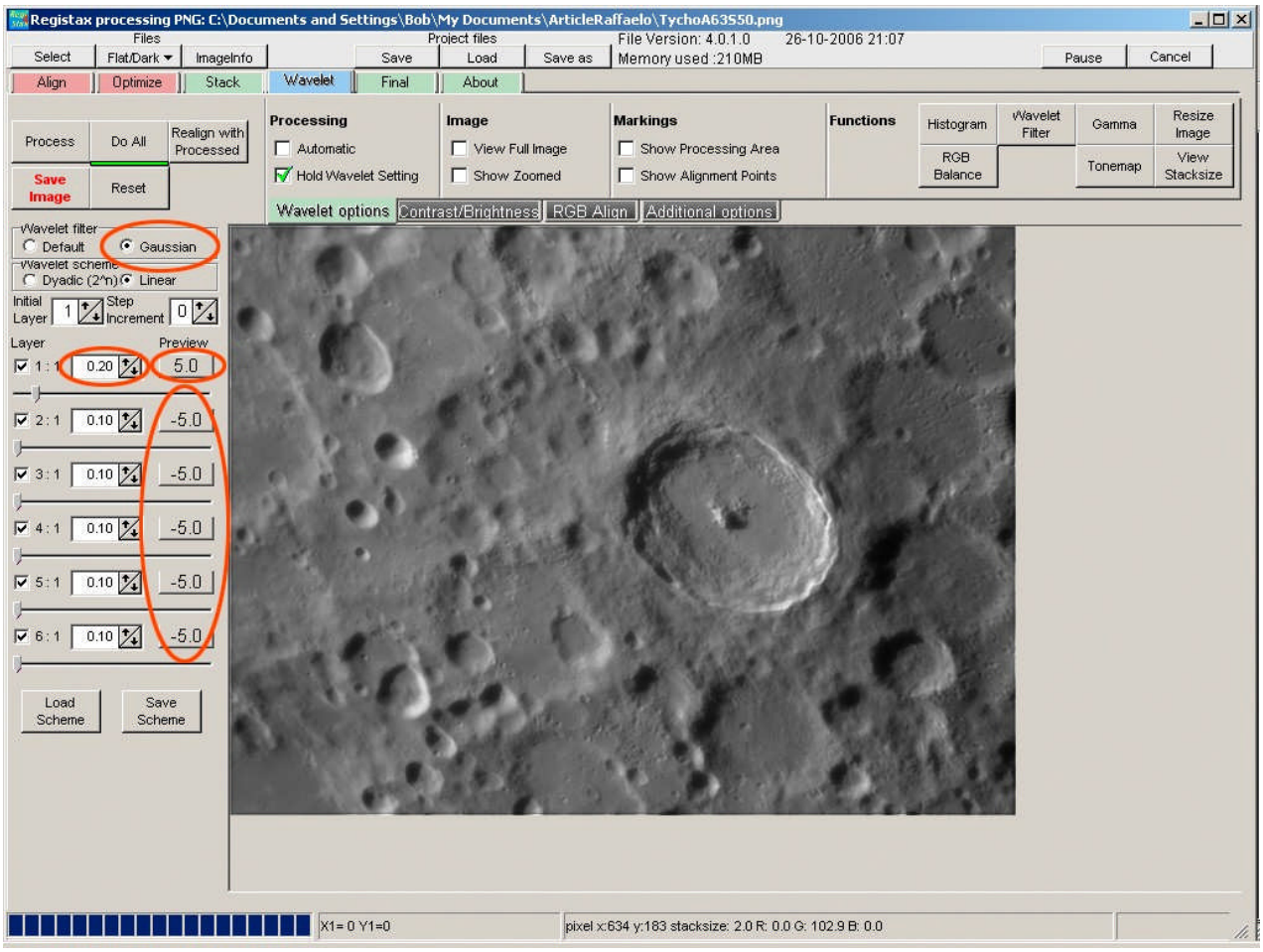

Figure 2 – Registax Wavelets Screen

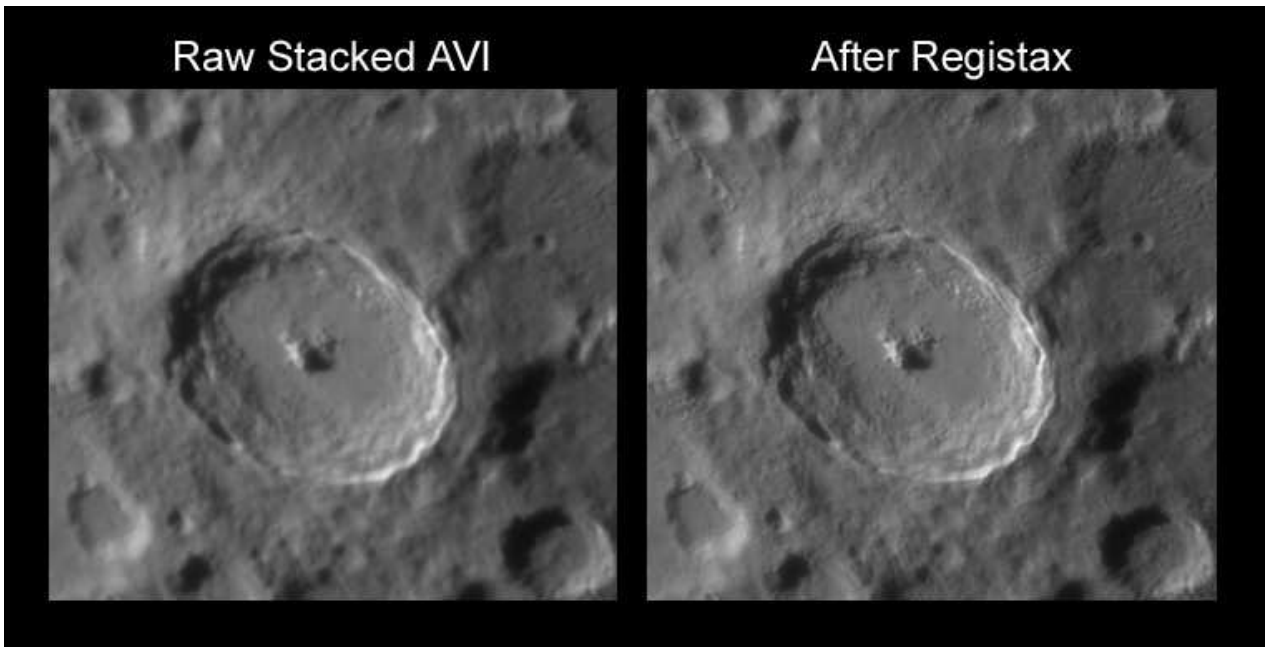

Figure 3 – Registax Wavelets Before and After

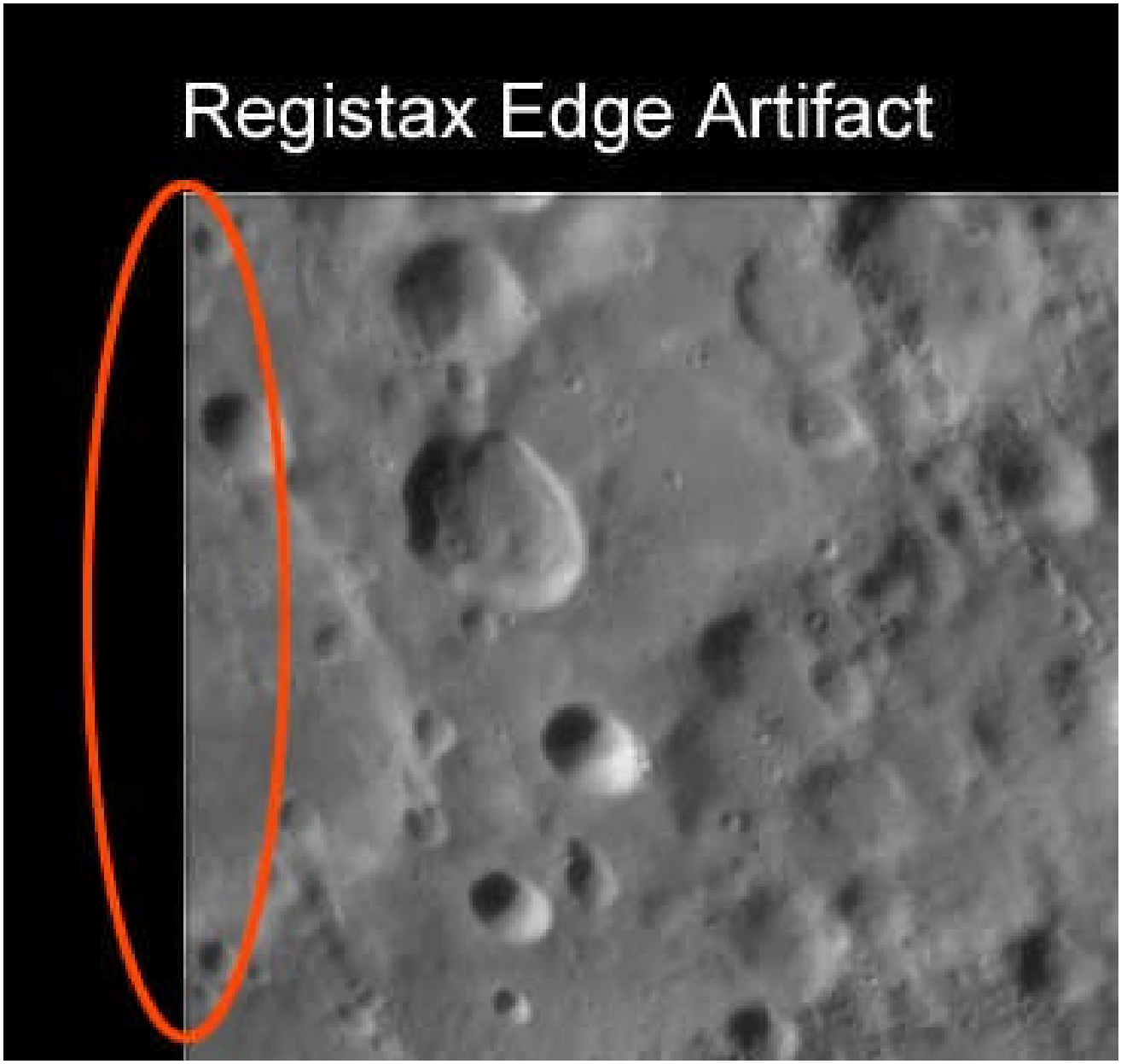

Figure 4 – Registax Wavelets Before and After

However, only the PS plug-in supports 16 bit images, and that is the only use that I recommend. The standalone program only supports JPEG images and will result in undesirable artifacts. After extensive trial and error, these steps and parameters have ended up working the best for me.

-I generally use FM twice on an image. The first application will be stronger. In order to avoid introducing artifacts or noise, first enlarge the image to 2x. I use Photoshop's resize capabilities. Specifically: "Image" → "Image Size" where I've found it simple to just double the resolution from, in this case 300 to 600, using "Bicubic Smoother" as the method (see Figure 6).

-Next I need to choose an "Image Source". FM attempts to provide optimal sharpening depending on the characteristics of the source media. This isn't relevant for my use, since I'm always using an image derived from a video. However, I've found that the choices can be used to modify the strength of the resulting sharpening action. The ones I use, varying from less to more strength, are:

- "Conventional (Film) Camera"
- "Digital Camera"
- "Forensic"

I tend to think of these as low, medium and high strength. The others are some variation and haven't seemed useful. Once again only with experience will you find when to use which parameter. For a stack size of 50, camera gain value of 35% that was used during recording and the brightness of the image, I know that "Forensic" can be used without causing noise to ultimately become apparent. Figure 7 shows a comparison of these three "Image Source" parameters.

-Next I need to set the "Blur Width". FM will suggest a value based on its analysis. It almost always is too high. With the mouse, pull the red box over a feature of interest and see the effect in the "Before" and "After" boxes. I find it best to use a little less than the maximum that seems okay. For example, a value of 6 might look bad and 5 might look fairly good, but I would choose 4 instead. This seems to give the most natural look when combined with the second application of FM. Figure 8 shows a comparison of the effect of a number of different "Blur Width" settings. Note how higher settings eventually create artifacts and an over-sharpened look. In this case a "Blur Width" of 4 was used.

-Finally, I need to set the percentage "Amount". This can be set smaller and larger than 100%. For this first application of FM, I've found 100% gives the best results. At this point all needed parameters have been set. The left and middle images in Figure 9 show a before and after view of this action. Note that all images have been resized to a common 1.25x for ease of comparison.

-After processing completes, I resize the image down to whatever final display size I plan to use. For me that is often from 2x down to 1.25x. Why 1.25x? Displaying an image at native, 1x, size certainly provides the sharpest appearing image, but it is difficult (or even impossible) to see the smallest details. I've found 1.25x to be a good compromise between apparent sharpness and detail made easily visible.

I use PS "Image" → "Image Size" where I change the resolution from, in this case 600 to 375, using "Bicubic Sharper" as the method. Note: In PS it is important for best

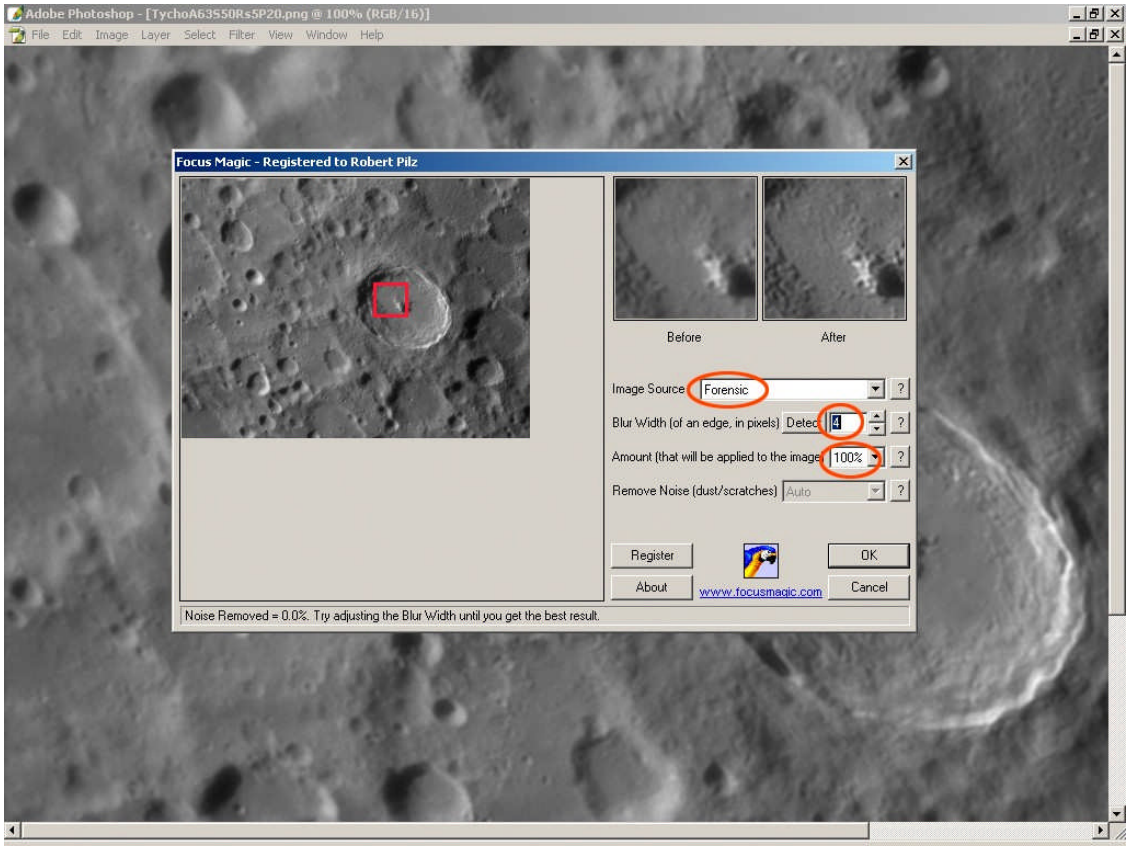

Figure 5 – FocusMagic Screen – First Application

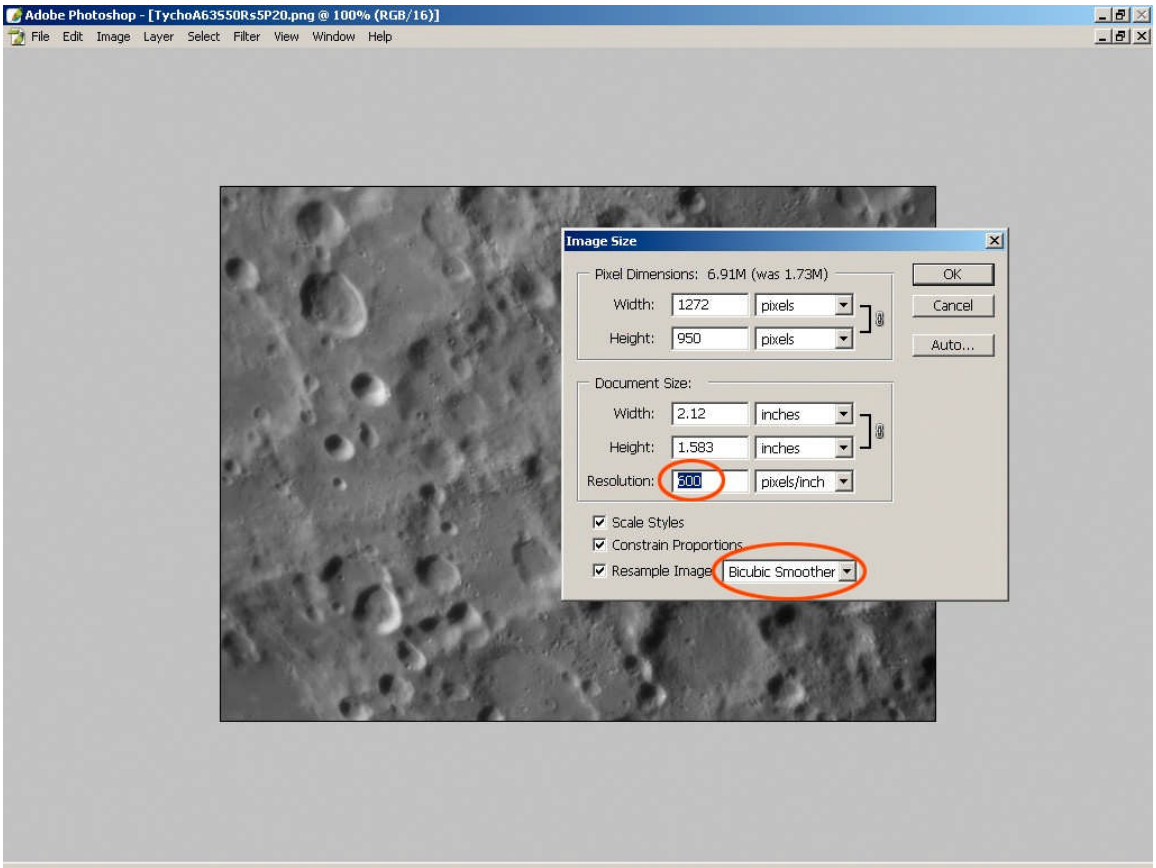

Figure 6 – Resize Image Upwards

results to always use "Bicubic Smoother" when enlarging and "Bicubic Sharper" when reducing!

- After I resize the image downward, I apply a second weaker application of FM. However, this second application will make a significant difference. A typical application would be to use "Conventional (Film) Camera" or "Digital Camera", generally with "Blur Width" of 1 and an "Amount" from 50% to 100%. In this case I used "Digital Camera", "Blur Width" of 1 and "Amount" at 100%. Once again I can use the "Before" and "After" boxes to see the effect in real-time. The middle and right images in Figure 9 show a before and after view of this action.
- Occasionally I've found that a third application of FM can produce even better results. A typical application would be to use "Conventional (Film) Camera" with "Blur Width" of 1 and an "Amount" of 50%. In this case a third application would have introduced more noise and created an over-sharpened appearance.

Evaluation

At this point I need to evaluate the image to see whether the correct sharpening choices have been made. Here I'll use the criteria for evaluating a sharpening workflow that I mentioned at the beginning of this article.

Detail – Figure 10 shows part of the entire image at 1.25x size after all sharpening steps have been done. I'm showing only a part to ensure that full detail will be visible when this article is viewed online. The image shows a wealth of small details and compares favorably to any I've seen taken with an 8" scope. However, how do I know for sure that this is the most detail I can get from the image? Would different sharpening parameters make the image better? Would a different stack size produce better results?

Based on experience, I already know that certain sharpening parameters are optimal. The Registax Wavelet setting used here I know is as much as can be used without introducing adverse noise, and I know a smaller setting won't reveal quite as much detail. However, in FM I generally will try a number of variations with the intent of applying the maximum sharpening that can be done without noise appearing or producing an over-sharpened look. This can take a number of iterations, since there can be two or even three applications of FM each with different strengths and blur widths. Only with experience will you get a feel for which ones are worth trying for a given stack size and camera gain. It's worth noting though, that the same values will definitely not be optimal for each image. Differences in stack size, camera gain, brightness and possibly image scale will all demand different sharpening settings to achieve optimal results.

The question of optimal stack size is an interesting one. There are two competing factors: 1) Increasing the stack size decreases noise and potentially allows more sharpening and 2) Decreasing stack size increases the average quality of frames being used in the stack but increases image noise and reduces how much sharpening can be applied. Anyone who has used Registax for AVI processing is familiar with the "quality graph" that is available for each alignment point. Even in very good seeing it shows that a small number of frames tend to have significantly higher

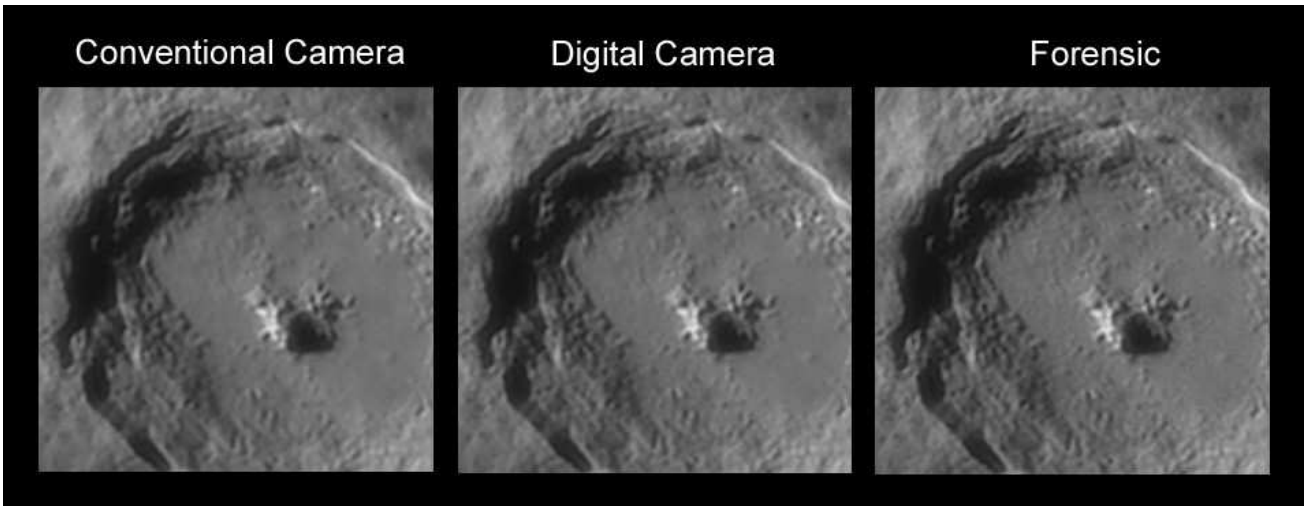

Figure 7 – Comparison of "Image Source" Settings

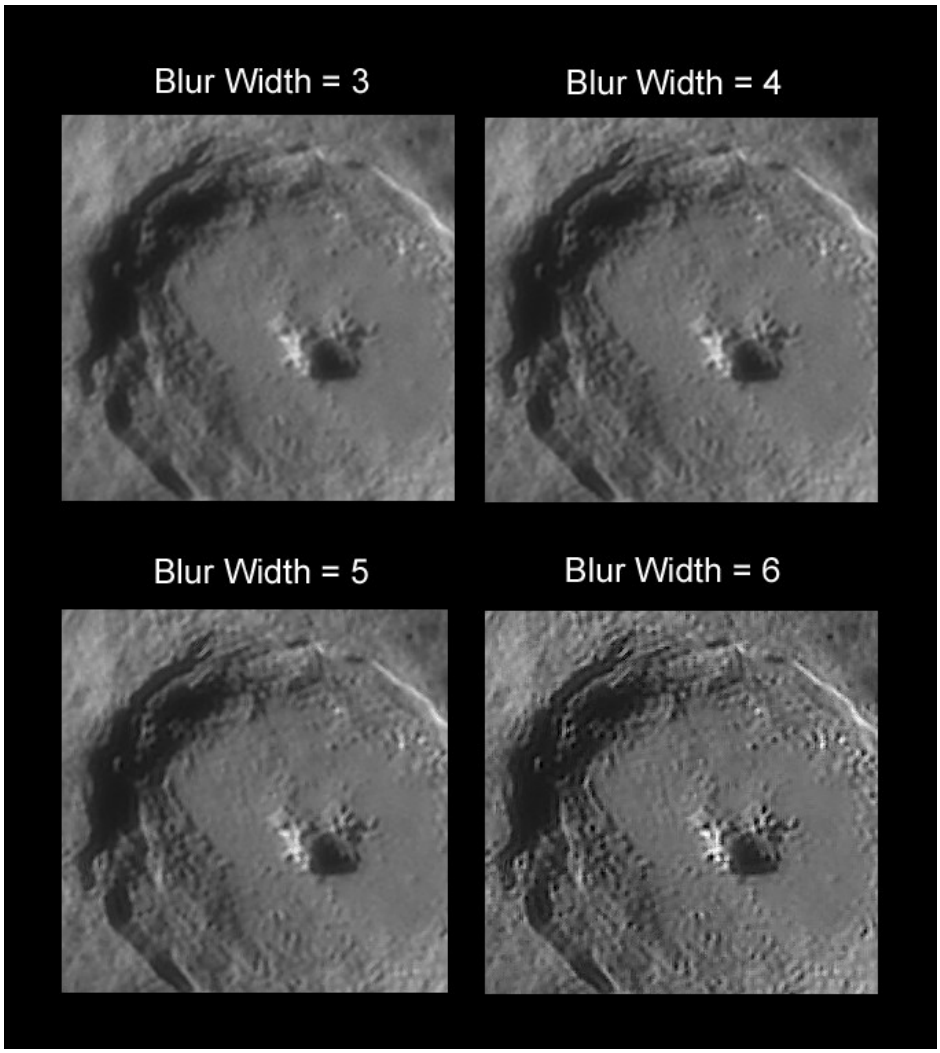

Figure 8 – Comparison of "Blur Width" Settings

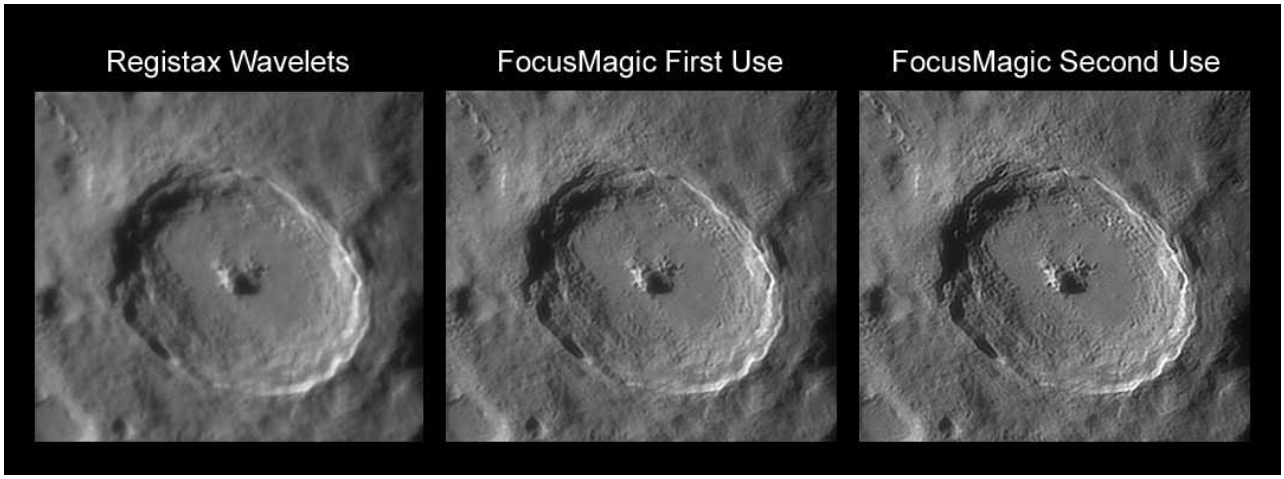

Figure 9a – FocusMagic Before and After

Figure 9b- Enlarged image

quality than the average. When I record an AVI containing 9000 frames, it is typical for the top 50 or so to have significantly better quality. Using fewer higher quality frames has potential for achieving more detail in the final image. Figure 11 shows a section of the image at 2x with stack sizes of 20, 30, 50 and 75 frames. In each case I took great pains to develop the optimum sharpening parameters. The image with a stack size of 50 has the best detail. You'll have to look critically, but the differences are there. Even though a stack size of 20 would have had the highest average frame quality, the greater noise inherent in the image means that less sharpening could be tolerated which means less detail revealed. Conversely, the stack size of 75 was more noise free and could tolerate even more sharpening, but the addition of more, lower quality frames offset this.

This interaction between stack size and detail will vary depending on the seeing conditions. In this case seeing was very good and adding in additional frames from 20 to 50 didn't degrade the average frame quality that much. The stronger sharpening was still able to achieve more detail. In worse seeing a smaller stack size might have been better, since adding in more frames might have degraded the image quality faster than any increase in detail caused by being able to use stronger sharpening. This sensitivity to stack size is stronger with small stack sizes. The percentage difference in average frame quality from a change in stack size of 20 to 50 might require a change from 200 to 600 to get the same percentage delta.

I didn't fully realize all this until I was writing this article. To me this example reinforces the need to create a number of different stack sizes and process each in order to determine where the best detail can be obtained. This can be a lot of work, but it can really pay off in revealed detail.

Noise **–** Figure 12 shows a 2x enlargement of several areas lacking detail in the image. Both a light and a dark area are shown. Noise is not evident. This is a good result for a stack size of 50 frames, but it was only possible because the gain during exposure was low and the image fairly bright.

Tonality **–** Figure 13 shows a section of the image before any sharpening and after all the above sharpening steps have been completed (but before any other tonality enhancements) At this stage I feel the sharpening actions performed above have not created an over-sharpened appearance or over-exaggerated topographical details. However, even though sharpening deals with concrete details, different individuals will have different opinions as to how the image should look. More or less sharpening than I'm doing here may be preferred by some.

It is evident that some areas on the rim of Tycho have become blown-out and have lost any detail. It might look as if many rim areas are blown-out, but use of the PS info palette/eyedropper tool in Photoshop shows that it is only a very few pixels. These areas went from a pixel value of 226 in one case and 232 in another to a value of 255. This isn't a very extensive change but any creation of blown-out pixels is undesirable.

There are two actions that could be taken to help avoid this:

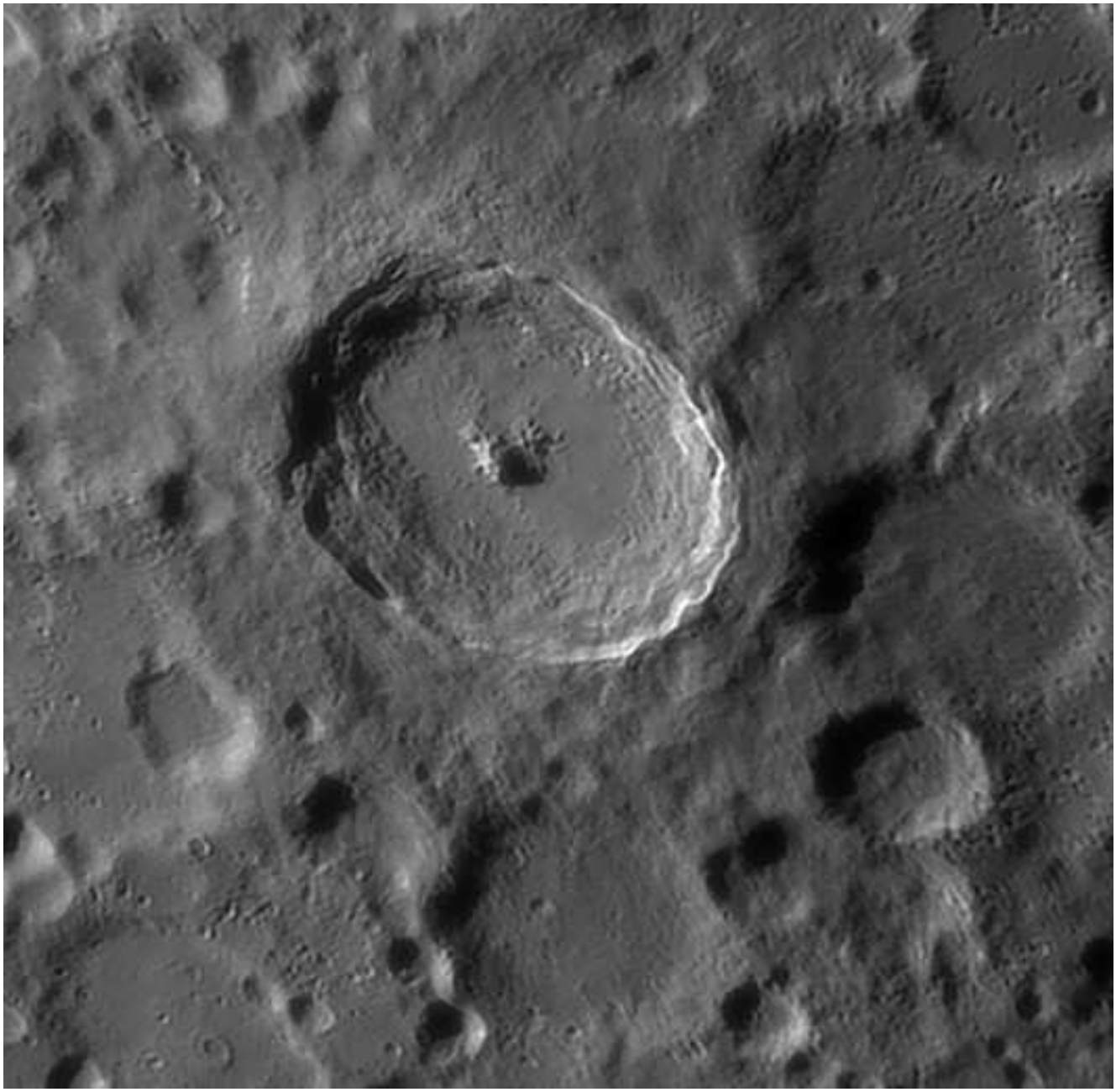

Figure 10 – Image After Sharpening Completed

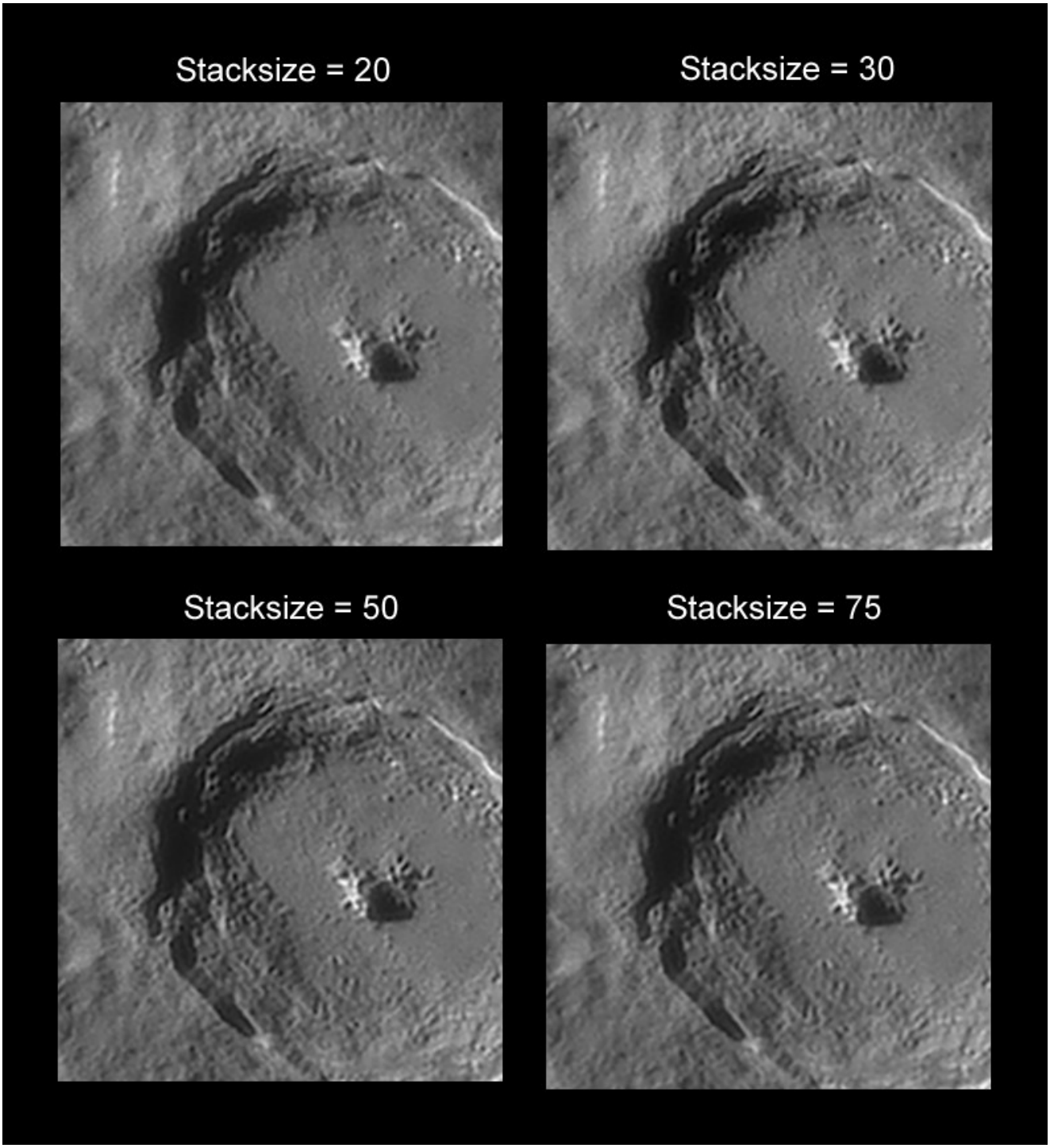

Figure 11 – Stack Size Comparison

1. Record the AVI with a smaller maximum histogram reading. Typically I try for a maximum reading in the 200 – 225 range but evidently slightly exceeded that in this case.
2. Prior to the first sharpening action using Registax wavelets, I could have used Photoshop to selectively reduce the brightness of highlights.

At this point it might be interesting to see what this image would have looked like if sharpened with the workflow I used nine months ago (see Figure 14). The level of detail is a little less, but the tonal changes caused topographical details to be somewhat exaggerated or thickened. For me this now looks somewhat over-sharpened.

Artifacts - Generally sharpening based on some form of deconvolution such as wavelets will produce a visible artifact where there is a sharp edge between areas of widely different brightness. In the literature this is often called 'ringing'. Subsequent sharpening/tonal adjustment steps generally just make it more evident. Figure 15 shows a 2x enlargement of Tycho (see Fig 15a and b). The leftmost arrow points to an area showing that this 'ringing' effect has created false light areas inside areas that should be totally dark. The pattern is typical – a light area surrounded by a moat of darkness. This is an obvious artifact which can be ignored or the more visible portions removed in Photoshop to create a more aesthetically pleasing image. A much less obvious potential artifact is indicated by the rightmost arrow where 'ringing' may have created a dark line outside of a very bright area. I used the word 'potential', because I am actually not sure whether this shadow line is a 'ringing' artifact or represents a slight elevation of the rim above the surrounding area. This kind of artifact is clearly more serious, since it can lead to a mistake in interpretation.

Both types of artifacts are objectionable, but I currently have no way to completely eliminate them. Both are introduced by the Registax wavelets sharpening action and made more visible by subsequent sharpening and tonal adjustments. My future goal is to find a way to further suppress these artifacts while maintaining the other desirable characteristics of this sharpening workflow. Lastly, Figure 16 represents the final image after all sharpening and tonal enhancements have been made.

Conclusion

Every six months or so, I seem to find a new program or new parameters that make a useful difference in my sharpening results. I don't believe this process is finished yet. This sharpening workflow is just a step on a continuing road of discovery, but it has been giving me the best results I've ever had. However, other folks produce terrific images with totally different workflows. There is a lot of room for creativity here. You can get additional insight and help by joining groups like Yahoo's Lunar-Observing forum, reading past posts and asking questions. If you have any comments or questions about this article, you can email me at **lunarimaging at earthlink dot net**.

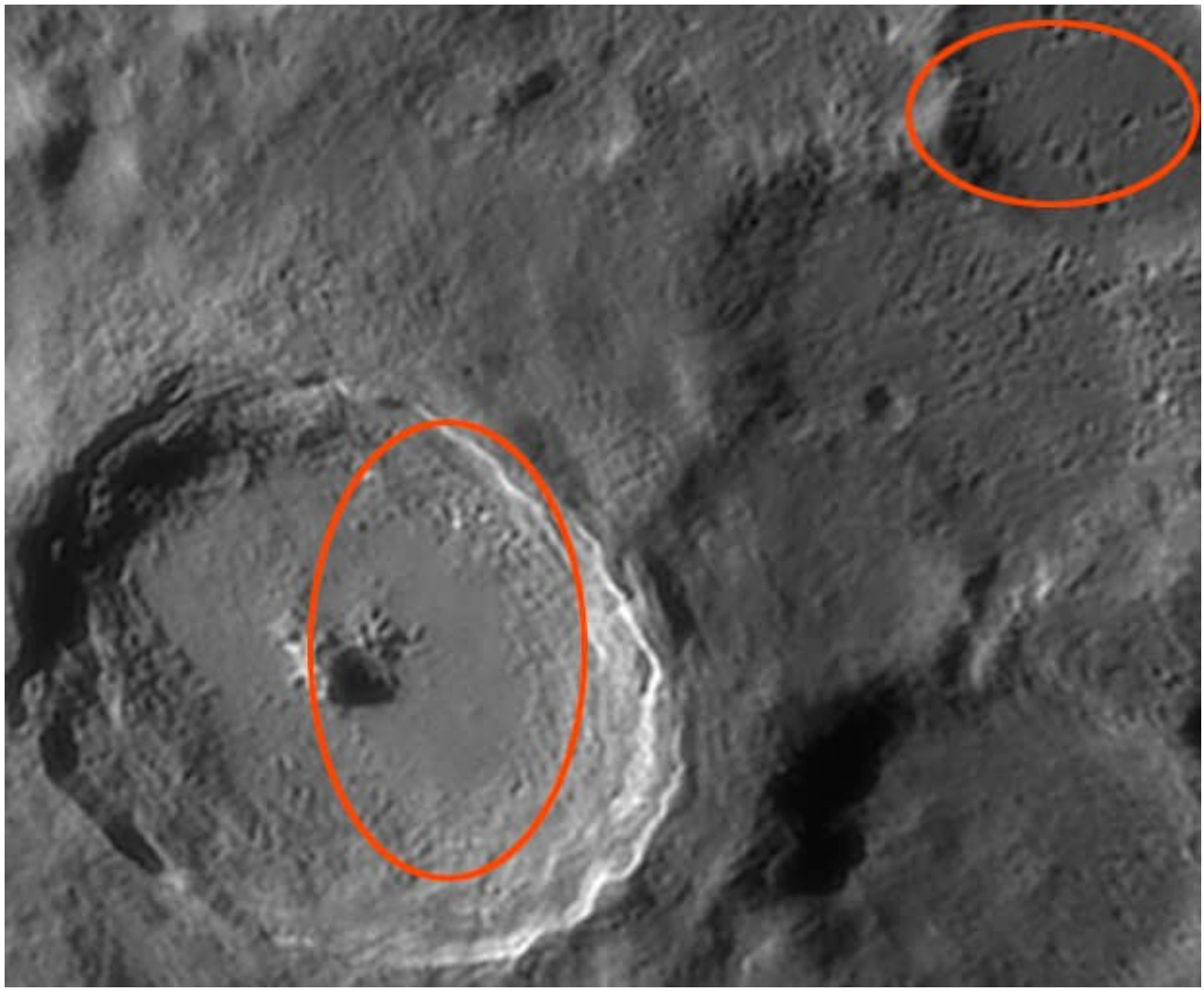

Figure 12 – Examine for Noise

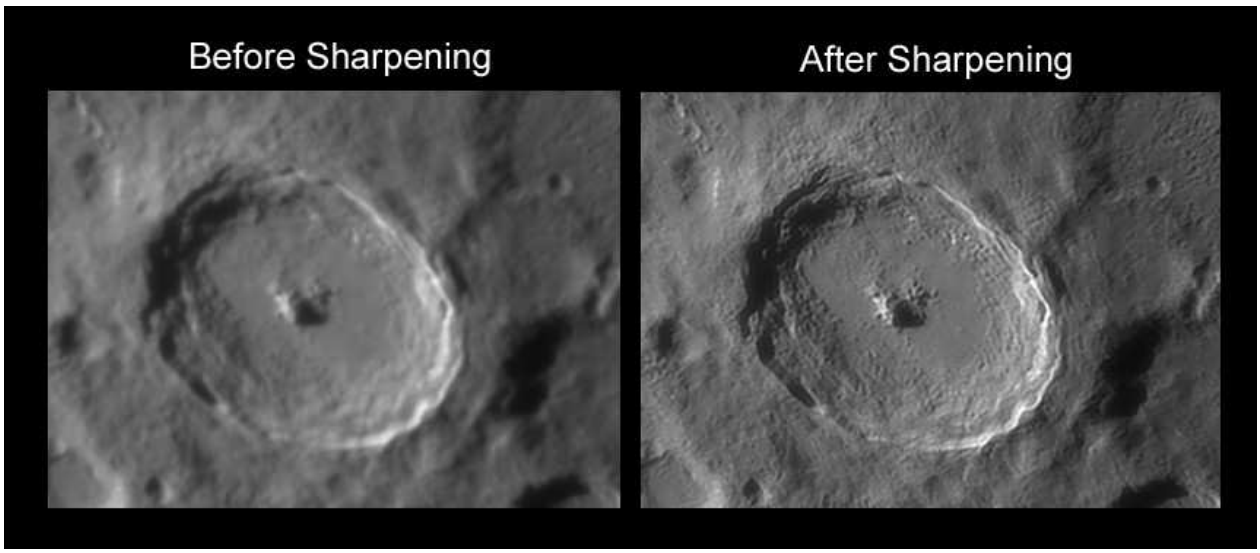

Figure 13– Tonality Changes Due To Sharpening

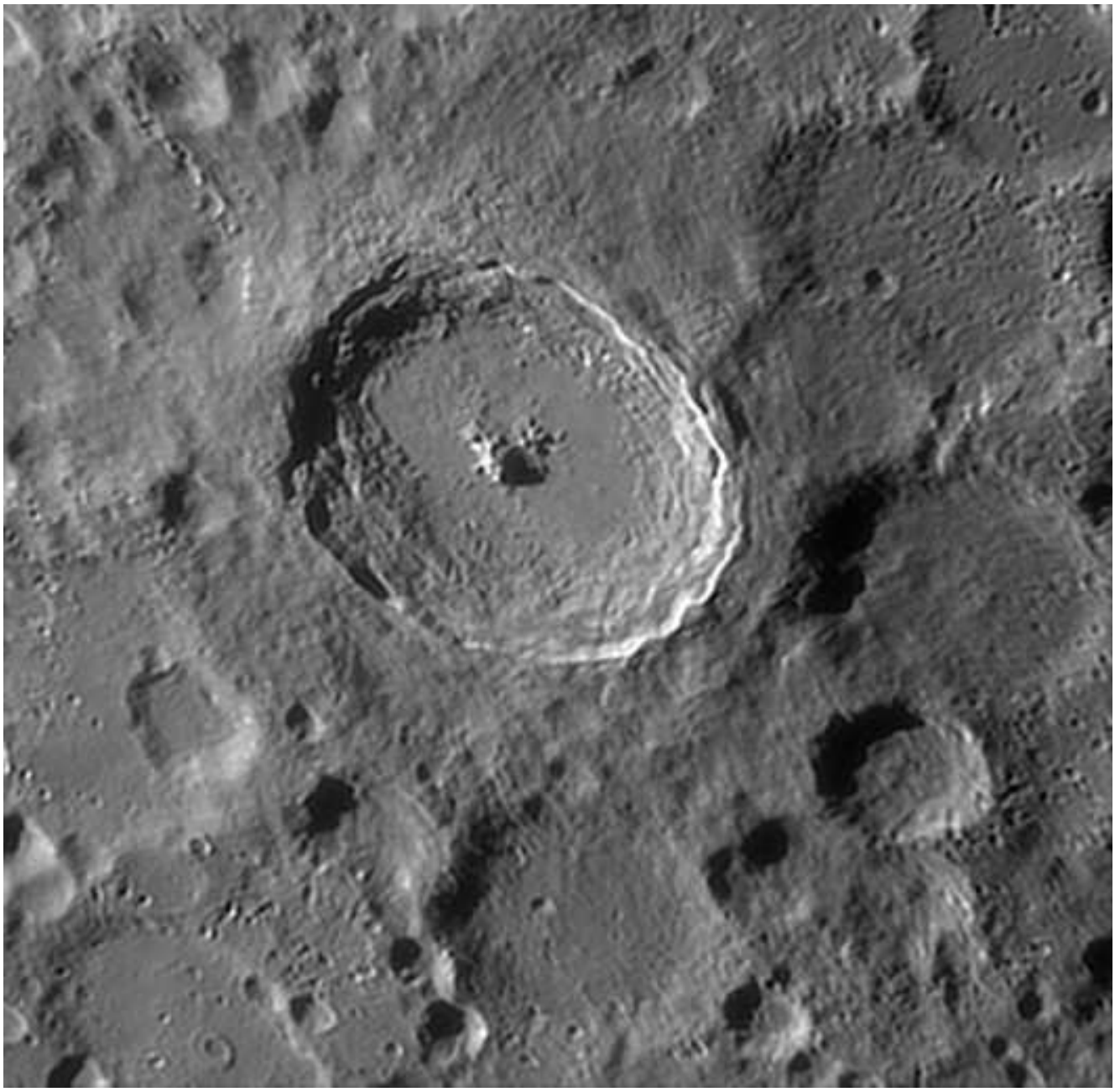

Figure 14 – Previous Sharpening Workflow Results

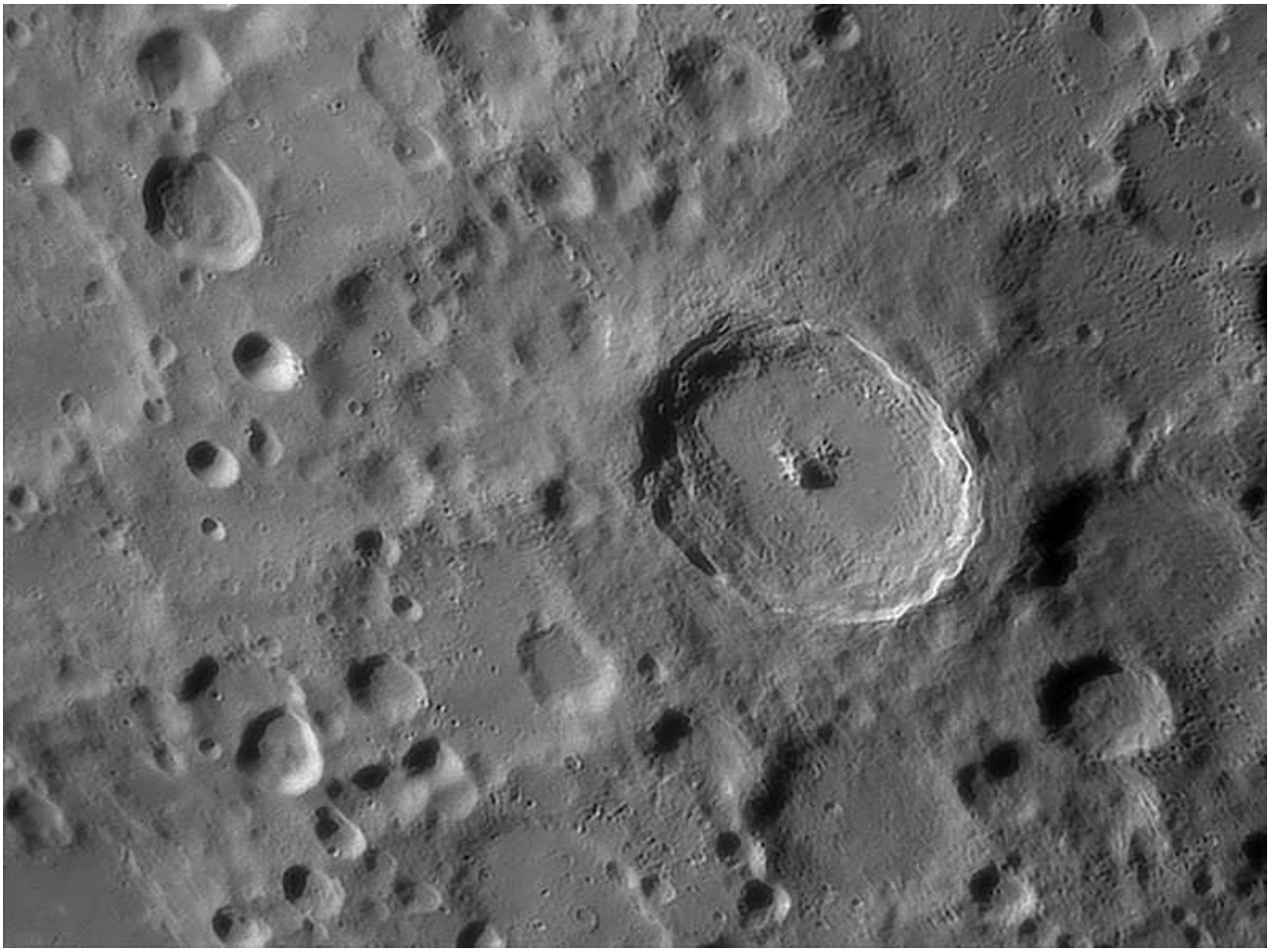

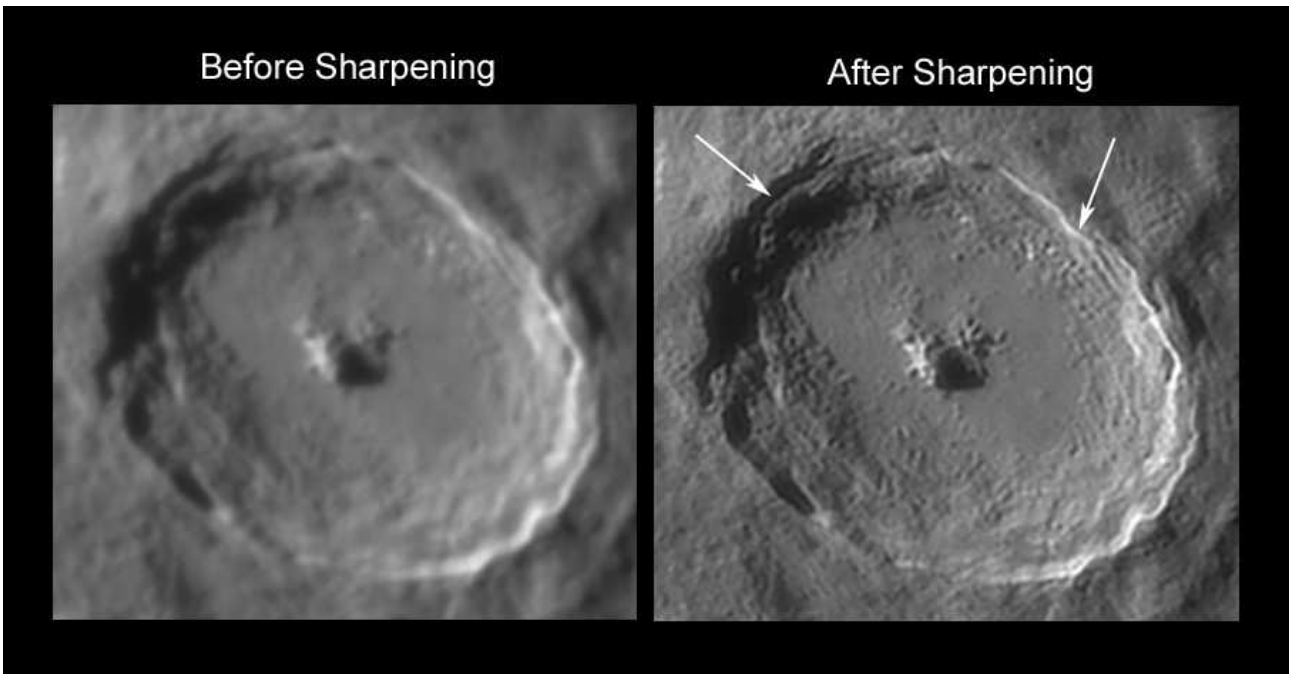

Figure 15 a and b – Sharpening Artifacts

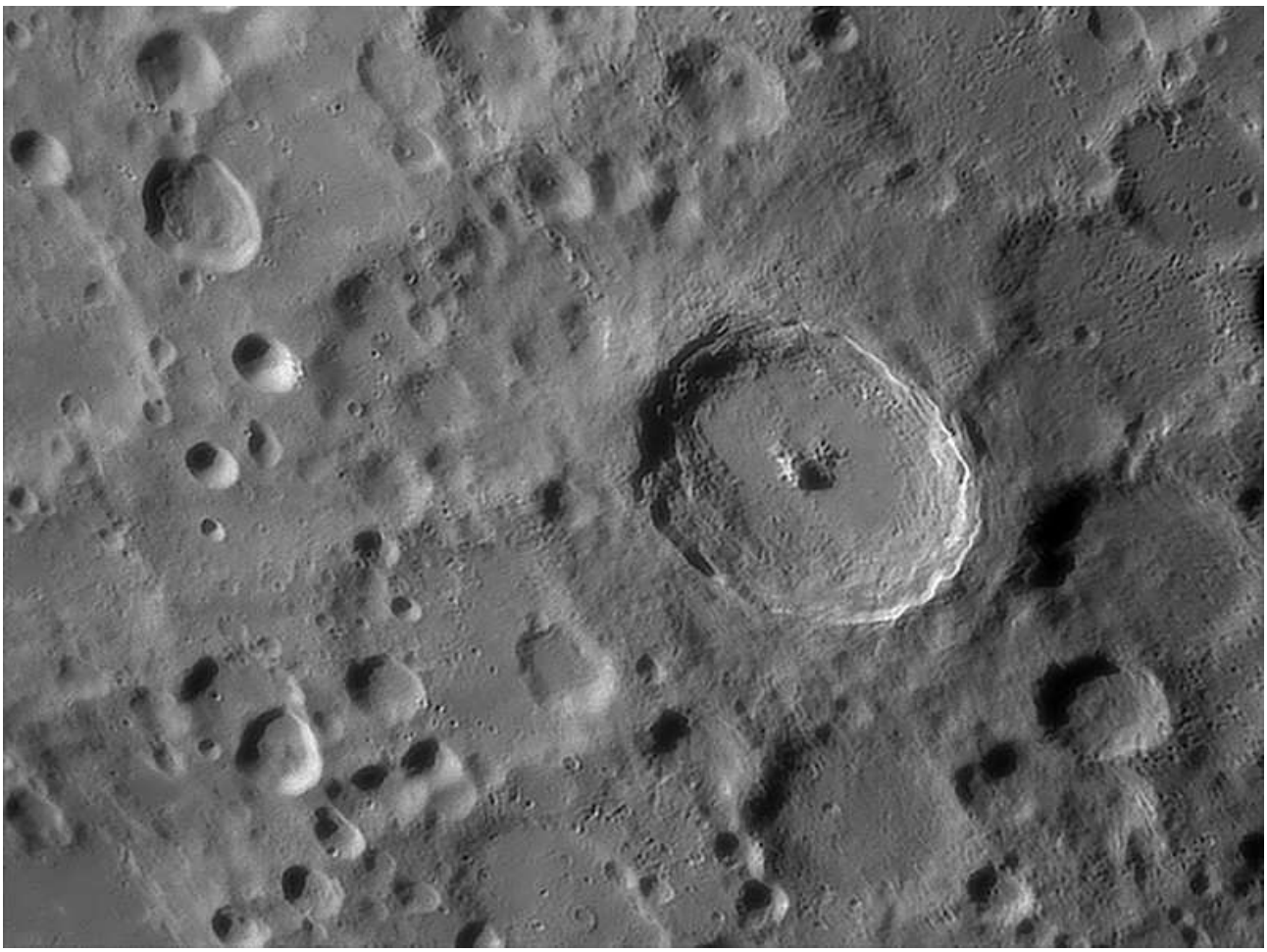

Figure 16 – Final Image Result After All Sharpening and Tonal Adjustments

Observation for Lunar Meteoroid Impacts: Review of Current Techniques

By Raffaello Lena and Richard Evans

Geologic Lunar Research (GLR) Group

Abstract

This paper reviews the historical context of recording lunar meteoroid impacts using small Earth based telescopes, discusses current techniques and methodologies, and presents recent GLR experience. Pertinent equipment including telescopes, cameras, and use of time encoders is discussed as are techniques such as the use of Hartmann masks, diffraction gratings, and near infrared imaging. Review of recorded footage using a slow motion viewer with frame stepping capability is described. Finally, GLR experience using the specialized software program Lunarscan is discussed. The sensitivity of the Lunarscan program at detecting simulated flashes involving a single frame and varying in size and brightness was examined. Simulated flashes were positioned on an avi of the dark side of the lunar terminator adjacent to Sinus Iridium. These simulated flashes were created using Screenblast Movie Studio 3.0 and detection was attempted in Lunarscan at several sensitivity levels determined by values of the k1 coefficient in the program configuration file. Lunar impact surveillance carried out during the Orionids, Leonids and Geminids is discussed and our results are reported.

1.Introduction

The first lunar meteorite impact may have been witnessed by a group of Canterbury monks on June 25, 1178 according to a historical account by Gervaise of Canterbury. The account is anecdotal and it is unclear whether a large lunar asteroid impact was witnessed or simply the break-up of a terrestrial meteor in the Earth's atmosphere that occupied the same sky area as the 1.5 day old moon. In 1953, Dr. Leon Stuart, a radiologist in Oklahoma with a passion for amateur astronomy is credited with taking the first photograph of a possible meteorite impact on the moon. In 2003, a review of Clementine images revealed a fresh 1.5 km diameter candidate crater for this impact (Buratti and Johnson, 2003).

The development and widespread use of videorecording equipment has recently made it possible to conduct surveillance for flashes of light associated with lunar meteorite impacts in real time (Dunham et al., 2000). Spectacular successes using such equipment occurred during the Leonid meteor showers of 1999 and 2001 (Cudnik et al., 2002). Since these initial successes, other meteor swarms have been shown to produce lunar impacts (Yanagisawa et al., 2006; Ortiz et al. 2002, 2006).

2.Methods and Validation

As experience has been gained, it has become apparent that impact flashes can be caused spuriously by a number of factors including camera noise, cosmic rays, glints coming from space debris and satellites, and terrestrial meteorites with trajectories toward the observer. Methodologies have been crafted by

various groups that are intended to prevent spurious flashes being interpreted as being genuine. GLR developed such a methodology jointly with the American Lunar Society in 2002 (www.**glr**group.org/**lunar**impact/manual.htm).

The gold standard is to have an impact recorded simultaneously by at least two observers located a minimum of 20 to 30 km from each other. However, it is not always possible to conduct imaging in organized teams. Therefore much thought has been given to how a single observer can minimize the chances of a spurious result. The possibility that a recorded flash is due to camera noise or a cosmic ray can be eliminated by either slightly defocusing the image to be recorded, or by using a Hartmann mask. Cosmic rays and camera noise produce single pixel aberrations and defocusing an image spreads the light from a genuine impact flash over a larger area. A Hartmann mask is a completely opaque telescope objective cover that has three small (2.5 to 5 cm) holes cut into it at the apices of a triangle drawn around the center point. A star or impact flash viewed through a telescope with a Hartmann mask will produce a triplet image when slightly out of focus. Camera noise and cosmic rays will not produce a triplet image. The drawbacks to using a Hartmann mask are that it reduces the light gathering power of the telescope and requires that the image be slightly defocused. Another alternative is to use a low resolution blazed diffraction grating of about 100 lines/mm. Impact flashes should produce spectra with such a grating while cosmic rays and camera noise will not. The drawbacks to using a diffraction grating are that it accentuates glare, causes some degree of defocusing of the image, and produces multiple spectral images (zero order, 1st order, 2nd order etc.).

For comparison of recorded impact flash candidates with images taken by others, it becomes essential that the exact time of a flash be recorded. The best way to do this is by using a video time encoder coupled to a GPS unit. The exact universal time, down to the millisecond, is superimposed on the bottom of each frame of the video image while it is being recorded. Another alternative is to superimpose an audio time signal onto the audio track of a videorecording. A team of separated observers working simultaneously must work with the same synchronized time.

Imaging is typically done at prime focus, sometimes using a focal reducer. Any camera capable of generating a video image stream can be used but more light sensitive cameras are preferred. If an analog camera is used, the video signal can either be recorded on videotape or DVD disk, or saved to hard disk via a frame grabber. Flashes are more intense and last longer when recorded at near infrared wavelengths, but cameras sensitive at and above the 800 nm to 1100 nm range may be prone to noise and hot pixels. Most often imaging is done in the visual wavelength range.

Once a videostream is recorded it is converted to uncompressed avi format. The first step in image analysis is to view the videoclip using a slow motion player and it is very helpful to have manual frame stepping available as an option. This is a very good but time consuming way to detect an impact flash. Recently,

Peter Gural has made an automated impact flash detection software package availabe as freeware. The current version is called Lunarscan 1.3. This program will allow the masking of the time encoder block on each video frame which prevents the rapidly changing numbers from being recorded as false flashes. It also allows in depth analysis of flashes that are detected and allows the user to vary the sensitivity of a "detection" against background noise levels. Finally, the program can generate predictions of which areas of the moon will likely be impacted by an upcoming meteor swarm.

Differentiating between a genuine flash and a false flash requires strict criteria. Camera noise and the effects of atmospheric turbulence on glare diffusing onto the dark side of the terminator can produce effects simulating a low intensity flash. Therefore, a flash is not a good candidate for a lunar impact event unless its intensity is, at a minimum, equal to the adjacent background intensity plus five times the standard deviation of the background intensity. This criteria may exclude some real events of low intensity, but it will largely eliminate false flashes due to camera noise and atmospheric turbulence. Cosmic rays and camera hot pixels are single pixel events and can be excluded by using the defocusing, the Hartmann mask method, or a diffraction grating. Glints off of satellites and space debris can be excluded by their motion and or the periodicity of their light curves. Terrestrial meteors that happen to be in front of the moon should be detectable by their trajectories and light curves as well. The gold standard will always be to have simultaneous images recorded by two or more separate observers at different locations, but using the methodology described above, a single observer can minimize the possibility of a false detection.

Examples from sessions in lunar impact surveillance, carried out during the Orionids, Leonids and Geminids, are reported in **Appendix 1-3.**

3. Automatic detection with Lunarscan

The Lunarscan program is available at **http://www.gvarros.com/lunarscan.zip** The program was used to analyze a total of twenty two impact flash simulations. The simulated flashes were created in Screenblast Movie Studio 3.0 by superimposing a simulated flash onto an Avi of the dark side of the lunar terminator adjacent to Sinus Iridium taken with a small telescope and a Watec 120N camera. Each simulated flash was 1 frame long, had a 16 millisecond duration, and was positioned at the same x,y coordinates on frame 231 of the avi file. There must be at least 100 frames in the avi clip before the simulated flash occurs. This is required by Lunarscan to adequately assess the background brightness. The approximate pixel dimensions of the bright central area and the entire area of each simulated flash was determined. The latter varied between 7x7 pixels and 1x3 pixels for each simulated flash. The average simulated flash brightness (S) for the entire pixel group constituting the flash varied between 77 and 151 greyscale. The average greyscale value of the background adjacent to the simulated flash was constant at 68 greyscale for

each simulation. The ratio of the average flash brightness to the adjacent background brightness, the signal to noise ratio (S/N) was calculated for each simulation.

Figure 1 shows avi clip frame 231 from a simulated flash 7x7 pixels in diameter with an average brightness of 151 greyscale. From top to bottom, the three inset simulated flashes on the left side of the image have size/brightness values of 5x4/153; 4x4/114; and 4x3/127.

4.Results

Specific data for each of the twenty two simulated flashes is shown in Table 1. Other than the k1 value, which was varied as shown in the Table 1, all other configuration parameters remained at program default settings.

Figure 2 shows a series of flashes all of which are 7x7 pixels in diameter. The image shows simulated flash 1, while the inset from top to bottom respectively shows simulated flashes 7, 9, 12, and 17.

5.Discussion

The Lunarscan program uniformly detected all simulated flashes in which the average flash brightness divided by the average adjacent background brightness was greater than or equal to 1.29. Below this value, no flashes were detected regardless of flash size or increasing the sensitivity of detection by decreasing the k1 parameter in the program configuration file. When flashes were sufficiently brighter than the adjacent background, Lunarscan was able to detect flashes at least 4x3 pixels in diameter. This simulated flash testing demonstrates that Lunarscan is likely to be a sensitive and reliable program for the detection of genuine lunar impact flashes. The software programs Astroart 3.0 and the histogram feature in ImageJ were used to analyze the signal to noise profiles of the simulated flashes. Figure 3 displays the results obtained from several flashes, reported in Figure 2. The program has identified these flashes as stars but the corresponding light curves are referred to the maximum greyscale value for the brightest pixel of the group. With a manual procedure. The histogram feature in ImageJ produced the S/N ratio reported in Table 1.

From these experiments we report that Lunarscan detected the flashes with at least an S/N ratio of 1.29. The brightest simulated flash (see the flash #5 in Fig.3) has the highest value corresponding to a S/N ratio of about 2.2.

APPENDIX 1

Experience in Lunar Impact Surveillance by R. Lena (Italy) and R. Evans (USA):

ORIONIDS SURVEY: Session carried out on October, 21, 2007 Rome Italy

The telescope used was a TMB Refractor f/6 diameter 13 cm. A Lumenera CCD camera LU 075M was used at prime focus with a filter IR blocking. The Lumenera has an imaging array of 640 x 480 pixels. During the session some clouds were present. Seeing was estimated as 3/10 and trasparency 2/5.

The Time was synchronized with US PA ntp-2.ece.cmu.edu.

Table 1

-

Simul. Flash #	Center Area	Total Area	Max	Min	Avg	SD	Frames	Msec	Noise	S/N	k1	Detection
1	3x3	7x7	256	94	151.2	53.0	1	16	68.3	2.21	10	Yes
2	3x3	7x7	256	94	151.2	53.0	1	16	68.3	2.21	5	Yes
3	3x3	7x7	256	94	151.2	53.0	1	16	68.3	2.21	3	Yes
4	2x2	5x4	218	86	153.0	43.2	1	16	68.3	2.24	10	Yes
5	1x1	4x4	191	74	113.6	34.8	1	16	68.3	1.66	10	Yes
6	1x1	4x3	197	80	126.8	35.9	1	16	68.3	1.86	10	Yes
7	3x3	7x7	194	74	126.6	38.2	1	16	68.3	1.85	10	Yes
8	2x2	5x4	169	83	126.2	128.4	1	16	68.3	1.85	10	Yes
9	3x2	7x7	146	72	97	24.3	1	16	68.3	1.42	10	Yes
10	3x2	7x7	146	72	97	24.3	1	16	68.3	1.42	5	Yes
11	3x2	7x7	146	72	97	24.3	1	16	68.3	1.42	3	Yes
12	3x3	7x7	110	72	89	12.1	1	16	68.3	1.3	10	Yes
13	2x2	5x4	103	74	88.3	9.5	1	16	68.3	1.29	10	Yes
14	1x1	3x3	98	75	84.8	7.5	1	16	68.3	1.24	10	No
15	1x1	3x3	98	75	84.8	7.5	1	16	68.3	1.24	5	No
16	1x1	3x3	98	75	84.8	7.5	1	16	68.3	1.24	3	No
17	3x2	5x4	86	77	81.9	2.7	1	16	68.3	1.2	10	No
18	3x2	5x4	86	77	81.9	2.7	1	16	68.3	1.2	5	No
19	3x2	5x4	86	77	81.9	2.7	1	16	68.3	1.2	3	No
20	2x2	5x4	83	72	76.9	3.8	1	16	68.3	1.23	10	No
21	1x2	4x3	81	69	74.3	3.7	1	16	68.3	1.09	10	No
22	1x1	1x3	81	73	77.3	4.0	1	16	68.3	1.13	10	No

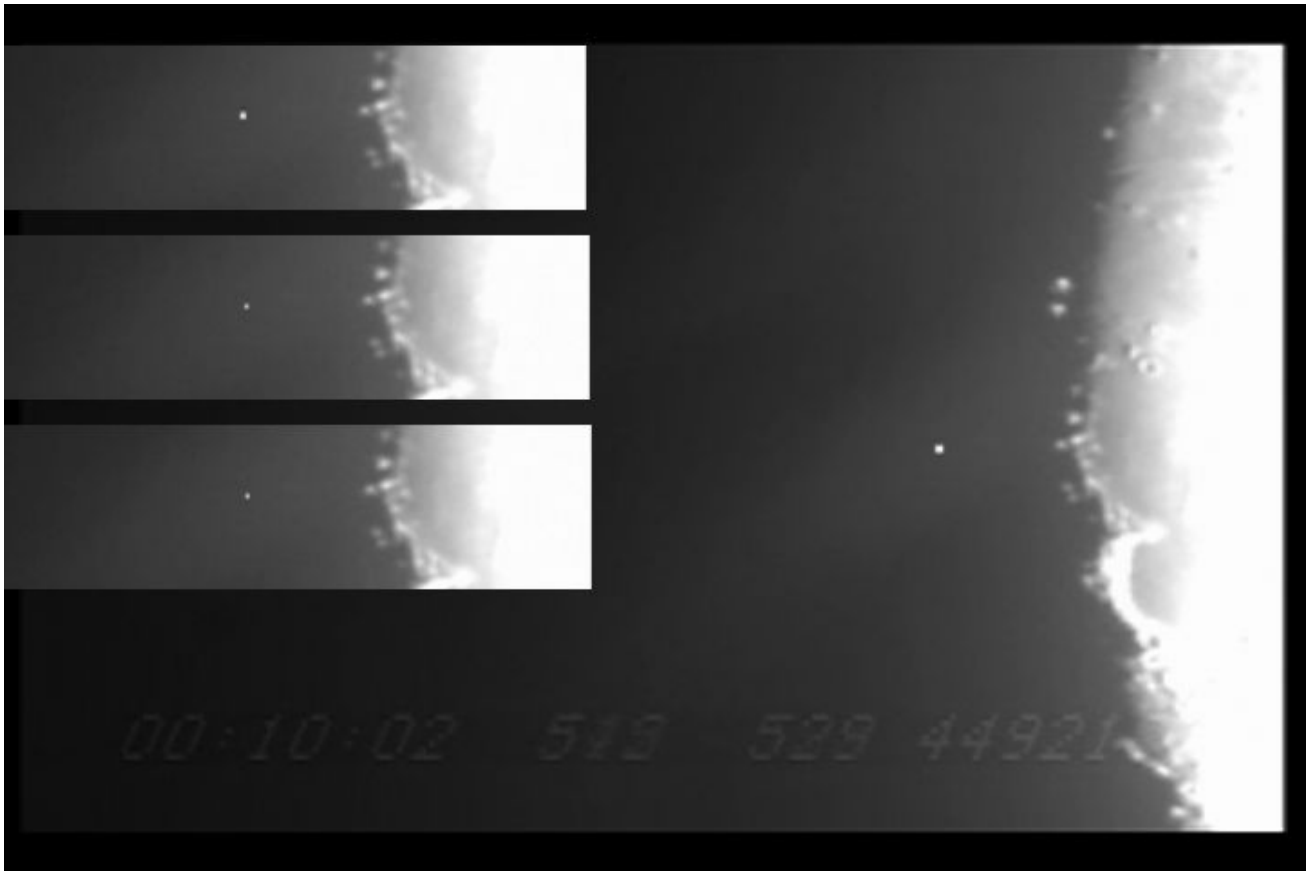

Figure 1 Simulated flash (see text for detail)

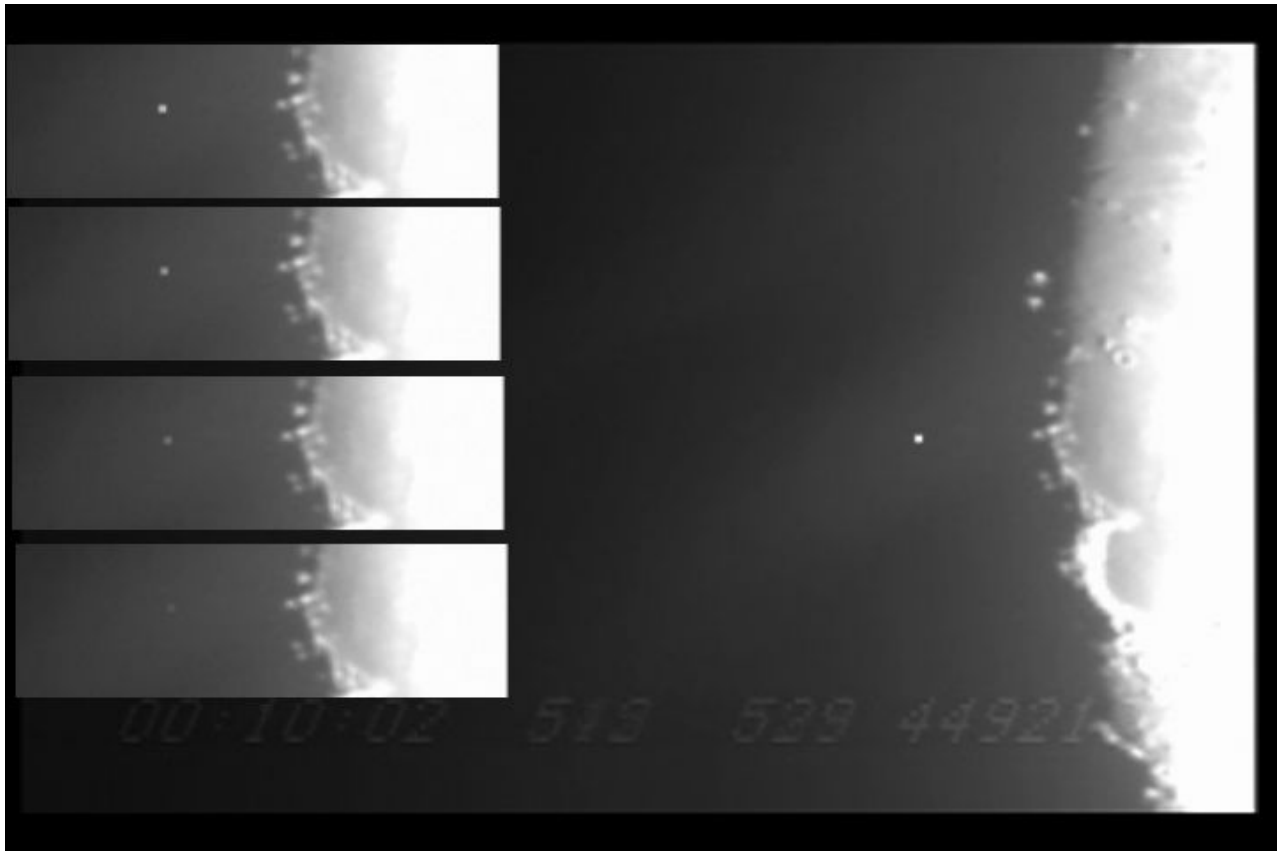

Figure 2 Simulated flash (see text for detail)

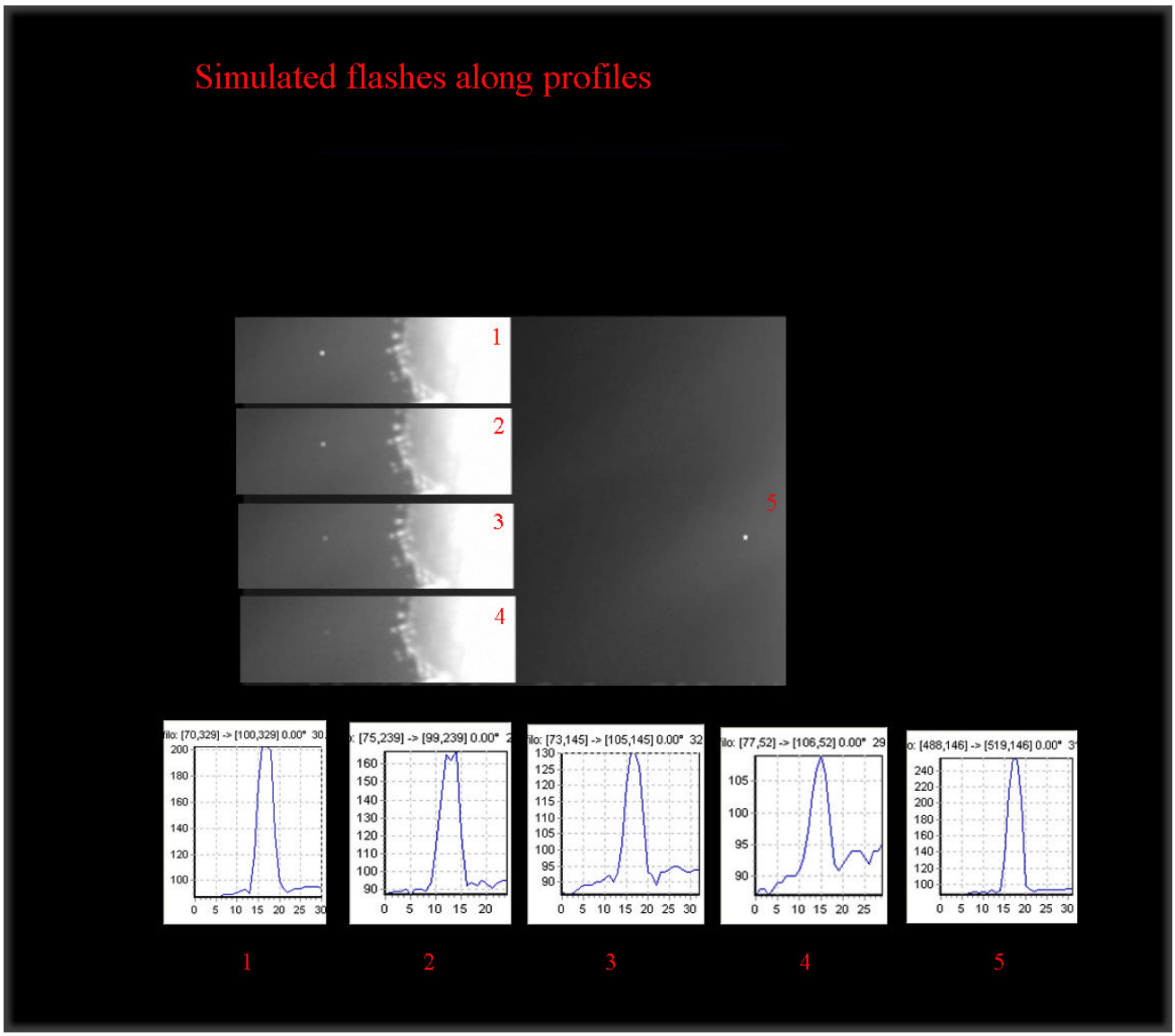

Figure 3

The Lumenera CCD camera was set at 15 fps. LTVT software packaging was used for lunar reference (Fig.4). The lunar quadrant for acquisition was the north - north west region. The lunar terminator was imaged at 18:45:32 UT (Fig.5). It was positioned in a horizontal plane with north to the right and east at the top. Sinus Iridium was used as the geographic reference of the frames (Fig.6). The session started at 18:53:52 UT until 19:22:26 UT. The Moon was blocked by dark clouds about 20% of the time.

The time variation is examined at a resolution of 1/15 sec by separating each frame. No contemporaneous session with independent observers was possible. A flash, which is restricted to a single frame on one single observation, is insufficient evidence to prove that a lunar impact has occurred. It is only suggestive. For this reason the acquired frames were slightly defocused. A lunar flash will be consequently defocused and will become a disk of comparable diameter. Defocusing will have no consequences on the images of spurious flashes, which will remain limited to a few pixels, thus allowing them to be distinguished from lunar flashes. Inspection of the avi films, for flash detection, was carried out with Lunarscan by P. Gural. Visual inspection using a video player was also employed. The shape of each point detected by the Lunascan software was studied. A real flash generally is detectable on two or more frames and its shape is round. Defocusing will have consequences on the images of spurious flashes, which do not appear as a small disk, but as single point. This approach clearly distinguishes possible real flash from cosmic ray hits or noise. No flashes were detected by Lunarscan and close visual inspection for the data analyzed. There are also no hot pixels and no cosmic rays signatures. An example of faint signal detection is shown in Fig. 7. Some bright points were not found to have a multiple spatial spread and they were rejected being single pixel noise spikes without any significant physical appearance consistent with a genuine flash.

The lunar phase after the survey for flash detection is shown in Fig.8.

ORIONIDS SURVEY: Session carried out on October, 21, 2007 Massachusetts, USA

Between October 21, 2007 22:30 UT and October 22, 2007 00:30 UT, the lunar terminator adjacent to Sinus Iridium was imaged using a 23.5 cm Schmidt Cassegrain telescope at F 6.3 to which a Hartmann mask with a total aperture of 13 cm was applied. Transparency was about 4 out of 5 and seeing was estimated at 6 out of 10. Soft focus was used so that a bright flash would produce a triplet image due to the Hartmann mask. The universal time to the millisecond level was encoded on the bottom of each video frame using KIWI OSD and a GPS unit. Tracking was done at lunar rate using a polar aligned equatorial mount. The camera, used at prime focus, was a Watec 120N analog videocamera used at a speed of 30 fps.

A total of 55 video clips, each approximately 1 Gb long, were recorded in wmv format. The total imaging time was approximately 30 minutes. The videoclips were converted to uncompressed avi format and viewed

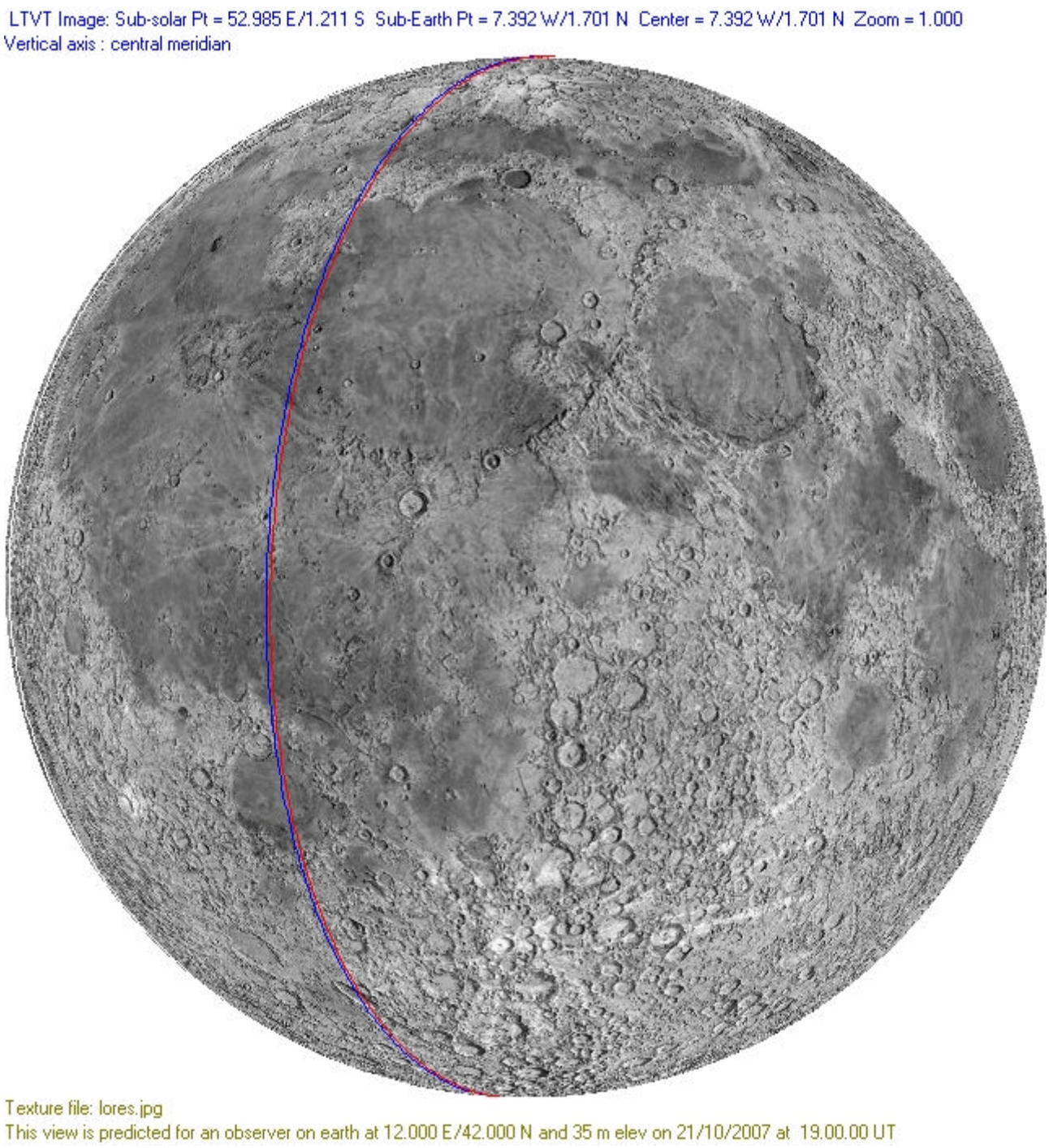

Figure 4. North at the top, West to the left

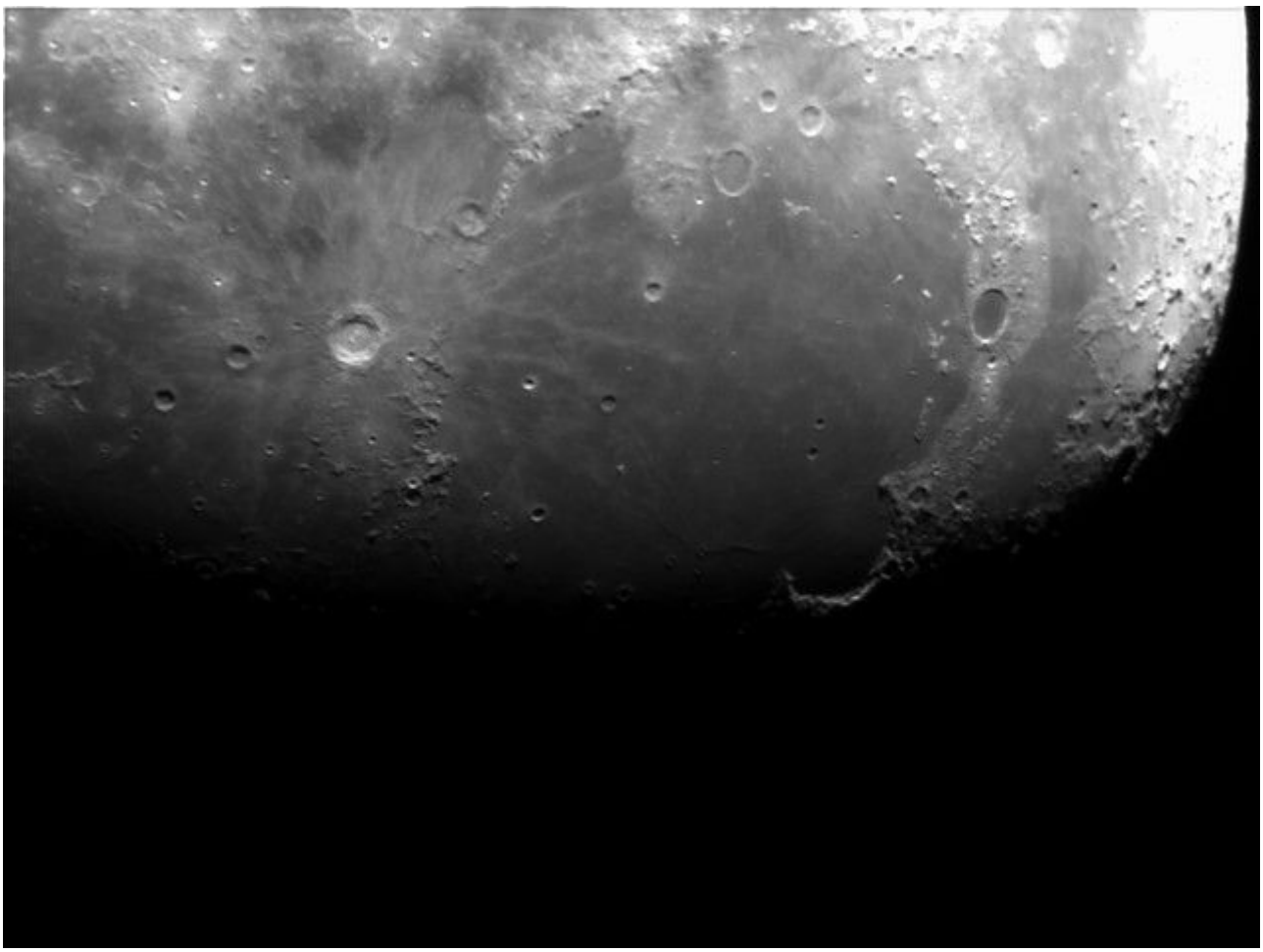

Figure 5 north to the right and east at the top

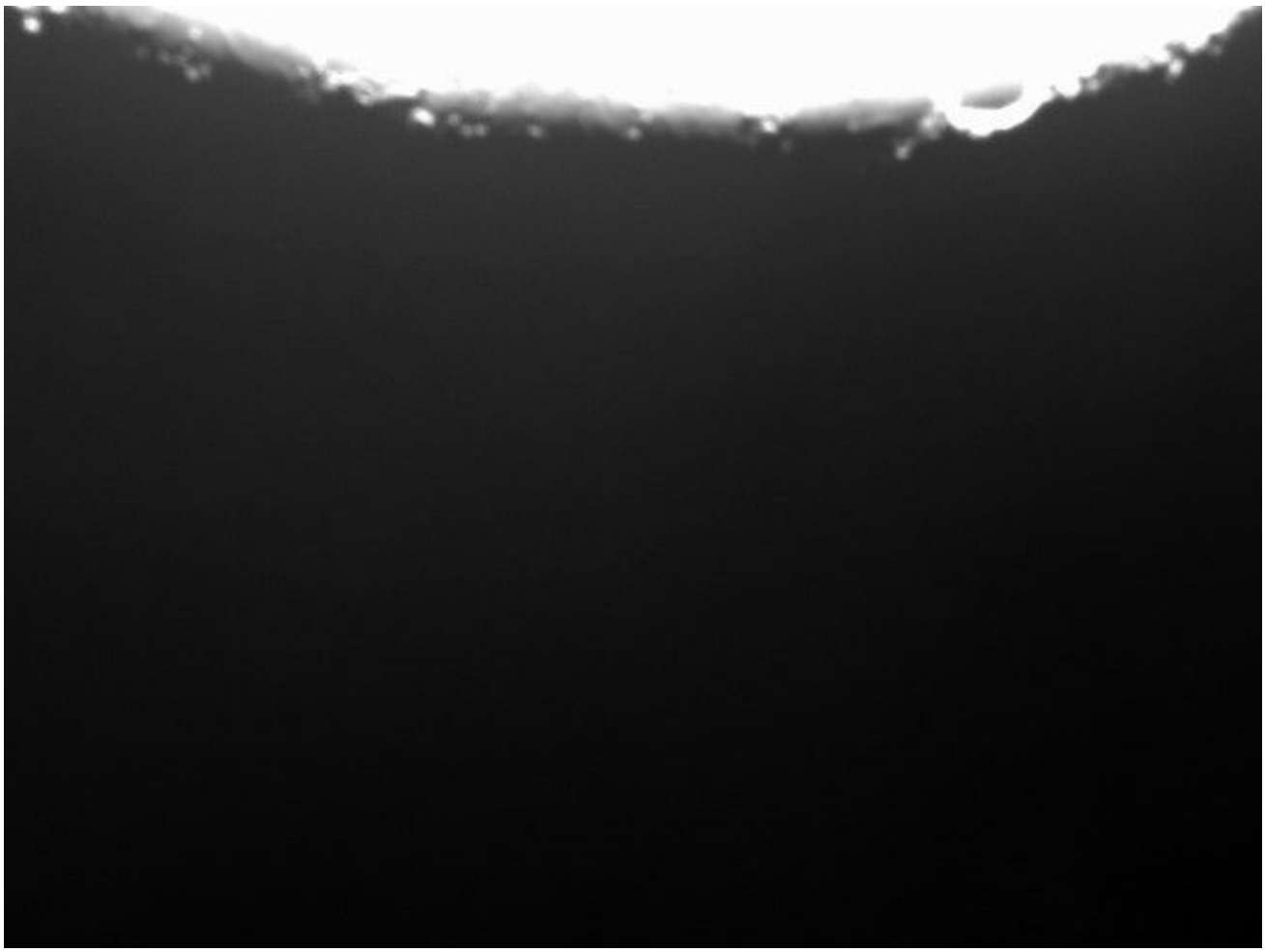

Figure 6

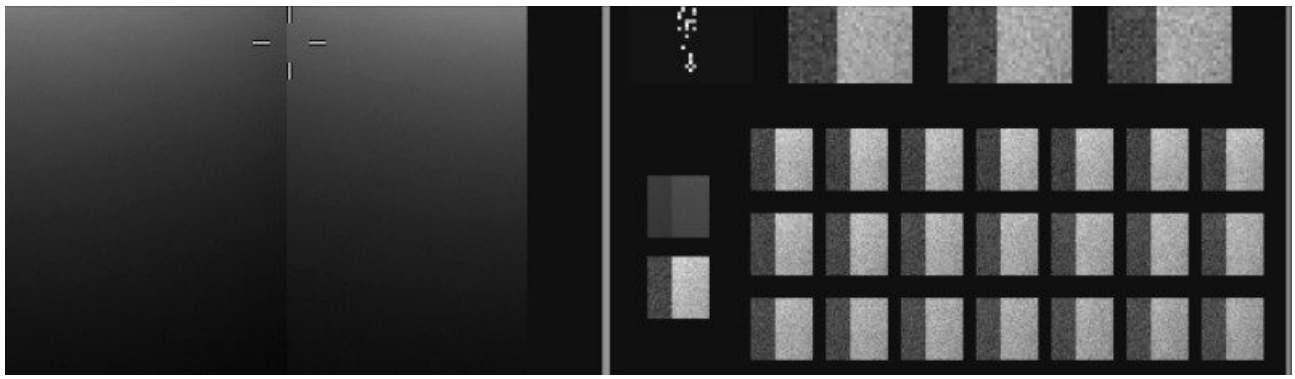

Figure 7 (Frame from Lunarscan)

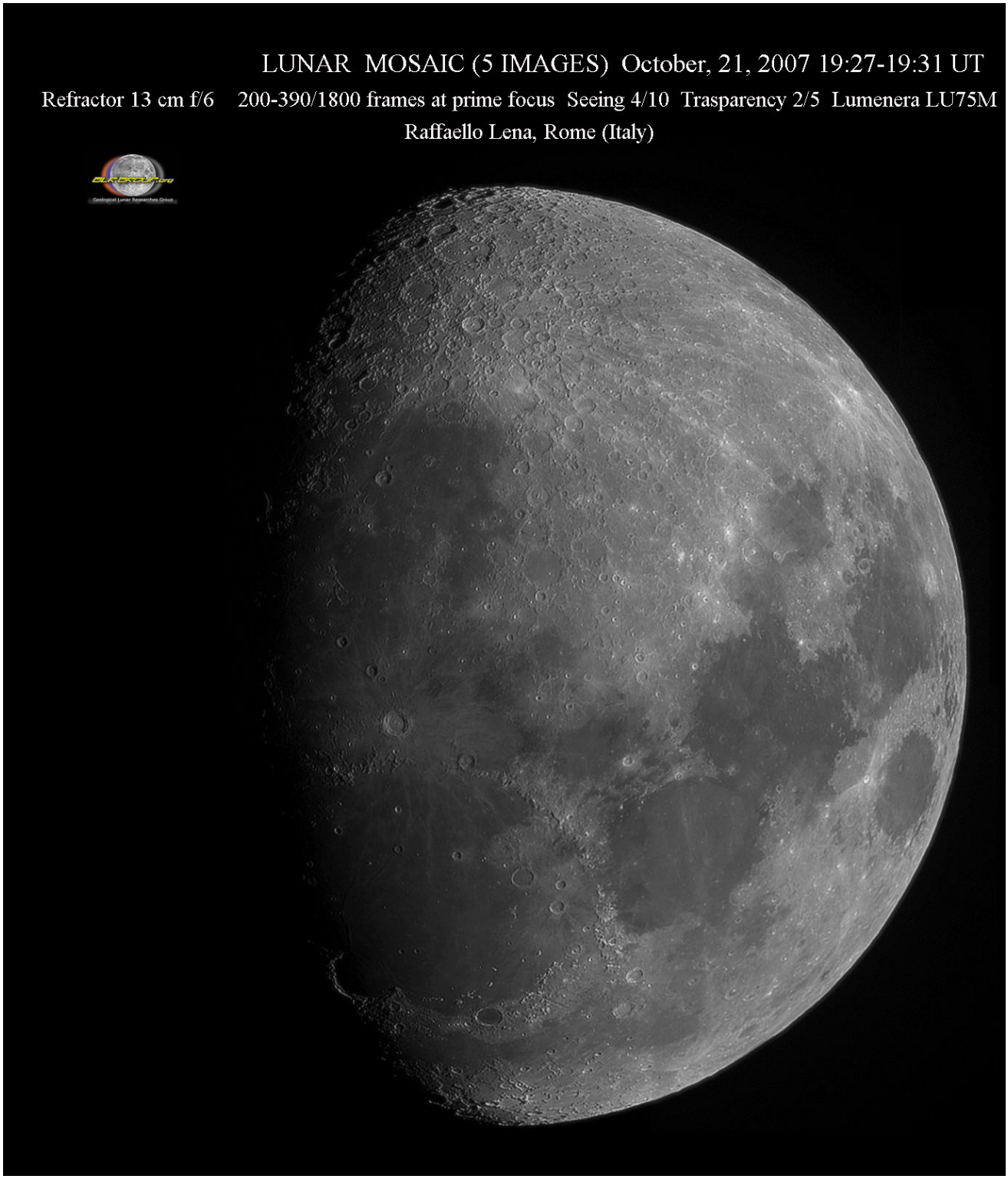
LUNAR MOSAIC (5 IMAGES) October, 21, 2007 19:27-19:31 UT
Refractor 13 cm f/6 200-390/1800 frames at prime focus Seeing 4/10 Trasparency 2/5 Lumenera LU75M
Raffaello Lena, Rome (Italy)

Figure 8

Figure 9

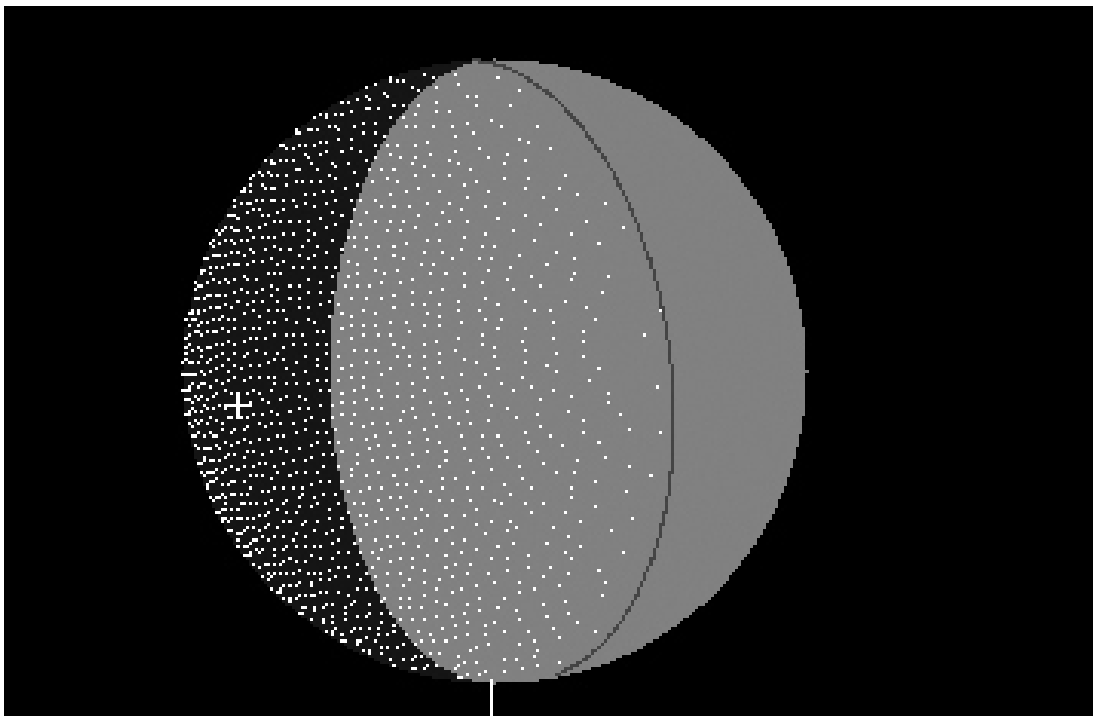

Figure 10 Prediction for area of impact

```
##########################################################
########   Confirmation of Scanned Data   ########
##########################################################

Enter the base filename:  0-12out
  1   00:00:01.200  00:00:01.200    229    481  Frame#      21
  2   00:00:01.233  00:00:01.233    231    479  Frame#      22
```

Figure 11 (from Lunarscan, see text for detail)

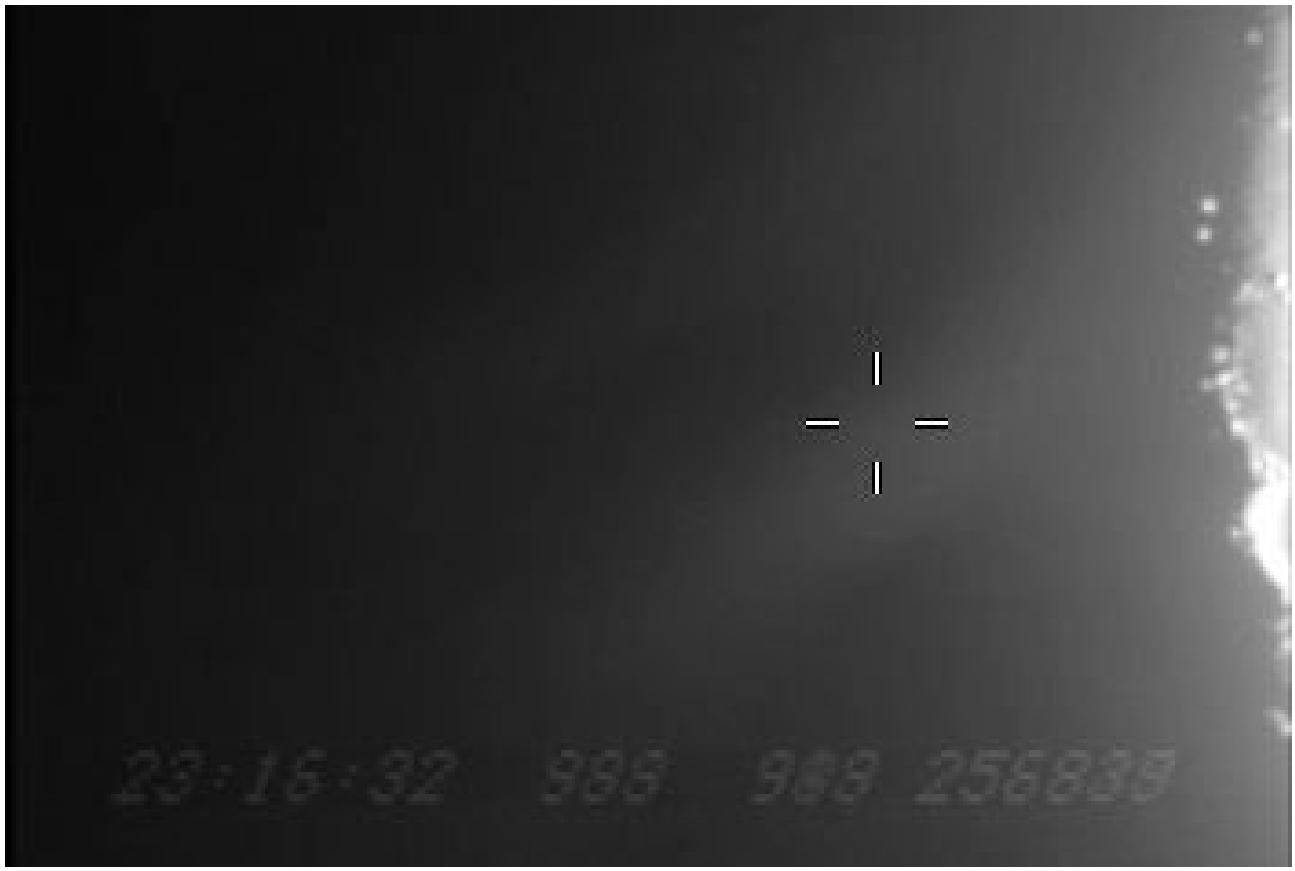

Figure 12 (from Lunarscan, see text for detail)

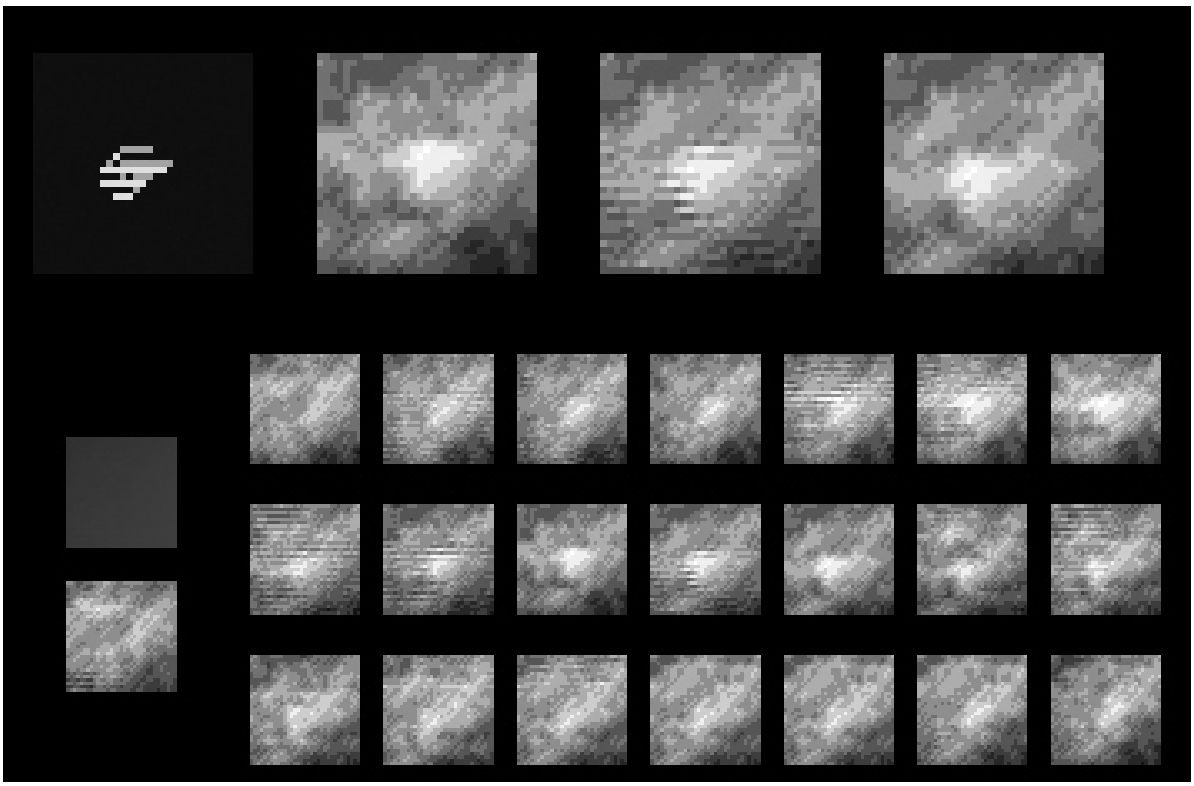

Figure 13 Frame 21 analyzed in Lunarscan

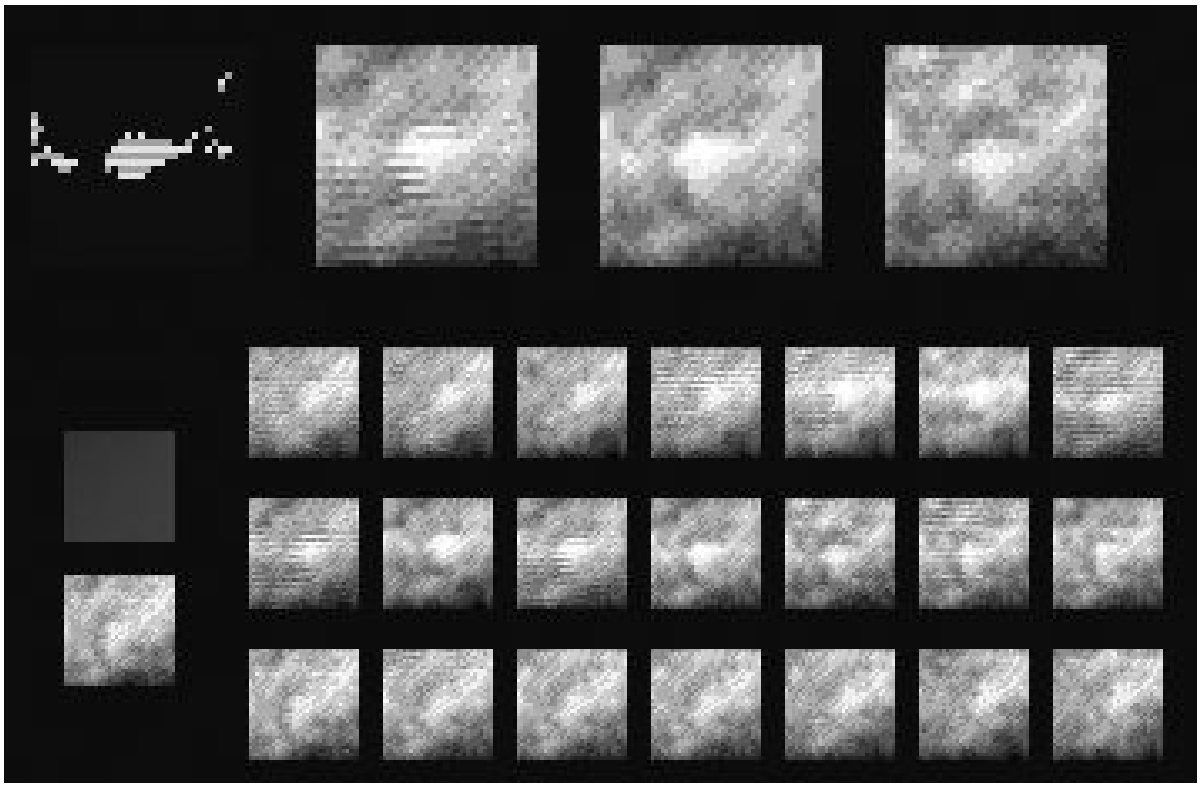

Figure 14 Frame 22 analyzed in Lunarscan

visually in slow motion and using manual frame stepping.

Each clip was then analyzed using Lunarscan 1.3, a freeware program for lunar meteorite impact analysis written by Peter Gural. The equipment setup is shown in Fig. 9.The object was to attempt to capture a lunar impact made by the Orionid swarm of meteoroids. A probability prediction for area of impact was made using Lunarscan for 23:00 UT on October 21, 2007 and is shown below. North is up in the diagram which indicates that the whole western limb is well placed for impact observation on that date and time.

No flashes visible to the eye were observed on review of the avi clips. Lunarscan analysis identified approximately 20 spurious flashes which were rapidly identified as being caused by either the shimmer of bright mountain peaks on the sunlit side of the terminator or by the effects of atmospheric turbulence on a circumscribed area of glare on the dark side of the terminator and located close to the terminator itself. Only one video clip showed an equivocal flash involving two adjacent frames (video clip 12, frames 21 and 22) at pixel locations row 229, column 481 and row 231, column 479 respectively. Time sequence for flash maximum is from 23:16:32:988 UT to 23:16:32:916 UT. Duration of detected flash maximum is 28 milliseconds. Unfortunately the flash is in an area of relative glare. The greyscale value of the central area of this flash (94.718) is equal to the average adjacent background greyscale value (64.418) plus five times the standard deviation (5*6.661) of the background. Because its brightness does not exceed this standard the flash is most likely spurious. Also, the low S/N ratio (1.47) is most likely attributable to a spurious noise effect. Moreover it was not confirmed by any other observer at a second location and it did not appear as a triplet image using the Hartmann mask. However, the analysis of the flash is quite an interesting example of flash analysis in Lunarscan and shows the importance of using the criteria that a genuine flash should likely be brighter than the background greyscale level plus five times the standard deviation of the background greyscale level, unless the flash is also confirmed by a second observer at another location.

APPENDIX 2

Detection of cosmic rays signature in Lunar Impact Surveillance by R. Lena (Italy) and R. Evans (USA):

LEONIDS SURVEY: Session carried out on November, 17, 2007 Rome Italy

The telescope used was a TMB Refractor f/6 diameter 13 cm. A Lumenera CCD camera LU 075M was used at prime focus with a filter IR blocking. Seeing was estimated as 6/10 and trasparency 2/5. The Time was synchronized with US PA ntp-2.ece.cmu.edu.

The Lumenera CCD camera was set at 30 fps. The lunar quadrant for acquisition was the north, north-west region. The session started at 18:13:12 UT until 19:00:03 UT. The Moon was blocked by dark clouds about 30% of the time. The time variation is examined at a resolution

of 1/30 sec by separating each frame.

The acquired frames were slightly defocused. A lunar flash will be consequently defocused and will become a disk of comparable diameter. Defocusing will have no consequences on the images of spurious flashes, which will remain limited to a few pixels, thus allowing them to be distinguished from lunar flashes. During the session were recorded several bright flashes interpreted as cosmic rays signature (see Fig. 15-17). The profiles (see section 5 Discussion) are referred to the maximum greyvalue for the brightest pixel. The analysis has shown their spurious nature because:

a) the presence of faint satellite flashes were recorded in the same frame. It seems to be a recurrent appearance for a cosmic ray nature. In the case of Figure 17 (time 18:22:00 UT) a double flash with the presence of another faint satellite flash was simultaneously imaged;

b) all the detected flashes (and their faint satellite flashes) were recorded in a single frame;

c) having strongly blurred the image during the acquisition the flashes are very sharp and cover one single (or 2-3 single) pixel in the image which is different with the broad PSF expected from a real impact.

Leonids Survey: Session carried out November 18, 2007 at Fitchburg, MA USA

The telescope used was a 235 mm (9.25 inch) Schmidt Cassegrain with a focal reducer used at prime focus at F 6.3. A Hartmann mask with three aperture holes of 7 cm diameter each giving a combined aperture area of 115 cm ^{2}, or 27 percent of the aperture of the instrument without the mask. When the image of a point source is slightly defocused, the Hartmann mask provides a triplet image of the source. Cosmic rays, however, do not produce triplet images. The imager used was a Watec 120N videocam at approximately approximately 30 to 40 frames per second. A Kiwi OSD video time encoder was used to superimpose universal time to the millisecond onto each video frame. The lunar quadrant imaged was the west southwest region. Imaging began at 22:00 UT on November 18, 2007 and continued through 00:30 UT on November 19, 2007. The seeing was estimated at 6/10 and the transparency at 3/5. The sky was mainly clear with an occasional passing cloud. Videoclips were recorded in wmv format and later converted to avi format with segmentation into 1 Gb lengths using VirtualDub. A single flash was detected and is shown in Figure 18. The single flash that was observed was recorded between 23:01:00.888 and 23:01:00.913 UT on November 18, 2007. The duration of the flash was a single frame, or about 0.025 seconds. The flash was analyzed using Lunarscan. The flash dimensions were 4 x 4 pixels and its margins were not particularly sharp. The magnitude of the flash could not be estimated as no stars were imaged during the session. Although the pixel dimensions of the flash were larger than expected from a cosmic ray which in our experience usually produces a 1 pixel flash with perhaps a couple of adjacent 1 pixel satellite flashes, the flash could not

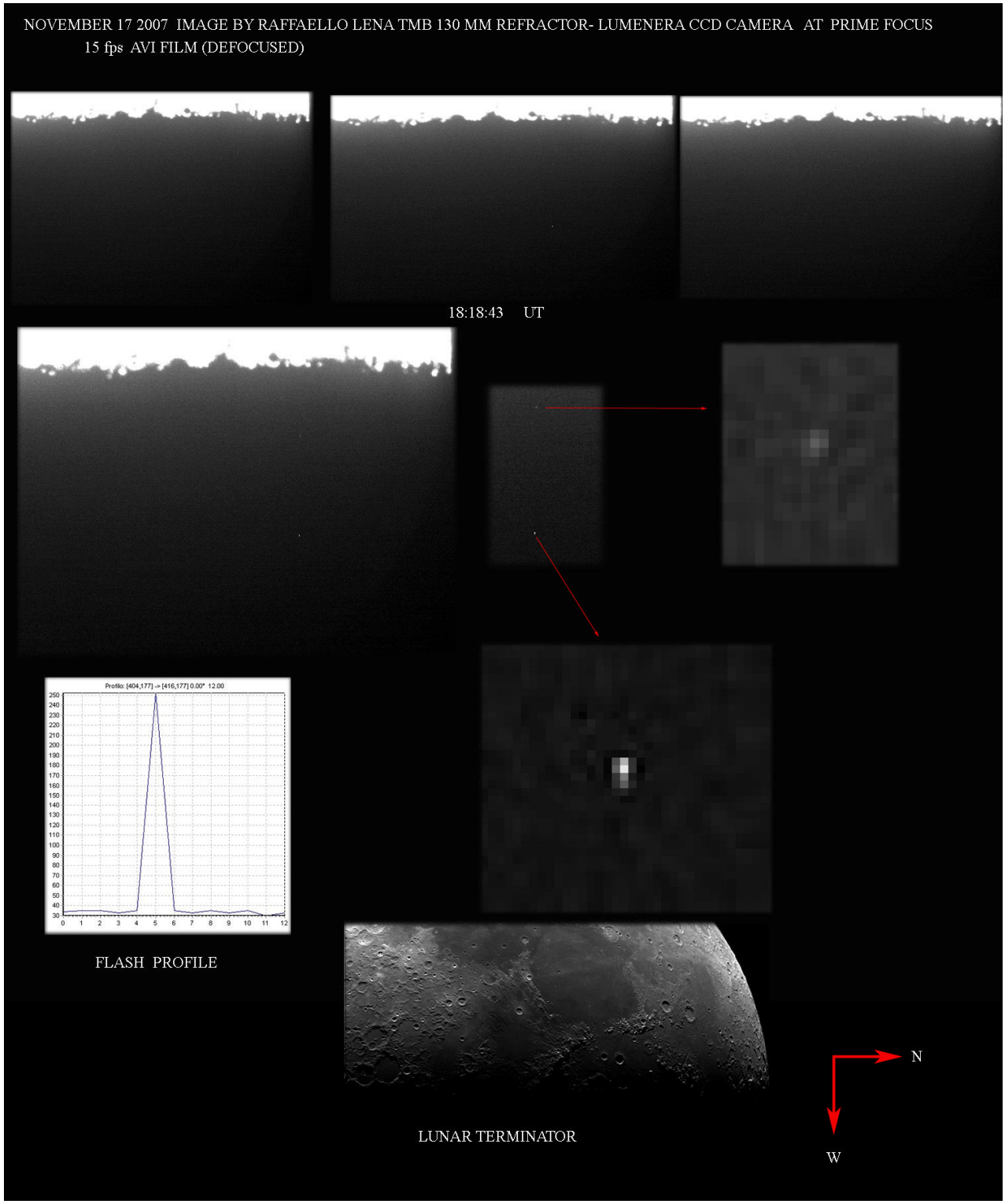
NOVEMBER 17 2007 IMAGE BY RAFFAELLO LENA TMB 130 MM REFRACTOR- LUMENERA CCD CAMERA AT PRIME FOCUS
15 fps AVI FILM (DEFOCUSED)
18:18:43 UT
FLASH PROFILE
LUNAR TERMINATOR
N
W

Figure 15

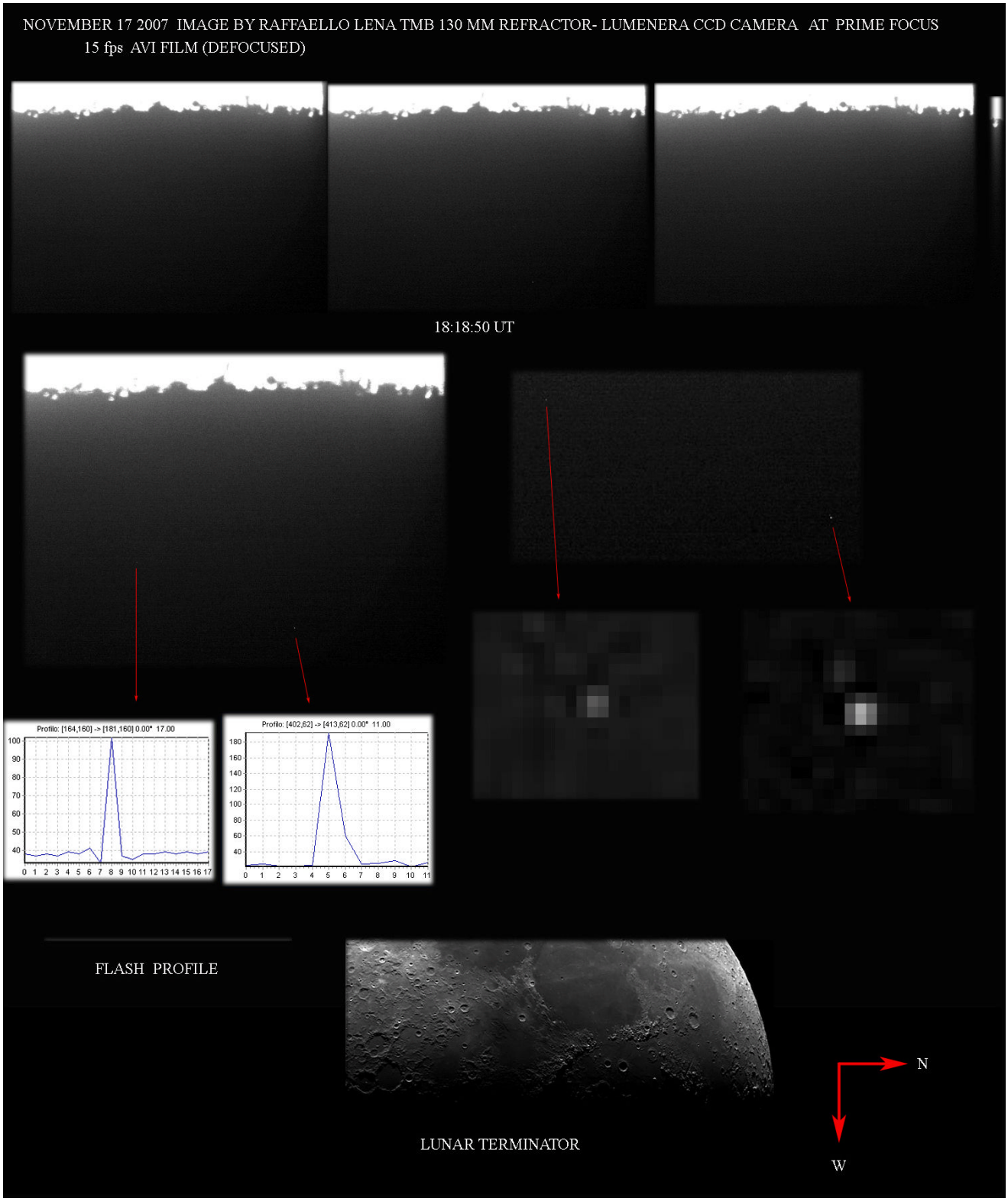
NOVEMBER 17 2007 IMAGE BY RAFFAELLO LENA TMB 130 MM REFRACTOR- LUMENERA CCD CAMERA AT PRIME FOCUS
15 fps AVI FILM (DEFOCUSED)
18:18:50 UT
Profilo: [164,160] -> [181,160] 0.00° 17.00
Profilo: [402,62] -> [413,62] 0.00° 11.00
FLASH PROFILE
LUNAR TERMINATOR
N
W

Figure 16

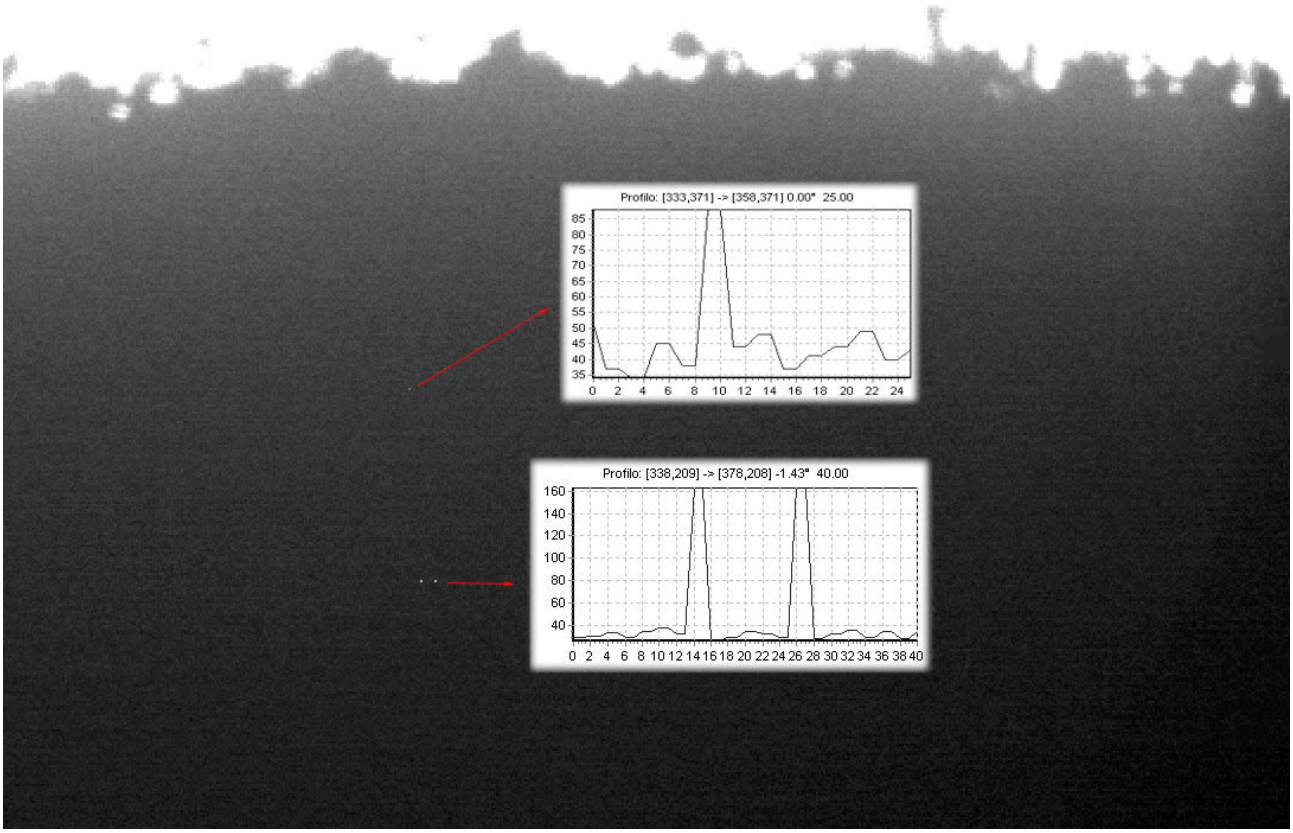
Profilo: [333,371] -> [358,371] 0.00° 25.00
85 80 75 70 65 60 55 50 45 40 35
0 2 4 6 8 10 12 14 16 18 20 22 24
Profilo: [338,209] -> [378,208] -1.43° 40.00
160 140 120 100 80 60 40
0 2 4 6 8 10 12 14 16 18 20 22 24 26 28 30 32 34 36 38 40

Figure 17

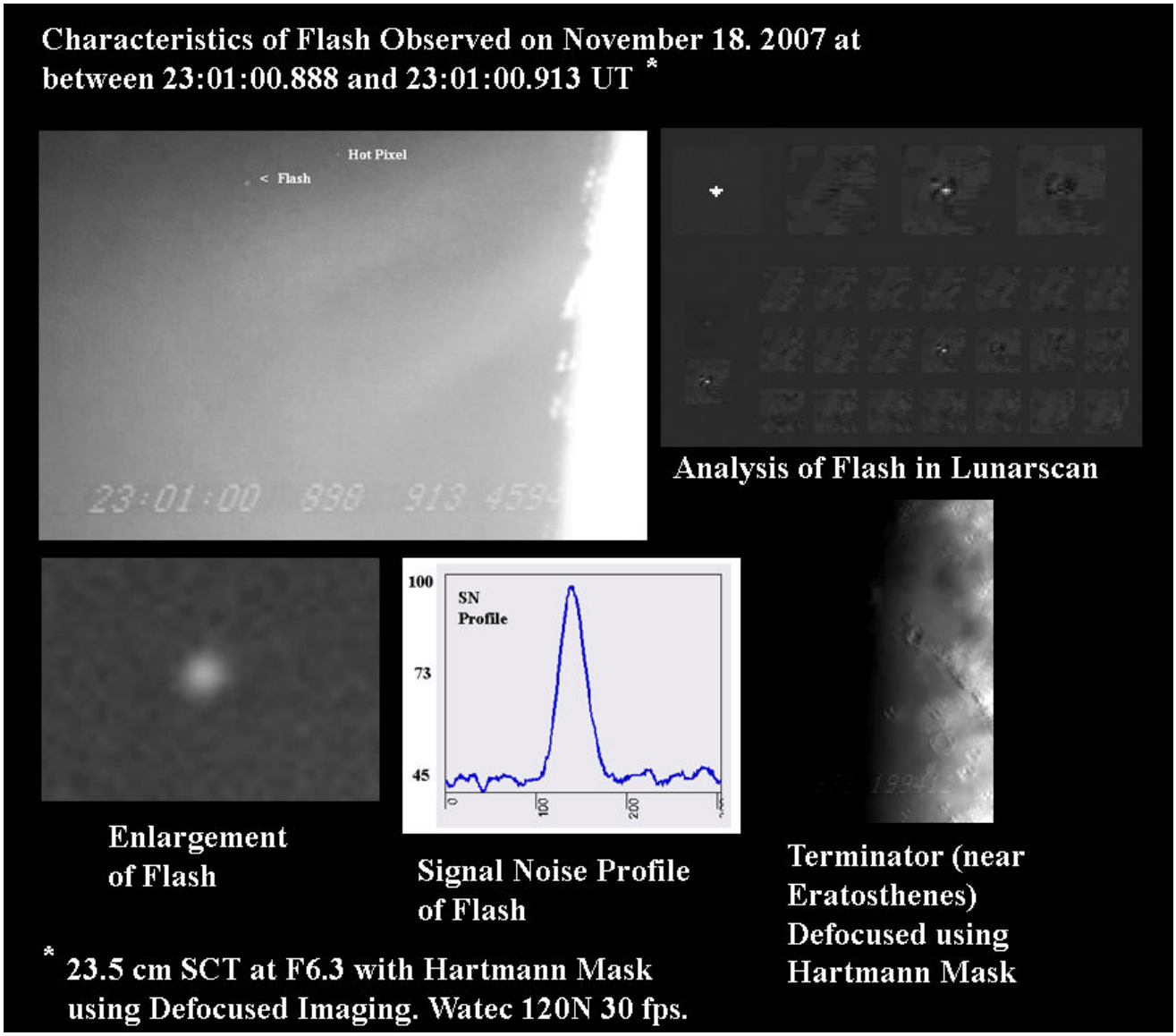
Characteristics of Flash Observed on November 18. 2007 at between 23:01:00.888 and 23:01:00.913 UT *
Hot Pixel
< Flash
23:01:00 898 913
Analysis of Flash in Lunarscan
Enlargement of Flash
100
73
45
SN Profile
0
100
200
Signal Noise Profile of Flash
Terminator (near Eratosthenes) Defocused using Hartmann Mask
* 23.5 cm SCT at F6.3 with Hartmann Mask using Defocused Imaging. Watec 120N 30 fps.

Figure 18

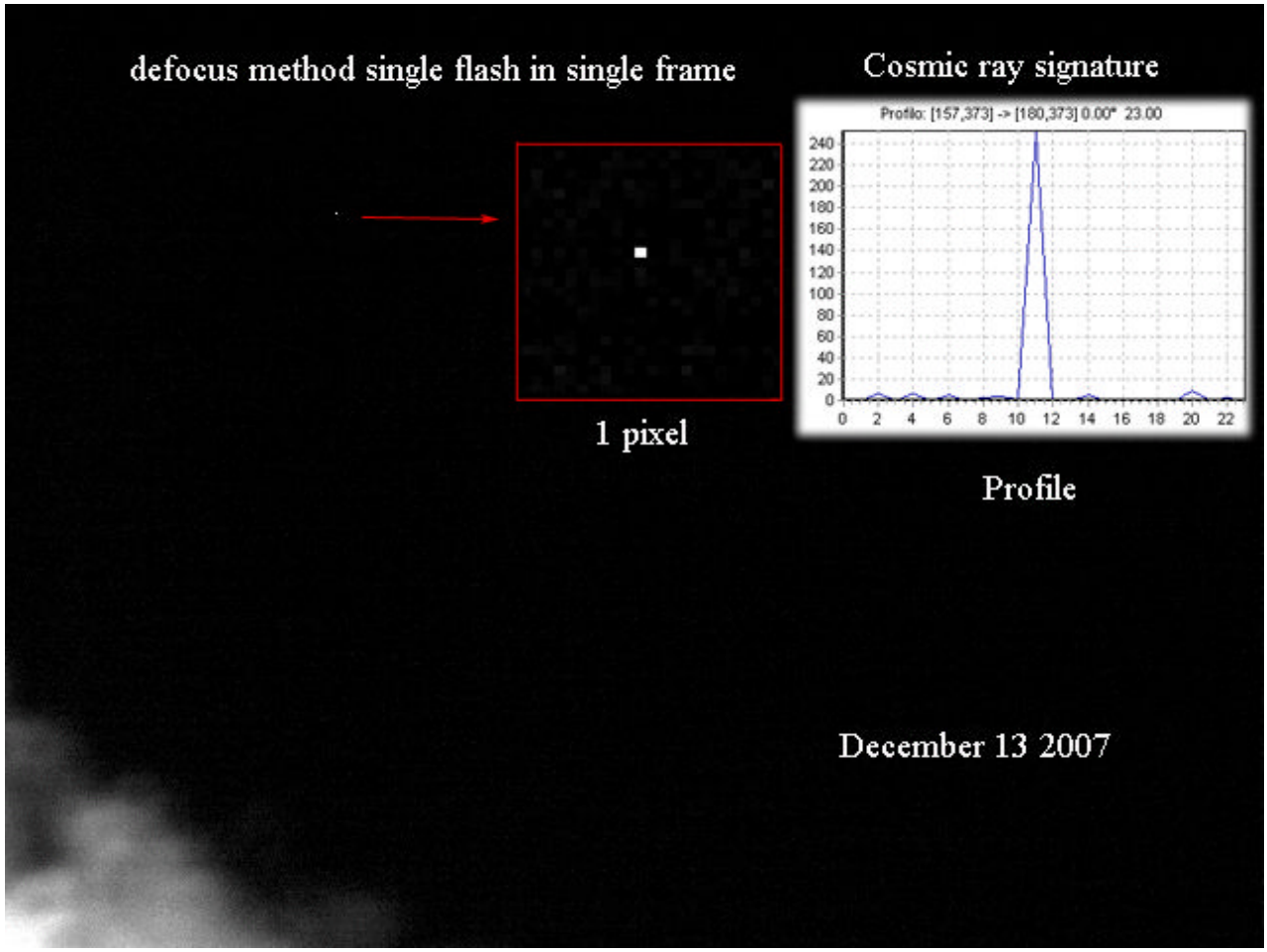
defocus method single flash in single frame
Cosmic ray signature
Profile: [157,373] -> [180,373] 0.00° 23.00
240
220
200
180
160
140
120
100
80
60
40
20
0
0 2 4 6 8 10 12 14 16 18 20 22
1 pixel
Profile
December 13 2007

Figure 19

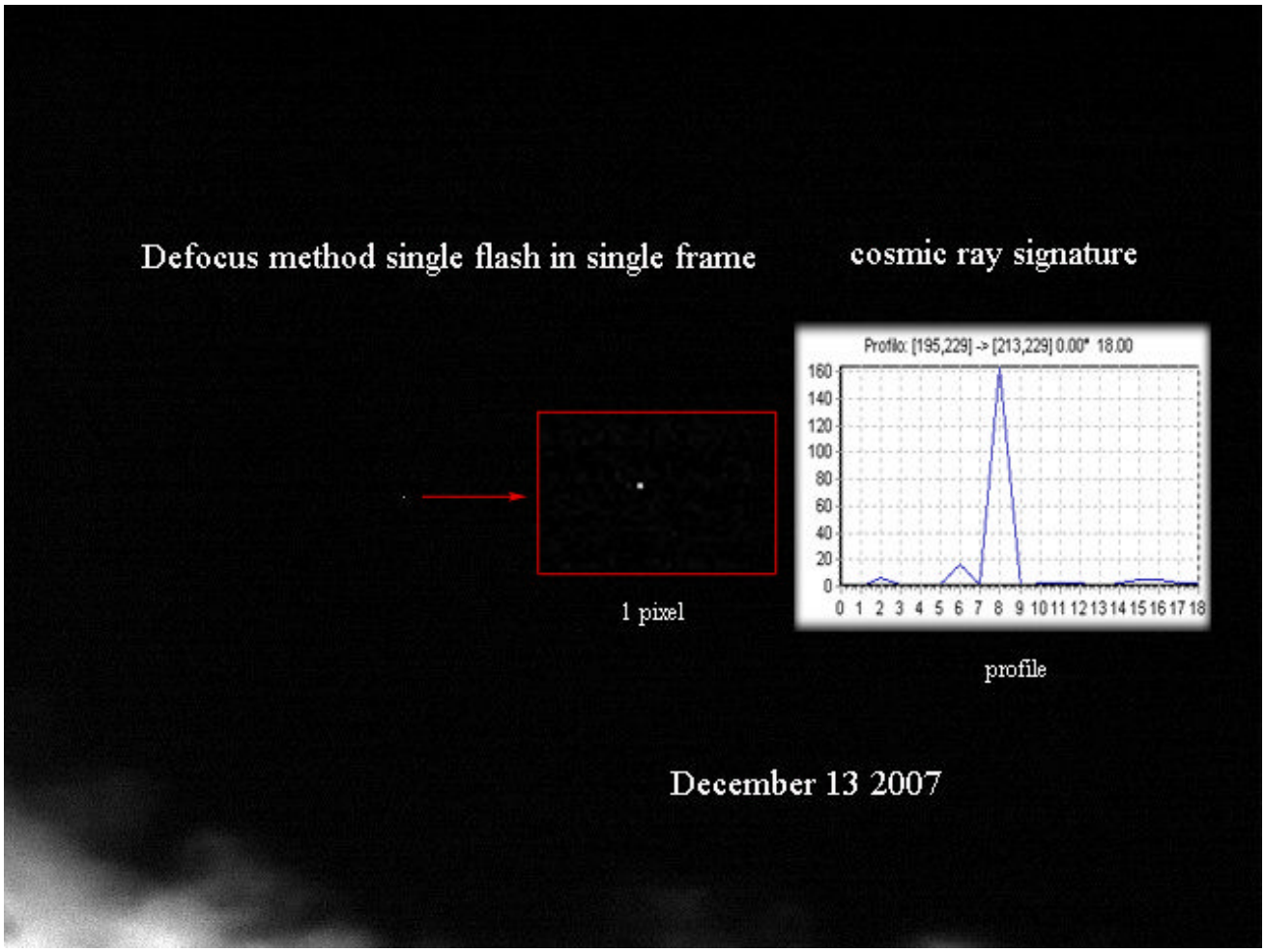
Defocus method single flash in single frame
cosmic ray signature
1 pixel
Profile: [195,229] -> [213,229] 0.00° 18.00
160
140
120
100
80
60
40
20
0
0 1 2 3 4 5 6 7 8 9 10 11 12 13 14 15 16 17 18
profile
December 13 2007

Figure 20

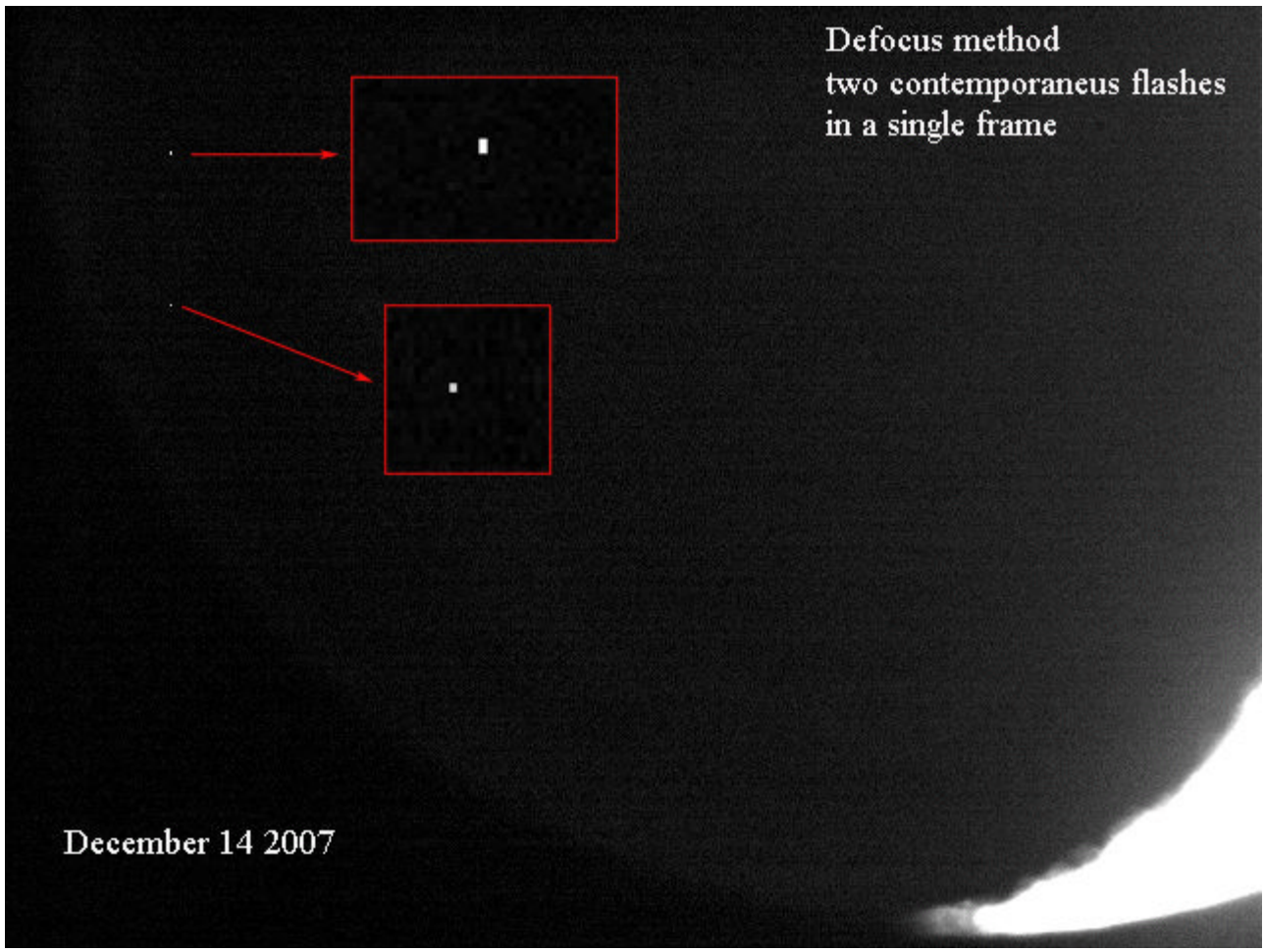
Defocus method
two contemporaneus flashes
in a single frame
December 14 2007

Figure 21

be confirmed as a true impact since it did not appear as a triplet image using the Hartmann mask.

It is therefore presumed to be spurious, possibly due to a cosmic ray.

APPENDIX 3

Detection of cosmic rays signature in Lunar Impact Surveillance by R. Lena (Italy)

GEMINIDS SURVEY: Sessions carried out on December, 13-14, 2007 Rome Italy

With the same procedure described in Appendix 1 and 2, two observing sessions were carried out during the Geminids.

A) December 13, 2007: the telescope used was a 180 mm Maksutov Cassegrain with a Lumenera CCD camera LU 075M used at prime focus with a filter IR blocking. Seeing was estimated as 3/10 and trasparency 2/5. The Lumenera CCD camera was set at 60 fps. The lunar quadrant for acquisition was the north - north west region. The session started at 16:10:10 UT until 16:25:04 UT. The Moon was blocked by dark clouds about 30% of the time. The lunar quadrant imaged was the north-west region.

B) December 14, 2007: the telescope used was a TMB Refractor f/6 diameter 13 cm with a Lumenera CCD camera LU 075M used at prime focus with a filter IR blocking. Seeing was estimated as 3/10 and trasparency 3/5. The Lumenera CCD camera was set at 30 fps. The session started at 16:48:13 UT until 17:52:50 UT.

The acquired frames during two sessions were slightly defocused. A lunar flash will be consequently defocused and will become a disk of comparable diameter. Defocusing will have no consequences on the images of spurious flashes, which will remain limited to a few pixels, thus allowing them to be distinguished from lunar flashes. During the sessions were recorded several bright flashes interpreted as spurious flashes (see Fig. 19-21) because of the presence of faint satellite flashes, recorded in a single frame and of dimension of 1 pixel. Moreover having blurred the image during the acquisition the flashes are very sharp and cover one single pixel in the image which is different with the broad PSF expected from a real impact. These flashes are therefore presumed to be spurious, possibly due to a cosmic ray.

References

[1] CudnikBM, Dunham DW, Palmer DM, et al. (2002) Ground-based observations of high velocity impacts on the moon's surface: The Lunar Leonid phenomena of 1999 and 2001. Lunar and Planetary Science 33 abstract #1329.

[2] Dunham DW, Palmer DM, Sada PV et al. (2000) The first recorded videorecordings of Lunar meteor impacts. Lunar and Planetary Science 31 abstract #1547.

[3] Cudnik BM, Dunham DW, Palmer DM et al. (2003) Ground-based observations of Lunar meteoritic phenomena. Earth, Moon and Planets. 93: 145-161.

[4] Adams MA, Schultz PA, Sugita S et al. (1998) Impact flash spectroscopy as a means to characterize asteroid surface compositions. Lunar and Planetary Science 28 abstract #1796.

[5] Cooke WJ, Suggs RM, Suggs RJ et al. (2007) Rate and distribution of Lunar kilogram impactors. Lunar and Planetary Science 38 abstract #1986.

[6] Ortiz JL, Sada PV, Bellot Rubio, LR et al. (2000) Optical detection of meteoroidal impacts on the moon. Letters to Nature. Nature 405: 921-923.

[7] Ortiz JL, Quesada JA, Aceituno FJ et al. (2002) Observation and interpretation of Leonid impact flashes on the moon in 2001. The Astrophysical Journal. 576: 567-573.

[8] Ortiz JL, Aceituno FJ, Quesada JA et al. (2006) Detection of sporadic impact flashes on the moon: Implications for the luminous efficiency of hypervelocity impacts and derived terrestrial impact rates. Icarus 184: 319-326.

[9] Yanagisawa M, Ohnishi K, Takamura Y et al. (2006) The first confirmed Perseid lunar impact flash. Icarus 182: 489-495.

[10] Sigismondi C and Imponente, G. (2001) The observation of Lunar impacts II. WGN (Journal of the IMO) 1:1-3.

[11] Buratti BJ and Johnson LL (2003) Identification of the lunar flash of 1953 with a fresh crater on the moon's surface. Icarus 161:192-197.

An Anomalous Transit on the Moon

By Alberto Baudà and Maria Teresa Bregante
Geologic Lunar Research (GLR) group

Abstract
In this article we analyze the transit of a "flying object" crossing the moon, recorded by an Italian amateur (A. Mayer from Busto Arsizio). The most reasonable hypothesis is that of a small weather balloon, of the "pilot" type for the study of the atmosphere.

1. Introduction

The transit of a "flying object" crossing the moon, is a rare event. In terms of probability the chance of such an occurrence is about 1 in 700 for each celestial hemisphere. The probability calculated from an object in motion in the air (or in space) is even less. Image analysis suggests that such transits are caused by birds, weather balloons, etc., and as a last resort unidentified flying objects. The description that follows is, in some aspects, an interesting anomaly.

2. The characteristics of the event

An analysis was made of a recording by A. Mayer from Bursto Arsizio (45.60° N, 8.852°, 214 meters elevation) at 19: 52 UT (21:52 local time). For a duration of 1 minute 52 seconds a dark spherical body of diameter ∂ 4.8 arc seconds flew across the moon with a linear trajectory at about a 45 degree angle. The telescope employed was a 20 cm Schmidt Cassegrain on a Meade LXD75 mount, used with eyepiece projection. The AVI film is stored at the link
http://www.youtube.com/watch?v=DIsOiWJ2DVw

The moon had an angular diameter of 29.7 arc minutes and was at a distance of 405000 kilometers from the Earth.
It was located at an altitude of 36° 43' above the horizon with an azimuth of 185° 26'. During the brief 55 second period of observation, the linearly moving object described an arc of 6' 13.6" on the moon with 17.7' due to its own apparent motion.

Therefore the object had crossed an arc of almucantarat (celestial circle drawn from points of equal height on the horizon) of size 6' 13,6"+ 17' 42"= 23' 55,6"
determined by using lunar coordinates.

But this represents relative motion on the moon. During the same time period the moon crossed an arc of around 16.5' and therefore the true angular size of the described arc is
23' 55.6" +16.5'= 24' 12.1"= 0.40336 °= $7.03998 * 10^{-3}$rad

at an angular speed of w= $1.279999 * 10^{-4}$ [rad]/ s. It is of interest that the object crossed an arc of longitude in the opposite direction from 57" toward 55" with relative motion opposite that of the moon. The apparent speed, after the change of trajectory, slows down and increased in altitude by an incalculable quantity. The dark disk was larger than the resolving capability of the instrument and therefore represents a true image (see Figure 1, single shot from the AVI).

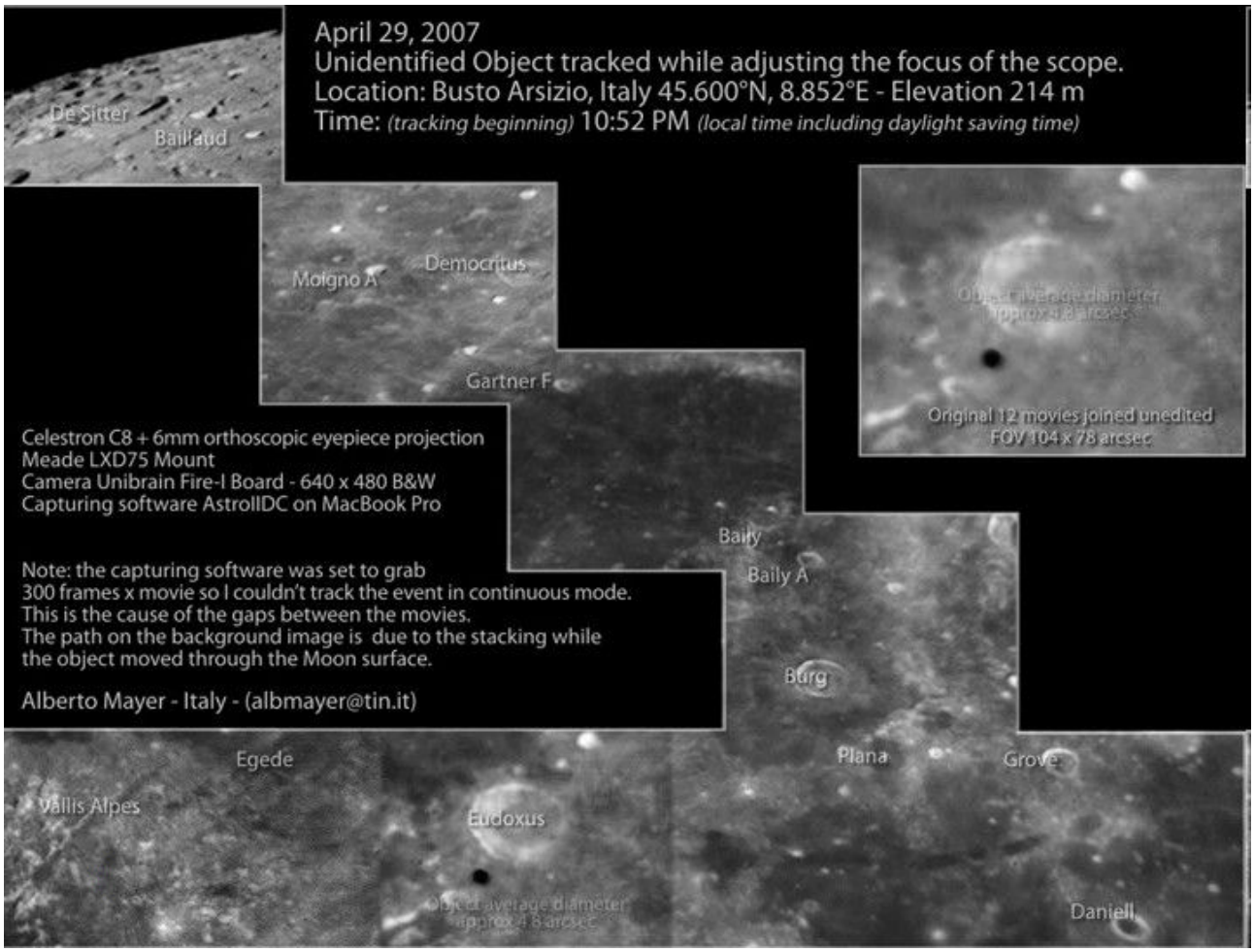
April 29, 2007
Unidentified Object tracked while adjusting the focus of the scope.
Location: Busto Arsizio, Italy 45.600°N, 8.852°E - Elevation 214 m
Time: (tracking beginning) 10:52 PM (local time including daylight saving time)
De Sitter
Baillaud
Moigno A
Democritus
Gartner F
Original 12 movies joined unedited
FOV 104 x 78 arcsec
Celestron C8 + 6mm orthoscopic eyepiece projection
Meade LXD75 Mount
Camera Unibrain Fire-I Board - 640 x 480 B&W
Capturing software AstroIIDC on MacBook Pro
Note: the capturing software was set to grab
300 frames x movie so I couldn't track the event in continuous mode.
This is the cause of the gaps between the movies.
The path on the background image is due to the stacking while
the object moved through the Moon surface.
Alberto Mayer - Italy - (albmayer@tin.it)
Baily
Baily A
Burg
Egede
Vallis Alpes
Eudoxus
Plana
Grove
Daniell

Figure 1

3. Object Exclusions

The first deals with trajectory, horizontal, which indicates a motion of length of 6' 13" in 55 s.
This corresponds to an angular speed of w= 3,29311* 10^{-5} [rad]/ s. A supposed satellite of the earth would have a period of T revolution in correspondence of the value of w:

$$T=2*\pi*(R+H)/vc$$

where:
R is the ray of the earth;
H the height from the terrestrial surface;
Vc the speed on circular orbit to the H. height
Since:
T= p/ w* 3600= 13.635 h

The H height can then draw from the relationship:

$$T=2*\pi*(R+H)/(G*M)/(R+H)^{0,5}$$

where:

G is the gravitational constant;
M the mass of the Earth;
R the ray middle earthling.

The altitude would be nearly 22,608 km. At this distance and a diameter of 4.8 arc sec, this would correspond to a size of 520 meters.
This would be a really large object, such as an asteroid. Besides the absolutely dark color indicates the absence of solar illumination, which, in those circumstances, should have had a height of over 400 km (diagrams of D. KING-HELE, Observing Earth Satellites, Van Nostrand Reinhold Company, pag.48). A body in motion at less than 400 km altitude would be most likely be fairly close to the terrestrial surface. Besides the form of the disk and the absence of lights makes it improbable that the object was an airplane or a bird in flight.

4. The Foundation of a Hypothesis
The more probable hypothesis is that of a neoprene balloon, also in relationship to the type of motion which is compatible with the action of the wind. In fact the variation of speed and trajectory is attributable to ascensional convective current. Considering a H= 11,000 km and, therefore, neglecting the terrestrial curvature, this gives a distance from the observer of L= 18,400 km. In relationship to the height of the moon above the local horizon, this allows the calculation of the true maximum diameter of the neoprene balloon using trigonometry:

$$DR = 2 * tang(\partial/2) * L = 0.43 m$$

As compared to the values of 1.8-2 m of those usually in production, which can inflate to a volume almost triple the originalsize. The true speed would be then:

v= 1,27999* 10^{-4}* L= 2.36 m/ s which is much reduced.

Smaller values would make the values of DR excessively reduced: for instance for H= 3000 m would be had DR= 0.12 m. It would then be necessary to hypothesize a value of

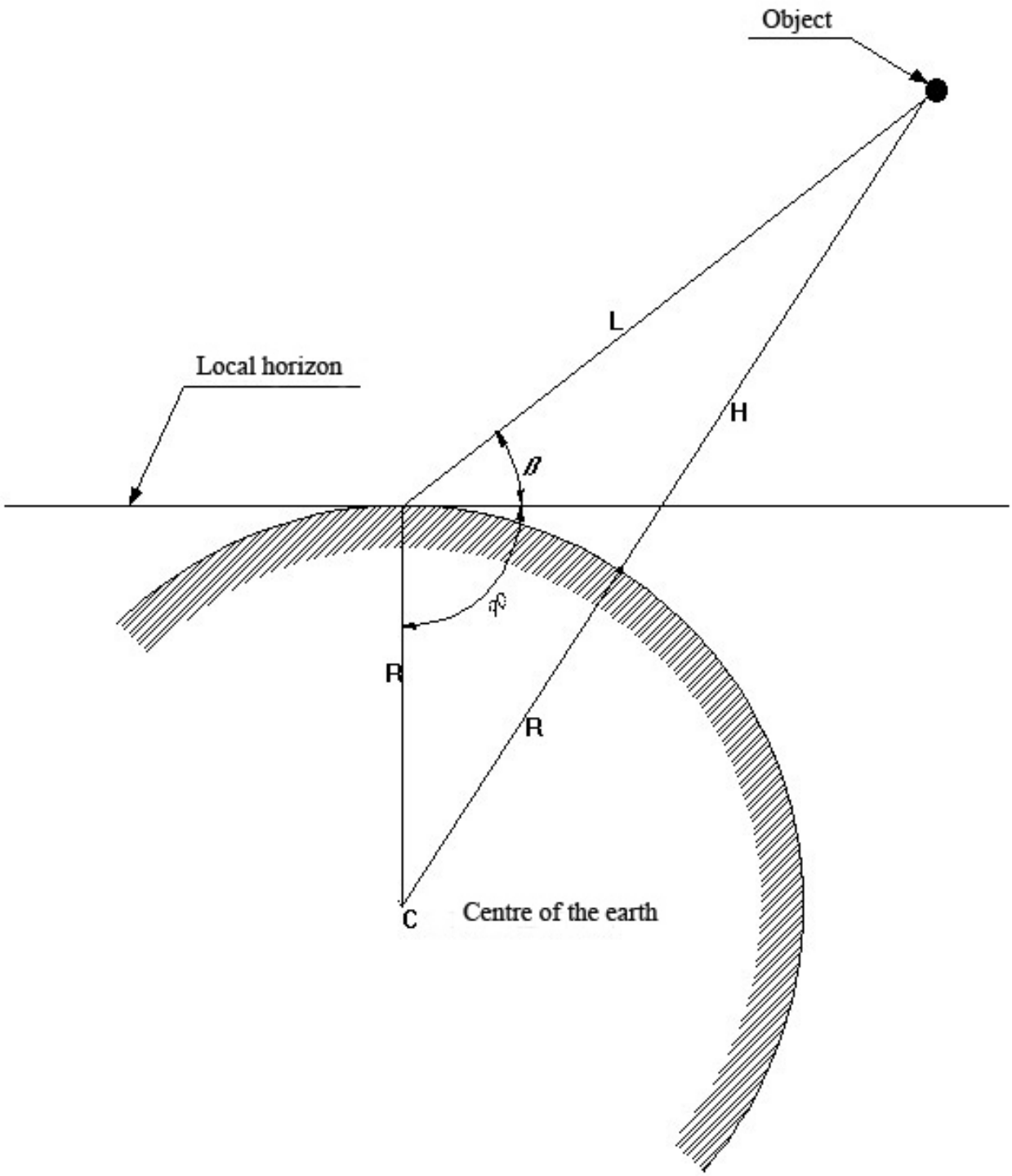

Figure 2

superior tangency to that normally reached to justify a reasonable diameter. Remember that the adiabatic value of tangency, which is not realistic for production of gas by heat, is better than an isothermal value. Besides the loss of useful load and favourable meteo-climatic conditions could have sensibly increased the value of true tangency.
Also, the maximum value depends on the difference between the densities of the air and of the gas to the values at lift-off, and are more favourable to summer temperatures, like those of the period of observation. In such a hypothesis the curvature of the terrestrial surface is not negligible. With reference to fig.2 it is possible using trigonometry to solve the triangles and verify the results through the relationship:

$$[\cos] (90° + ß) = (R^2 + L^2 - (R^2 + H^2) / (2 * R * L)$$

taken from a “satellite tracking” by S.MACKO, RIDER Publisher.

In the Table 1 has brought again the obtained data

Table 1

H (km)	L (km)	DR (m)
11	18,510	0,43
12	20,190	0,47
13	21,869	0,51
14	23,548	0,55
15	25,226	0,59
16	26,904	0,62
17	28,581	0,66
18	30,258	0.70

It is therefore reasonable to suppose an altitude of about at 18 km, reached in favourable conditions. An inclusive value between the maximum attainable adiabatic and the value of saturation. Probably the balloon, to any hours from the launch, had already lost some gas, a factor that could justifiably cause a reduction in volume. Balloons for children, on the other hand, could have a similar dimension but they don't reach those values of expansion and are not dark, but have better transparency.

5. Other hypothesis

The hypothesis of the balloon, therefore, would make reduced speeds justifiable but not a reduction in dimensions (Figures 3 and 4). The hypothesis would be of the stratospheric balloon or other balloon, that would can hypothetically reach values of 40 km altitude. But this is not probable: these balloons don't present a form so regularly spherical and their dimension is not compatible with the reduced angular diameter of the observed object.
The possibility also exists, as already mentioned, of a “night time” bird in linear flight (static gliding) at reduced speed. However, the expected dimensions would not cause a profile as perfectly round as the object against the lunar background and a motion of around 2000 m would make his real dimension too small :
L= 5,053 m, DR= 11,75 [cm].

6. Conclusion

The most reasonable hypothesis is that of a small weather balloon, of the "pilot" type for the study of the atmosphere.

These can have diameters that are much reduced relative to the value of tangency, respectably at between 11 and 18 km, given a series of favourable circumstances and meteo-climatic conditions that are particularly favourable.

.

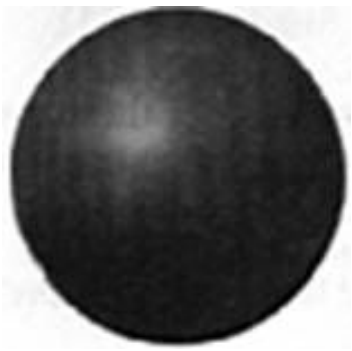

Figure 3: colour and shape of a neoprene balloon

Figure 4: a stratospheric balloon

Original AVI LINK

Report of an unlisted dome in Sinus Roris

by Jim Phillips and Raffaello Lena
Geologic Lunar Researches (GLR) group

Abstract
In this study we describe a previously unreported dome with a diameter of 20 km. It is located at coordinates 55.05° W and 50.52° N. The dome appears in the old image by Kuiper, but it has not been recognized as such. This dome, for its large dimension, and morphology could be interpreted as an intrusive swell, e.g laccolith.

1. Introduction

The GLR (Geologic Lunar Researches) Group is an International organization of amateur astronomers interested in conducting scientific studies of our Moon. Members of the GLR work together in a team effort. An area of prime interest for GLR is the study of lunar domes, including but not limited to, mapping, classification, and the identification of unlisted domes in ALPO catalogue and USGS geologic maps. This report describes an unlisted dome in Sinus Roris (The Bay of Dew) with preliminary data.

2. Observations and digital images

The image shown in Fig.1 of the approximately 20 km diameter dome was obtained by Phillips using a TMB 8" F/9 @ F/54 using a Skynyx 2.0 camera set on monochrome mode at 4:02-4:04 UT September 24, 2007 (solar altitude of 2.83°, solar azimuth 94.39° and colongitude 60.24°). The dome is located at longitude 55.05° W and latitude 50.52° N (ξ = -0.5211, η = +0.7718). The local solar altitude, azimuth and the Sun's selenographic colongitude, along the coordinates, were calculated using the LTVT software package by Mosher and Bondo (2006). It is, to our knowledge, previously unreported by any lunar dome survey.

In the images proposed as Figures 1 and 2, the shading on its antisolar slope is not black, indicating that the slope is of low inclination. Preliminary estimations indicate a diameter of about 20 km because the outline of the dome is not well-defined.
Figure 3 displays Lunar Orbiter frame IV-63-H3, where the dome is not recognisable for high solar angle (the frame covers half of the dome surface). In this image, an impact crater (feature A) on the dome surface is visible and it is filled with black shadow which supports our interpretation that is of impact origin. Looking at photographic lunar atlases published in the past, the dome could not be found on the Consolidated Lunar Atlas but, was found on a few plates from Kuiper's Photographic Lunar Atlas published in 1960 (fig. 4).

The dome appears indeed in the old image by Kuiper, but it has not been recognized as such. The Kuiper's Photographic Lunar Atlas is composed of the very best lunar photos taken at the top Observatories around the world in the first half of the 20th Century. It was meant to replace the Atlas by Julius Schmidt drawn with his 6.2" refractor and

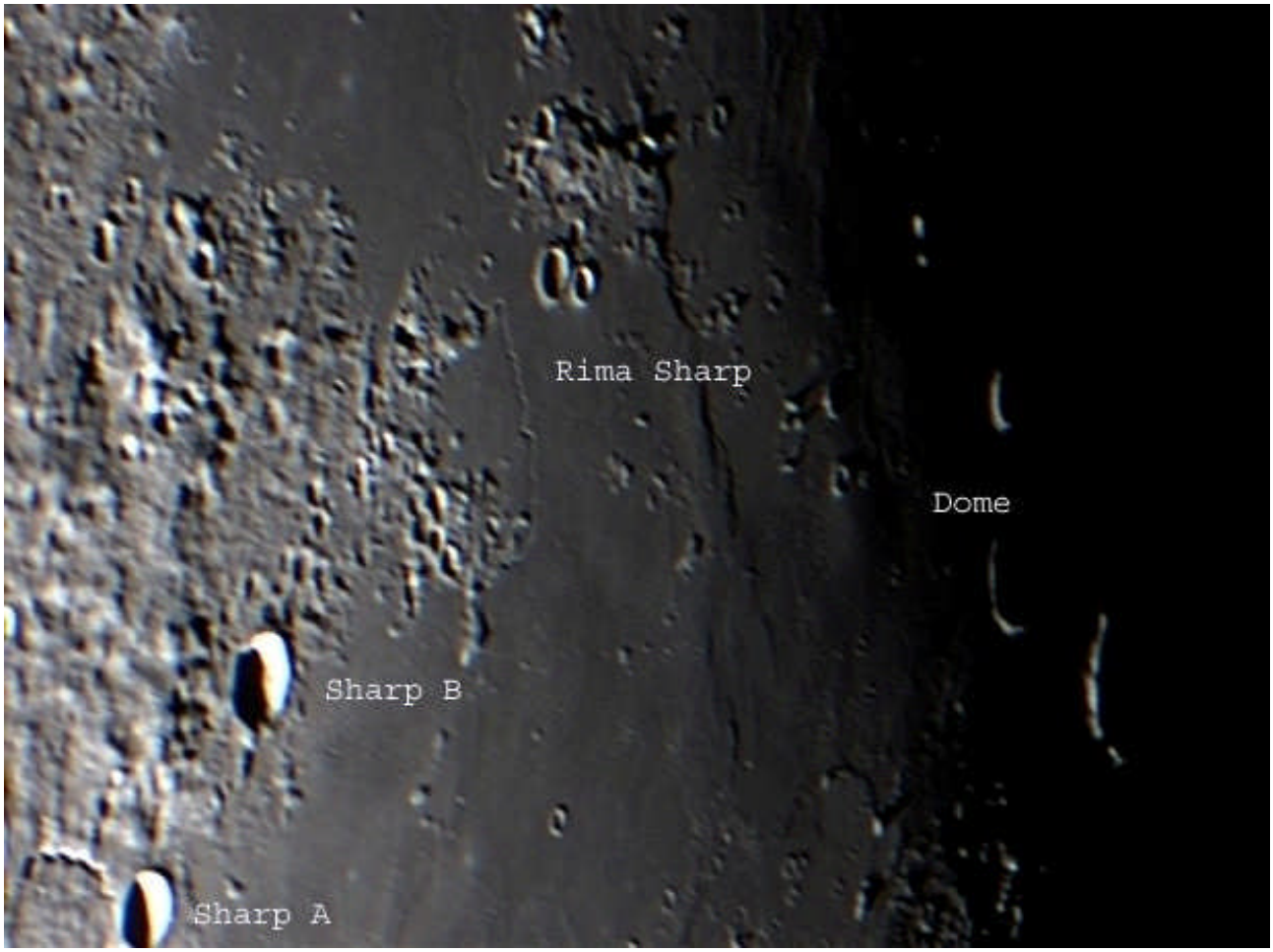

Figure 1

Figure 2

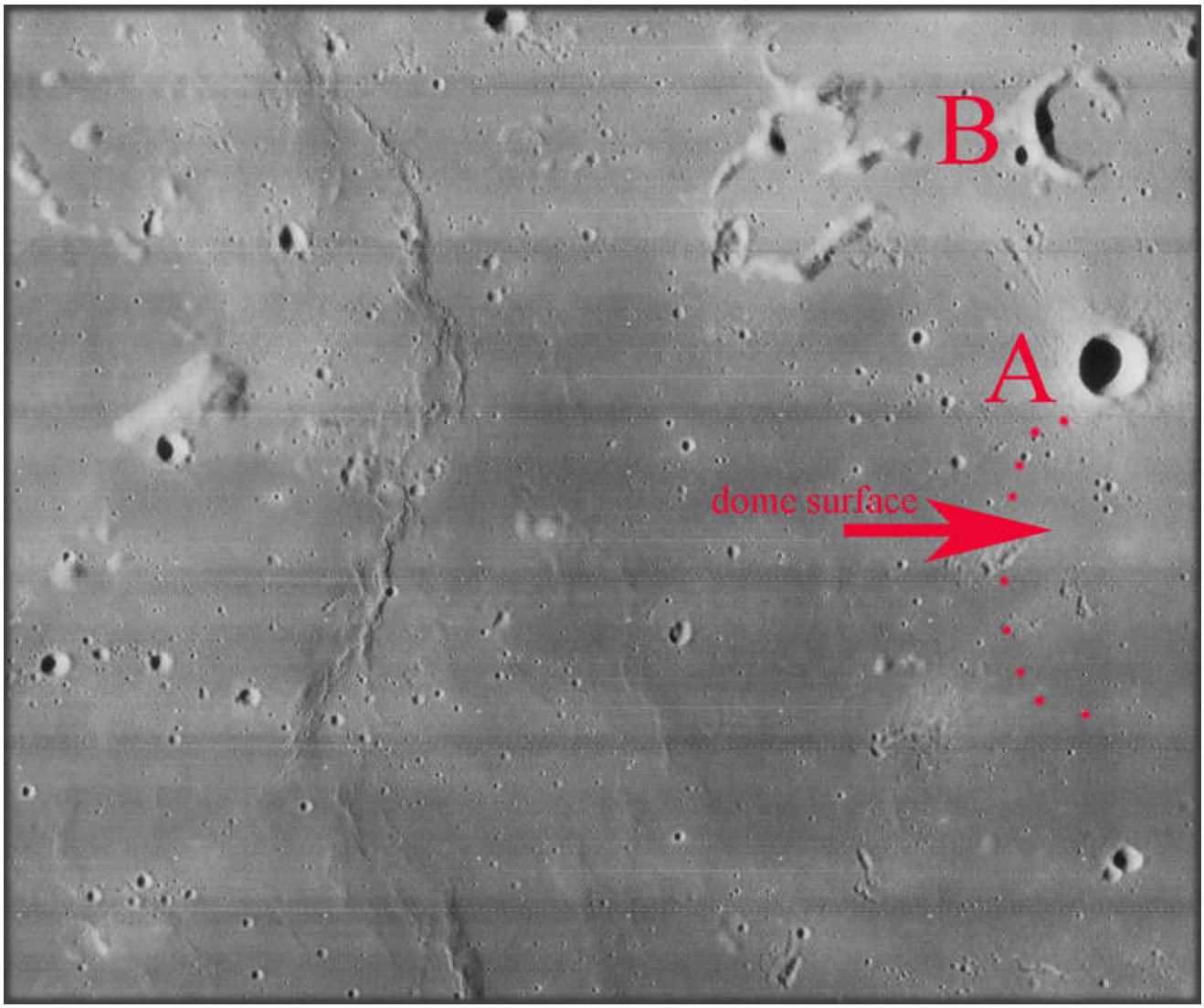

Figure 3

Figure 4

published in 1878! "The best resolution obtained is about 0.4" ... This matches the resolving power of an 11-inch visual telescope used under perfect conditions. This aperture may be compared with the 6-inch used by J. Schmidt in his great map published in 1878, a map that has not been exceeded in general usefulness..."(G. Kuiper 1960). Kuiper states later in the Introduction that "...only a small fraction of the photographs have as high a resolving power as 0.4.. Values between 0.6" and 1.0" are more common".

3. Discussion

The dome in Sinus Roris is located in a lunar area (50.52º N and 55.05° W) not included in the Geologic map of the Rumker quadrangle of the Moon (Scott and Eggleton, 1973, I- 805) and in the Geologic map of J. Herschel quadrangle of the Moon (Ulrich, 1969 I-604). In fact the USGS maps I-805 and I -604 cover only the region comprised from 48° N 50-60°W and from 50°N 50°W respectively.

Furthermore, in the ALPO catalogue the closest object is located at different coordinates of 46.64° W and 49.73°N (ξ = -0.470 η = +0.763) with a reported diameter of 9 km, which is significantly different from our data, not only for coordinates, but also for the diameter. Sinus Roris trough is concentric with both the Imbrium and Procellarum basins and contains generally bright and thin mare materials of different spectral classes from most of Oceanus Procellarum but similar to some of the older units in the adjacent part of northern Mare Imbrium (Wilhelms, 1987). The dome extends in a region of so called *Sharp lavas*, the younger and darker, close to the *Telemann lavas* (rough and bright) and ejecta from Harpalus crater. These several units, along the features, are visible in Clementine imagery. Figure 5 shows a high resolution image from Clementine, while Figure 6 displays the Clementine color ratio image (compare Fig. 3 with Figs. 5-6).

Different albedo distribution is also visible in Fig. 7, a high resolution image taken at 750 nm from Clementine.
The albedo distribution is non-uniform across the dome surface, such that single-image photoclinometry yields inaccurate results.

A second image acquired under different illumination conditions would allow to apply the ratio image based method described by Lena et al. (2006). This dome, for its large dimension , morphology and possibly low slope could be interpreted as an intrusive swell, e.g laccolith. In this scenario rising lavas accumulate within the lunar crust increasing in pressure slowly, causing the crustal rock above it to bow-outward. This creates a structure of low positive relief without ever necessarily having external eruptions.

4. Conclusion

In this study we have described a previously unreported dome with a diameter of 20 km. It is located at coordinates 55.05° W and 50.52º N. Future work will include an extension of our analysis with new images which brings us closer to understanding the morphometric properties of this dome, allowing a measurement of slope and height.

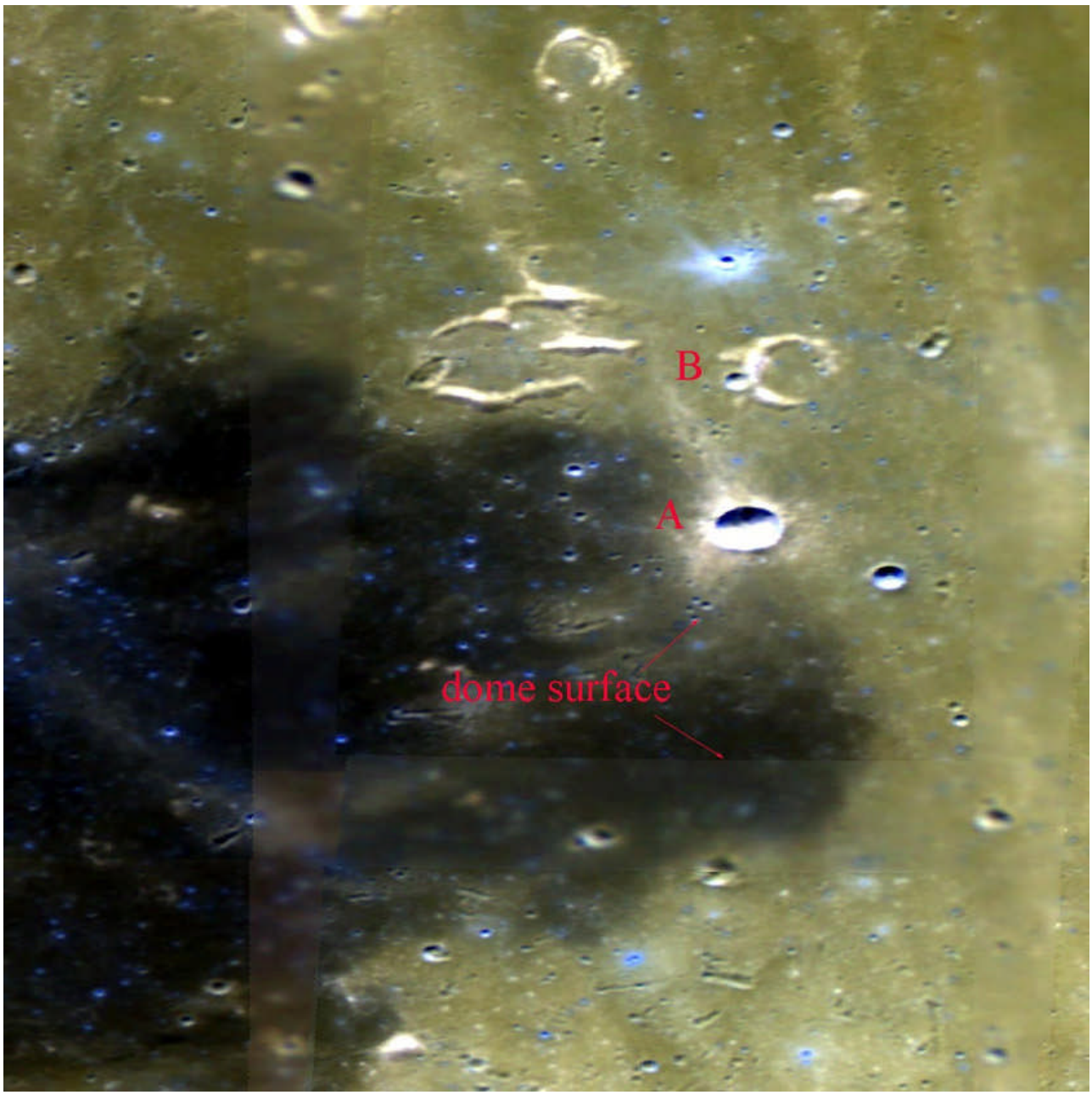

Figure 5

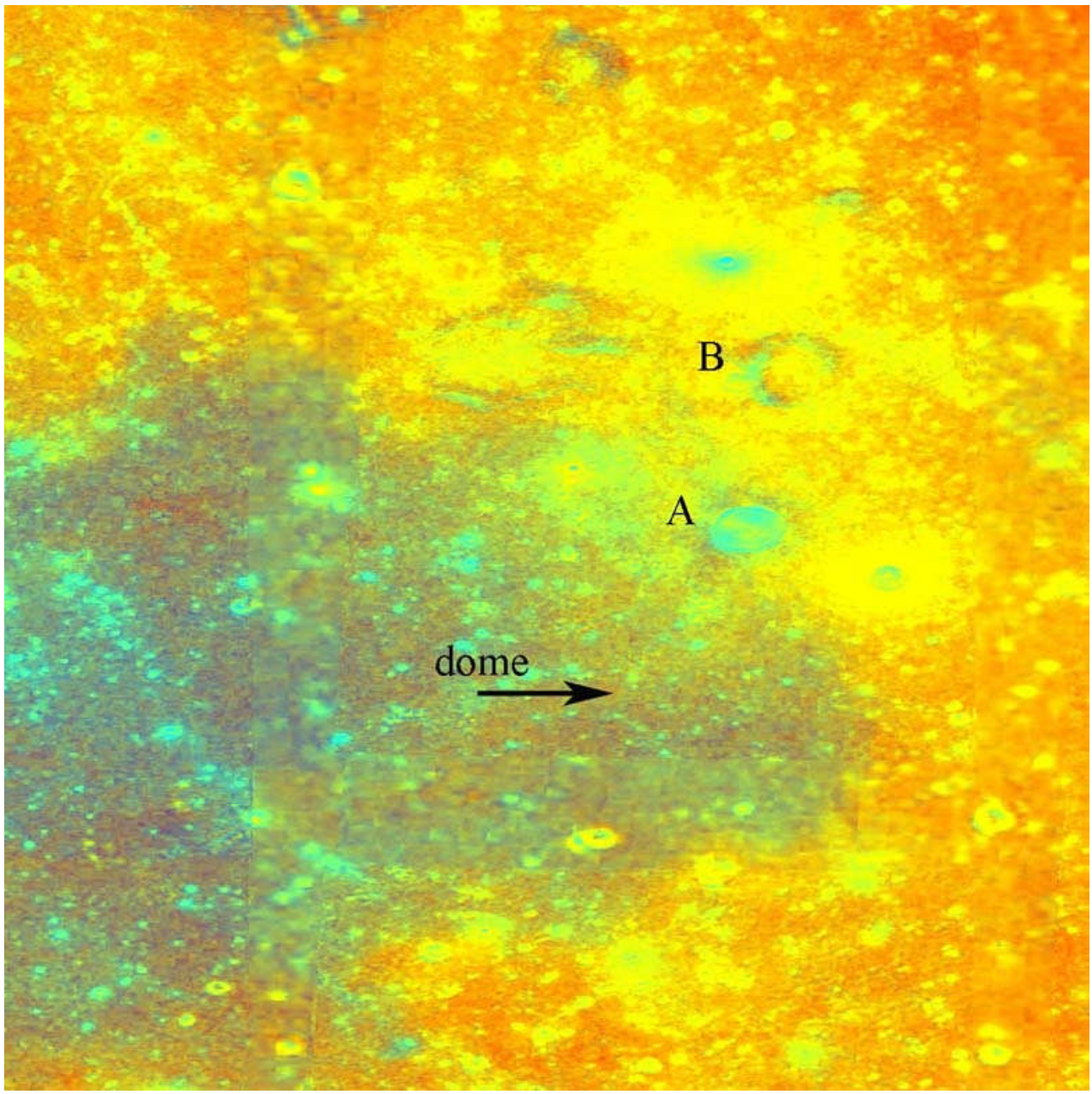

Figure 6

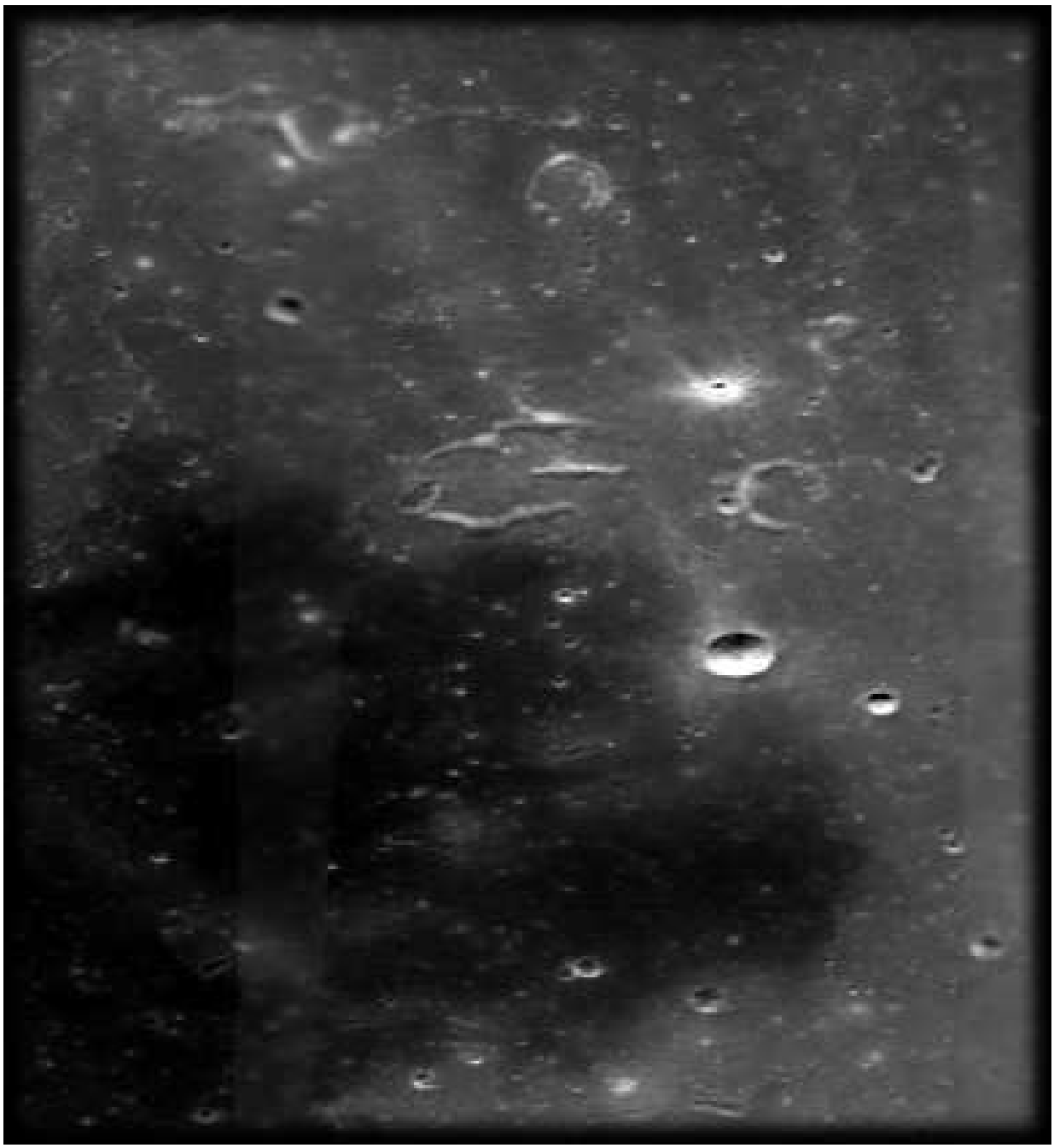

Figure 7

Acknowledgements: We wish to thank C. Wöhler and M.T. Bregante for their stimulating discussion and suggestions.

References

[1] Kuiper, G. P., PHOTOGRAPHIC LUNAR ATLAS, based on photographs taken at the Mount Wilson, Lick, Pic du Midi,McDonald and Yerkes observatories. Edited by G. P. Kuiper with the collaboration of D.W.G. Arthur, E. Moore, J.W. Tapscott and E.A. Whitaker 1960. University of Chicago Press.

[2] Lena, R., Wöhler, C., Bregante, M.T., Fattinnanzi, C., 2006. A combined morphometric and spectrophotometric study of the complex lunar volcanic region in the south of Petavius, JRASC 100(1), 14-25.

[3] Mosher, J., Bondo, H., 2006. Lunar Terminator Visualization Tool (LTVT). http://inet.uni2.dk/ d120588/henrik/jim ltvt.html

[4] Scott and Eggleton, 1973. USGS I- 805 http://www.lpi.usra.edu/resources/mapcatalog/usgs/I805/72dpi.jpg

[5] Ulrich, 1969. USGS I-604 http://www.lpi.usra.edu/resources/mapcatalog/usgs/I604/72dpi.jpg

[6] Wilhelms, D.,1987. The Geologic History of the Moon.
USGS Prof.Paper1348.

Dionysius West Wall Spectra Using Multiple Interference Filters and Processing in LTVT and ImageJ

By Richard Evans
Geologic Lunar Research (GLR) Group

Abstract
The purpose of this paper is to demonstrate a simple technique by which visible and infrared spectra of lunar features can be obtained using a small telescope, multiple interference filters, and two cameras. Image Calibration and co-registration are achieved using free software and the resulting image set is used to produce relative reflectance vs wavelength plots for lunar features of interest. The absorption trough near 1000 nm is analyzed. The west wall of Dionysius was studied. This western region within the crater wall has no visible superficial basaltic deposits (which can be seen easily in other areas of the rim). Small telescope reflectance spectra were compared with Clementine UVVIS and NIR reflectance spectra.

1. Introduction

Spectra of the west wall of Dionysius (2.8 degrees latitude, 17.15 degrees longitude) and the Apollo 16 landing site (-9.0 degrees latitude, 15.6 degrees longitude) were obtained with a 9.25 inch (23.5 cm) Schmidt Cassegrain telescope using a set of 73 interference filters between 500 nm and 1600 nm. The filters were in 10 nm increments below 1000 nm, 20 nm increments between 1000nm and 1300 nm, and in 100 nm increments above 1300 nm. Two cameras were necessary to cover the wavelength range. A Lumenera 075M was used from 500 nm to 1064 nm and a Goodrich Sensors Unlimited Su320-MX was used from 990nm to 1600 nm. Each image was divided by the average greyscale value of the Apollo 16 site present in that image, and then multiplied by the directional hemispheric reflectance of Apollo 16 speciman 62231 (Pieters, 1999). Images calibrated in this way were multiplied by 5 to achieve adequate visualization and converted to 8 bit TIFF format in ImageJ. Images from each camera were initially co-registered as separate image sets using BlinkComparator. These two image sets were then co-registered into a single image set using the program LTVT and cropped. They were then imported into ImageJ as an 8 bit greyscale image sequence and a group of pixels was boxed for the lunar feature of interest. The histogram of the pixel box was examined and the average greyscale reflectance value and standard deviation were recorded for each wavelength image. Resulting data was then divided by 255 to ensure uniformity of the reflectance scale and a plot of relative reflectance versus wavelength was created which included the standard deviation at each wavelength. Analysis of this plot yielded information about the characteristics of the absorption trough near 1000 nm. Results were compared to those obtained using Clementine UVVIS and NIR reflectance data. Clementine spectral data were obtained using ISIS 2.0 (a free Linux based software package maintained by the USGS) from archived .cub image files.

NIR data in .cub format can be

downloaded from http://astrogeology.usgs.gov/Projects/ClementineNIR/. UVVIS data in .cub format can be downloaded from http://ser.sese.asu.edu/MOON/clem_color.html.

2.Methodology

On August 30, 2007 at 02:00 UT a series of images of the Descartes/Cayley plains region (Giguere, 2005) were obtained using a 9.25 inch (23.5 cm) F10 Schmidt Cassegrain telescope and a series of 74 interference filters at increments described above. A Lumenera 075M was used to record images from 500 nm to 1064 nm and a Goodrich Sensors Unlimited Su320-MX camera was used to record images from 990 nm to 1600 nm. Images were converted to 8 bit TIFF format and calibration was achieved by Apollo 16 site division and Apollo 16 speciman 62231 multiplication as described above. Image sets from each camera were initially co-registered separately using BlinkComparator. Images from both cameras were then imported into LTVT where they were co-registered to produce a single combined image set. The image sequence was imported into ImageJ and cropped. The west wall of Dionysius centered at 2.8 degrees latitude and 17.15 degrees longitude was studied. A box of 8 x 8 pixels at 1350 meters/pixel resolution was defined and the average greyscale reflectance value and the standard deviation for the pixel group was determined for each wavelength using the histogram function in ImageJ. Results were divided by 255 to insure uniformity of the reflectance scale. Data points with excessive standard deviation represented data from underexposed images and were excluded from the data set. Spline smoothing of the resulting data set was performed in TableCurve2D and a continuum line tangent to the curve from roughly 750 nm to 1250 nm was defined. Continuum division of the reflectance data by this tangent line was performed to enable study of the mafic absorption trough near 1000 nm. Finally, results were compared to a reflectance plot made from Clementine UVVIS and NIR data for approximately the same area of the west wall of Dionysius. The area of sampling was centered at 2.8 degrees latitude and 17.15 degrees longitude. The pixel area sampled was 21 x 21 pixels at 500 meters per pixel resolution. Trough parameters were calculated after spline smoothing of the data and division by a continuum line taken through 779 nm and 1143 nm. Clementine UVVIS and NIR data were obtained from archived .cub files using ISIS 2.0, a free Linux based program maintained by the USGS (see http://isis.astrogeology.usgs.gov/documents/Isis2UserDocs/index.html).

3.Results

Spectra for the west wall of Dionysius and of Theon Junior are presented below.

West Wall of Dionysius

Figure 1, courtesy of the USGS map-a-planet website (http://pdsmaps.wr.usgs.gov/PDS/public/explorer/html/moonpick.htm) shows Dionysius with a superimposed grid to enable visualization of the west wall area studied at 2.8 degrees latitude and 17.15 degrees longitude. Figure 2 shows the relative reflectance vs wavelength plot for the west wall of Dionysius while figures 3 and 4 respectively show the spline smoothed reflectance plot with

Figure 1

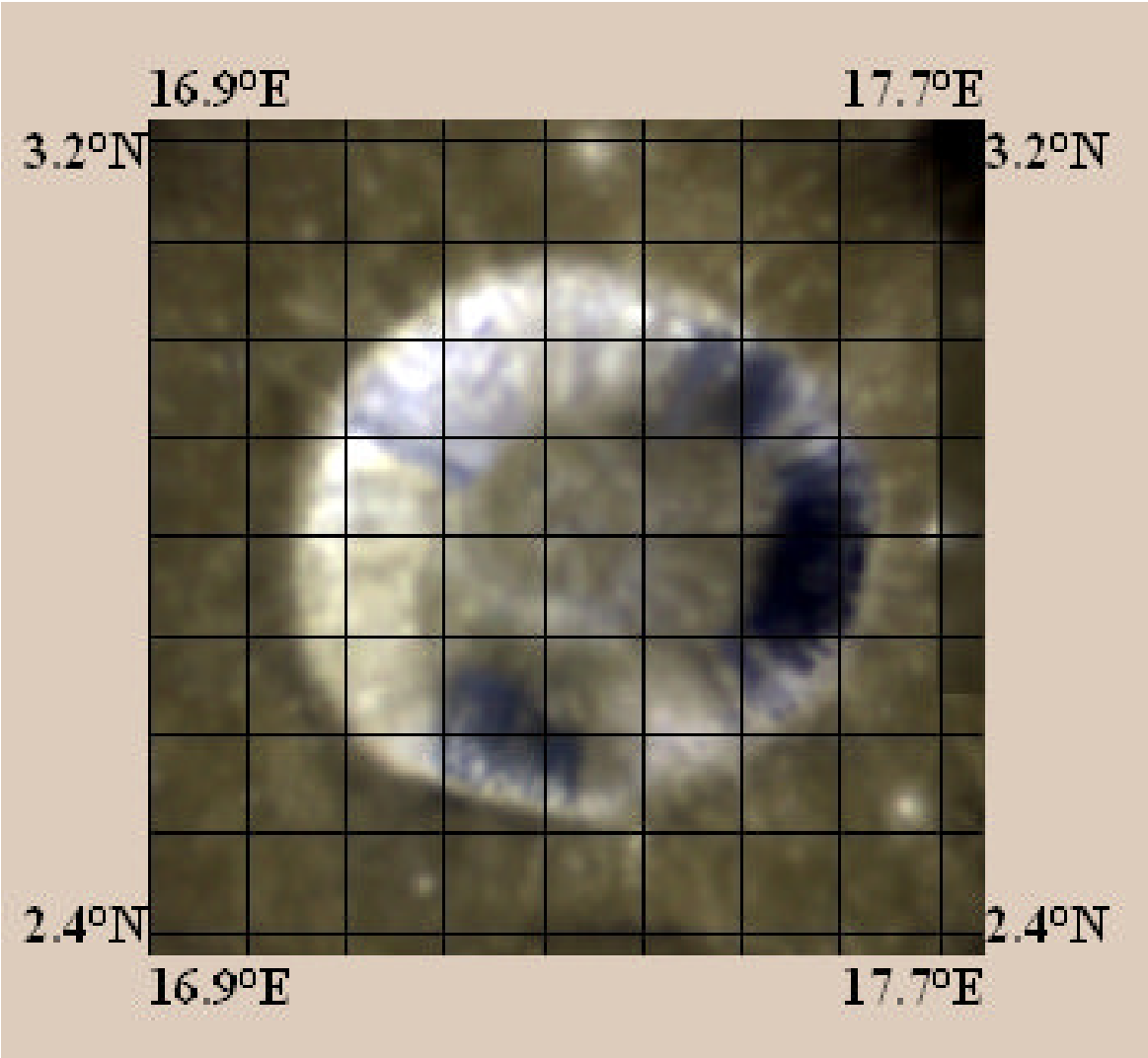

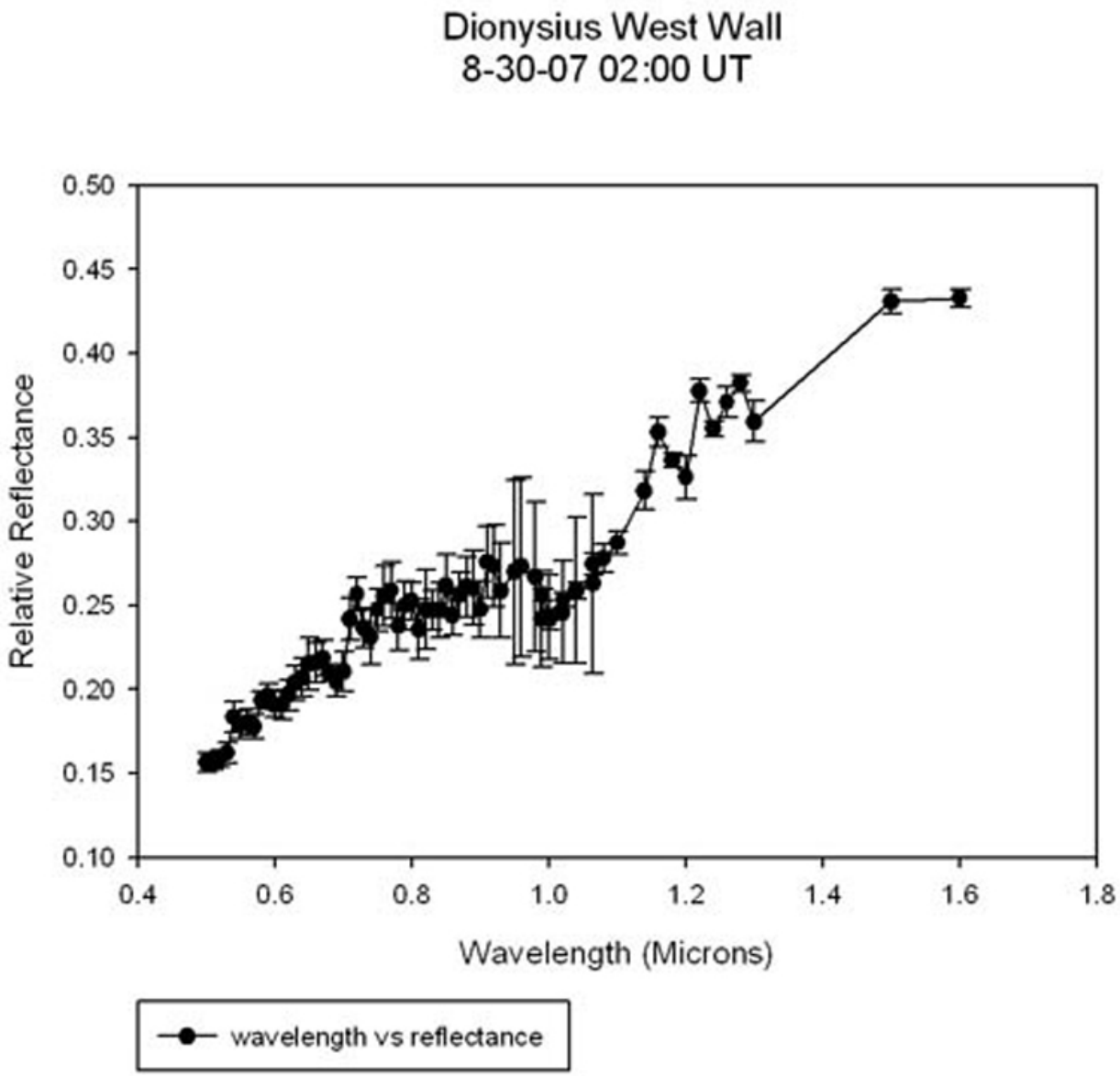
Dionysius West Wall
8-30-07 02:00 UT
Relative Reflectance
0.50
0.45
0.40
0.35
0.30
0.25
0.20
0.15
0.10
0.4
0.6
0.8
1.0
1.2
1.4
1.6
1.8
Wavelength (Microns)
wavelength vs reflectance

Figure 2

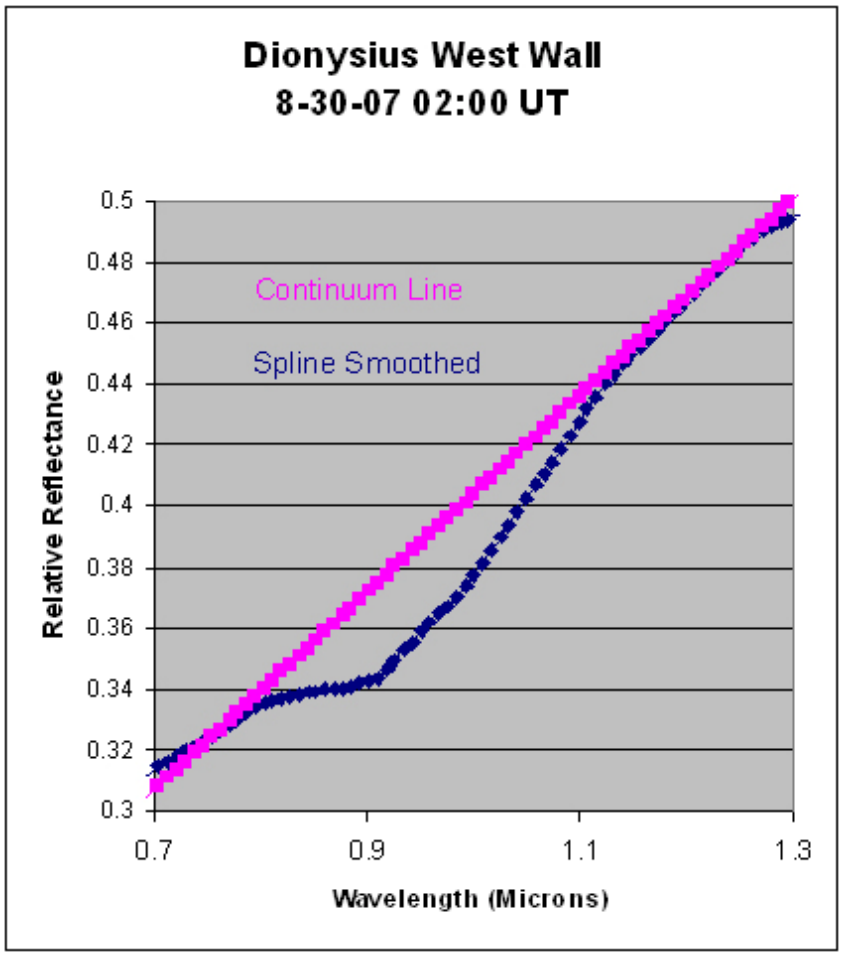

Figure 3

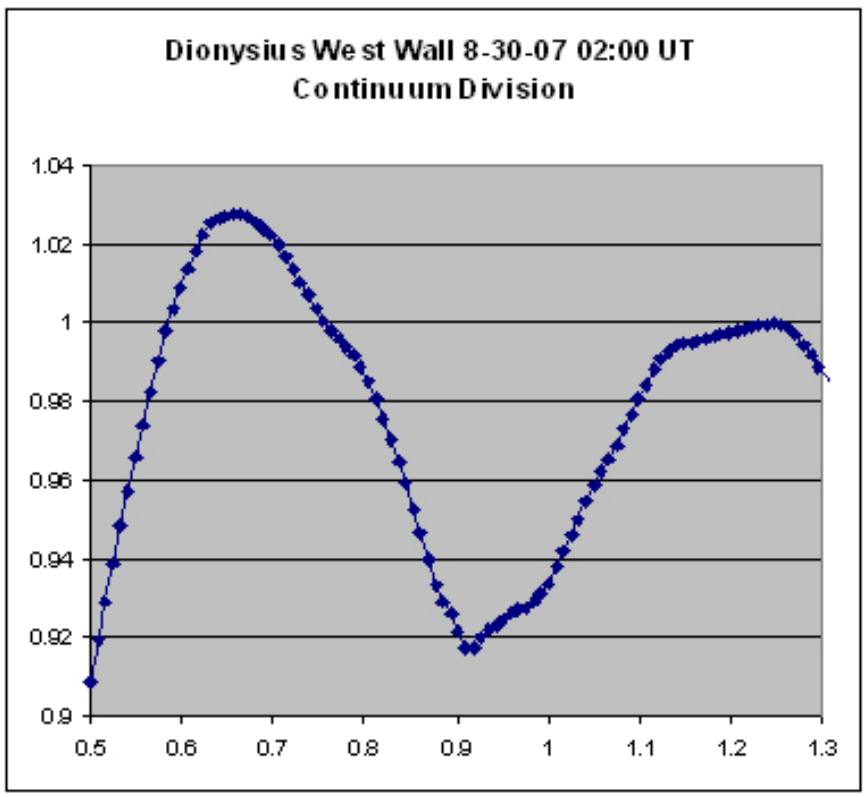

Figure 4

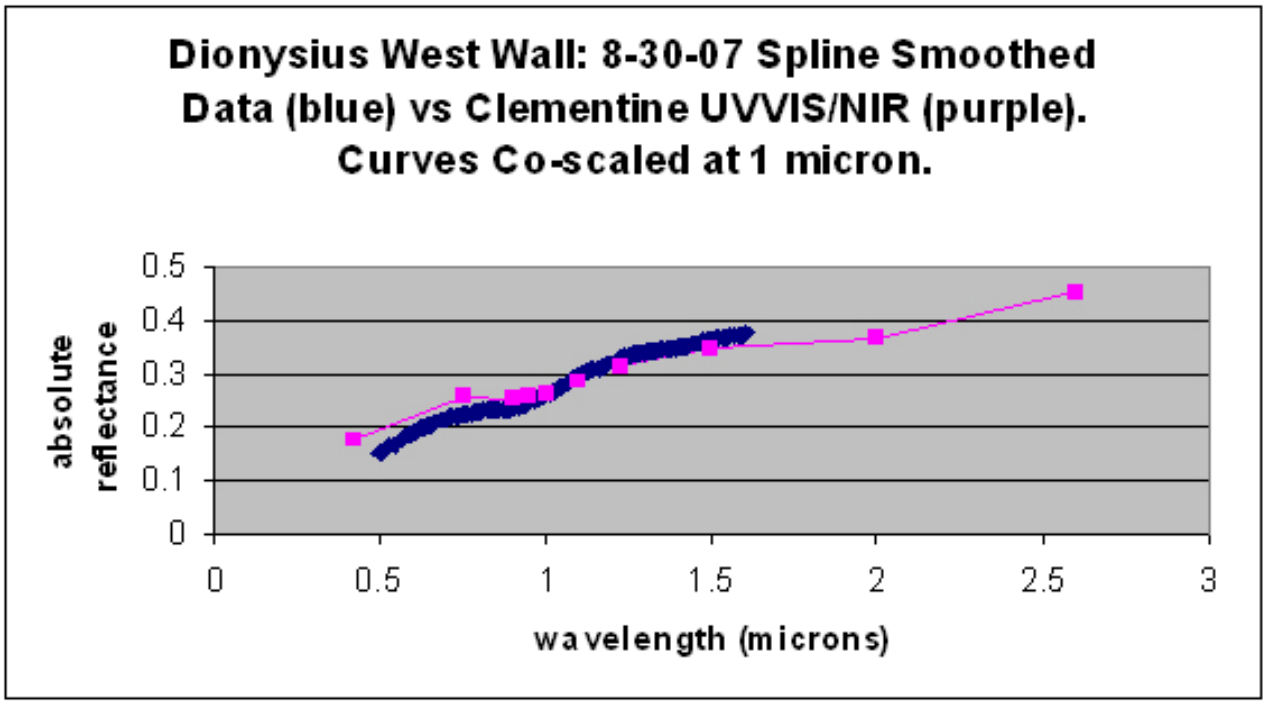

Figure 5

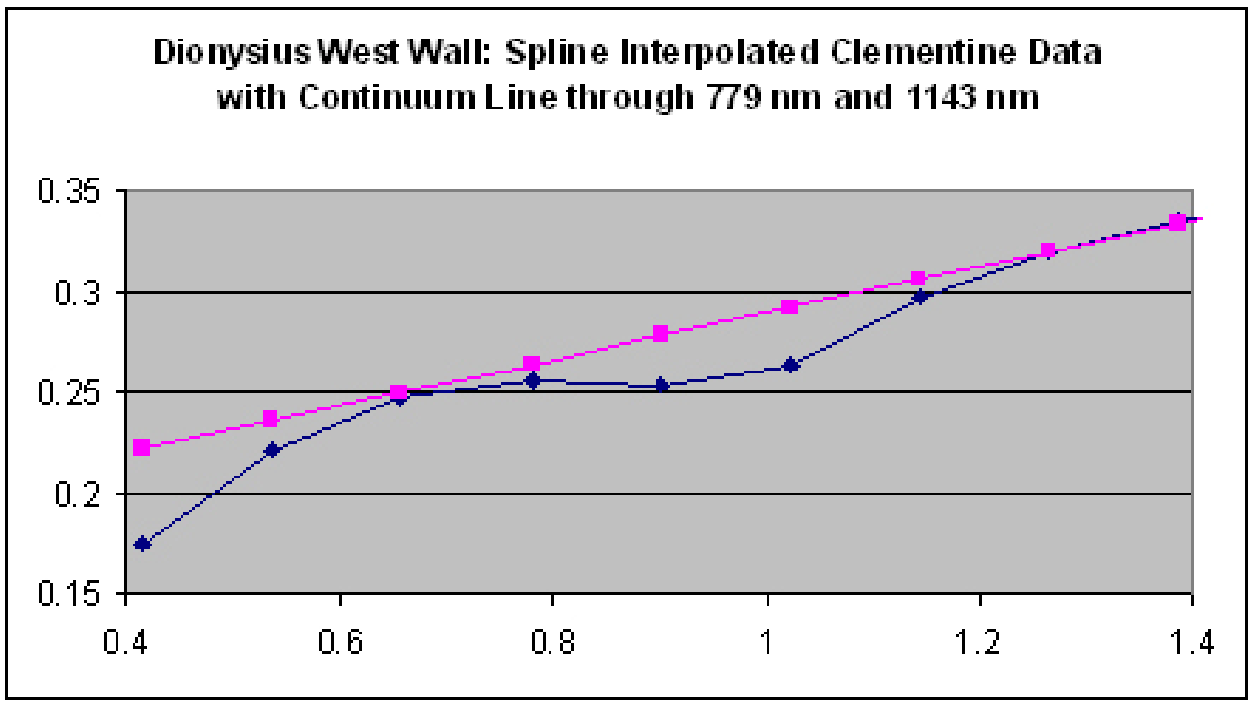

Figure 6

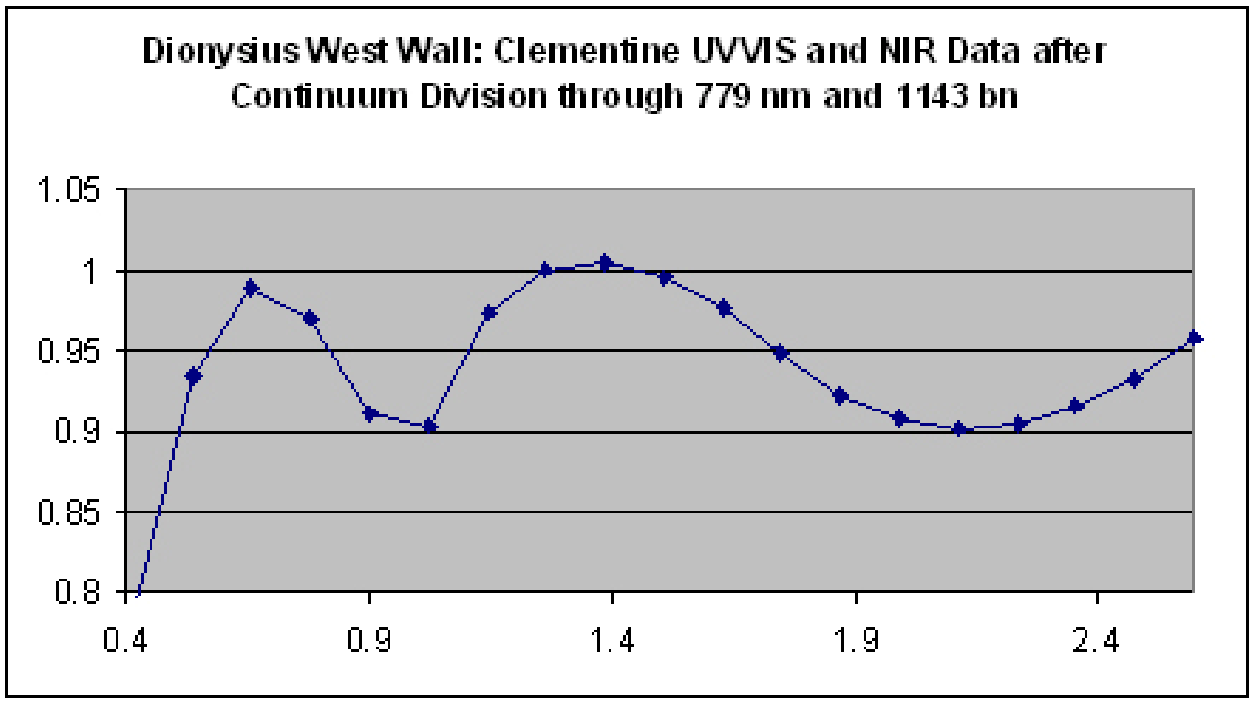
Dionysius West Wall: Clementine UVVIS and NIR Data after Continuum Division through 779 nm and 1143 bn
1.05
1
0.95
0.9
0.85
0.8
0.4
0.9
1.4
1.9
2.4

Figure 7

tangent line applied, and the result of division of the reflectance data by the tangent line (approximating the lunar continuum between 756 nm and 1220 nm). Trough parameters can be read from Figure 4 and show a trough center of about 919 nm, a trough width of about 328 nm, and a trough depth of about 8.3 percent. The integrated area of the trough is about 24 nm reflectance units. The area of a Gaussian is given by 1.77*trough half width*trough depth. Figure 5 compares the spline smoothed data with Clementine UVVIS and NIR data for the same area of the west wall of Dionysius, by co-scaling it with the Clementine reflectance curve at 1000 nm.

Trough parameters were calculated from the Clementine data after spline smoothing and division by a continuum line taken through 779 nm and 1143 nm. The resulting trough was centered at 960 nm, had a width of 404 nm, and a trough depth of 7.7 percent. The integrated area of the trough was 27 nm reflectance units. The spline interpolated Clementine data with continuum line placement is shown in Figure 6 and the continuum division plot is shown in Figure 7. Trough data are compared in Table 1.

4.Discussion

This paper illustrates a simple method by which UVVIS and NIR spectra for lunar features can be obtained with a small telescope, a set of interference filters, and two cameras. An area of the west wall of Dionysius was studied and compared to spectra obtained using Clementine UVVIS and NIR reflectance data. Techniques for image calibration and co-registration of the images into a single image set are discussed. Characteristics of the absorption trough near 1000 nm are determined from the resulting data. These results provide a basis for better understanding the mineral composition of the lunar feature and are distinct from analysis based on the shape of Clementine five band UVVIS spectra described by Tompkins and Pieters (1997) in that the entire trough is visualized. Results were compared to reflectance plots of Clementine UVVIS and NIR data accessed via ISIS 2.0. The trough width, depth and area were quite similar but a variation in the band center of 41 nm was observed. It was felt that the greater number of data points available from the telescopic study helped to better define this parameter than was possible with the more limited Clementine data set.

Table 1

	Trough Center	Trough Width	Trough Depth	Trough Area
Dionysius West (present study)	919 nm	328 nm	8.3 percent	24 nm refl. u.
Dionysius West Clementine UV-VIS & NIR data	960 nm	404 nm	7.7 percent	27 nm refl. u.

References

[1] Anderson JA et al. (2004) Modernization of the Integrated Software for Imagers and Spectrometers, LPSC XXXV abstract #2039.

[2] Giguere TA, Hawke BR, Gaddis LR et al. (2005) "Remote Sensing Studies of the Dionysius Region of the Moon". Lunar and Planetary Science XXXVI, abstract #1092.

[3] Gaddis LR et al. (1997) An overview of the Integrated Software for Imaging Spectrometers (abs), Lunar and Planetary Science XXVIII p. 387-388.

[4] Pieters CM (1999) The moon as a spectral calibration standard enabled by lunar samples The Clementine example. Workshop on new views of the moon2: Understanding the moon through the integration of diverse datasets. Flagstaff, Az. abstract #8025.

[5] Tompkins, S and Pieters CM (1997) Composition of the lunar crust beneath megaregolith. Lunar and Planetary Science XXVIII #1251.

LETTERS TO THE EDITORS

Some Interesting Features in Mare Vaporum

By Achille Giordano

Geologic Lunar Research (GLR) group

In this note some interesting features in Mare Vaporum are described. The features Manilius domes, elusive rille located south of Manilius and Ina caldera have been imaged using a Maksutov ETX 125 f/15. The results obtained suggest strongly that this elusive rille near Manilius and the caldera Ina can be detected in telescope of small diameter under low illumination and good seeing. We invite all readers of Selenology Today to send observations of Ina caldera to the editorial board

selenology_today@christian-woehler.de

1.Introduction

Mare Vaporum is located in the central region of the Moon (13.3°N-3.6°E), immediately south of the Appenines. It measures approximately 245 Km in diameter and has a surface area of 30,000 square Kms. In this great plain we can find many structures of remarkable importance, such as the crater Manilius as well as the Ariadaeus and Hyginus rilles. In this article I will focus my attention on three structures that were recorded on one my lunar images under ideal conditions of solar lighting. These three features are the caldera Ina, three domes on the west of Manilius, already known in literature but still not completely investigated in terms of accurate height and slope measurements, and one elusive rille located south of Manilius, imaged by Pau and previously identified by the GLR Group (Lena et al., 2007).

2. Instrument and methods

The image shown in Fig.1 was taken on October 2, 2007 at 23:40UT (Colongitude 167.4°) from Casalnuovo di Napoli, Italy. The seeing was estimated as 7 and transparency as 3 (scales between 1 poor to 10 excellent). It was obtained from an AVI using a Maksutov ETX 125 f/15, a 2x Barlow lens and a DMK 21AF04 As camera. Registax 4 software was used with 5 alignment points having a dimension of 128x128. After alignment and stacking the raw image (287 of 800 frames was stacked), it was then processed using the wavelet filter, in Gaussian mode, as follows :

For “Layer 1” a slider value of 30 was used. For the remaining layers I set all sliders to a value of “0”. The final image was resample (1.5x) and then imported into Microsoft Digital Image and further processed using a gauss filter of 0.3. The resulting final image was saved as a BMP file.

3. Description

We can see the disposition of the three different subjects in Fig1. Ina (Fig 1, number 1), is located at 18.7° N and 5.3° E was discovered during the Apollo missions. It measures 2.9 Km in diameter and has a depth of approximately 30 meters. It is also

known as Caldera D because of its characteristic shape (Fig.2). Ina, because of its small dimension is a difficult target, but when seeing is good and solar lighting right it can be seen with a telescopes of small aperture including the 125 mm scope used to make this image. Only recently has it been studied in deep, thanks to multi-spectral images taken from the probe Clementine using a color ratio it shows a typical "blue color" of "fresh" material (Fig. 3). We can notice this colour in many impact craters, but Ina is not an impact crater.

Schultz et al (2006) suggested the possibility of the release of gas related to a volcanic activity. It is not easy to determine the age of Ina, but it appears to be relatively young. The preservation state of relief, the number of superimposed small craters, and the 'freshness' (spectral maturity) of the regolith together indicate that features within this structure must be as young as 10 Myr (Schultz et al, 2006).

We now pass to examine the three domes seen in a Lunar Orbiter picture (fig 4). The first dome (2) is obvious enough It is circular with a modest height. There are superimposed tiny craters, likely of impact origin. The second (4) has also generous dimensions, and it is found placed near one small ridge: it is small compared to the previous dome discussed. Initial analysis shows the typical morphologic characteristics of domes. Finally, the third dome (3) is less obvious. It has small dimensions but it has rounded shape and the presence on the summit of a possible pit.

Finally, I want to cite the elusive rille located south of Manilius and indicated as 5 (fig 4). It has rectilinear shape and is approximately 100 km long. It is a difficult target, but can be detected with good seeing and the proper solar angle with telescopes of small aperture like the 125 mm used in this image. Already detected in the past by K.C. Pau , the rille is not visible in high resolution images from Lunar Orbiter, but is visible in Clementine images (Lena et al, 2007). The ideal time for its observation is one day after First Quarter and one day before Last Quarter.

The results obtained suggest strongly that this elusive rille and the caldera Ina can be detected in telescope of small diameter under low illumination and good seeing.

Lena (private communication) has planned to investigate this observation under the same specific lighting conditions, as shown in Table 1, for future repeat illumination conditions that match the image I have taken, in sunset, on October 2, 2007.

References

[1] Lena R., Wöhler C., Pau K.C, Bregante M. T. (2007). A study about the Manilius region and a dome located at 08.26° E and 10.52° N. Selenology Today, 3, pp 9-24.

[2] Schultz P.H., Staid M. I., Pieters C. M. (2006). Lunar activity from recent gas release. Nature, 444, pp. 184-186.

Table 1 Future prediction times in UT for repeat illumination conditions that will match the image taken on October 2, 2007, at 23:40 UT. Predictions are calculated from Rome (Italy) D=daylight. It is not suggested to image when the Moon is under 20 degrees above the local horizon in order to ensure sufficient altitude above to avoid the worst aspects of poor seeing.

UT Date	Time	Alt°	Semi-diam"	Long°	Lat°	Colong°
2007/10/ 2	23:40	28.36	958.63	6.86	-5.93	167.54
2007/12/ 1	02:21	44.08	930.24	7.52	0.24	167.31
2008/ 1/29	08:12D	11.90	898.28	2.62	6.02	167.67
2008/ 4/27	01:30	13.24	907.30	-5.74	3.81	168.35
2008/ 6/24	23:56	18.88	938.05	-7.06	-2.82	168.23
2008/ 9/21	08:27D	36.74	977.17	1.07	-5.77	167.49
2008/11/19	10:39D	11.16	954.17	6.79	1.09	167.33
2008/12/19	01:20	27.30	944.51	7.66	4.57	167.48
2009/ 2/16	07:24D	14.32	910.35	5.24	6.70	168.03

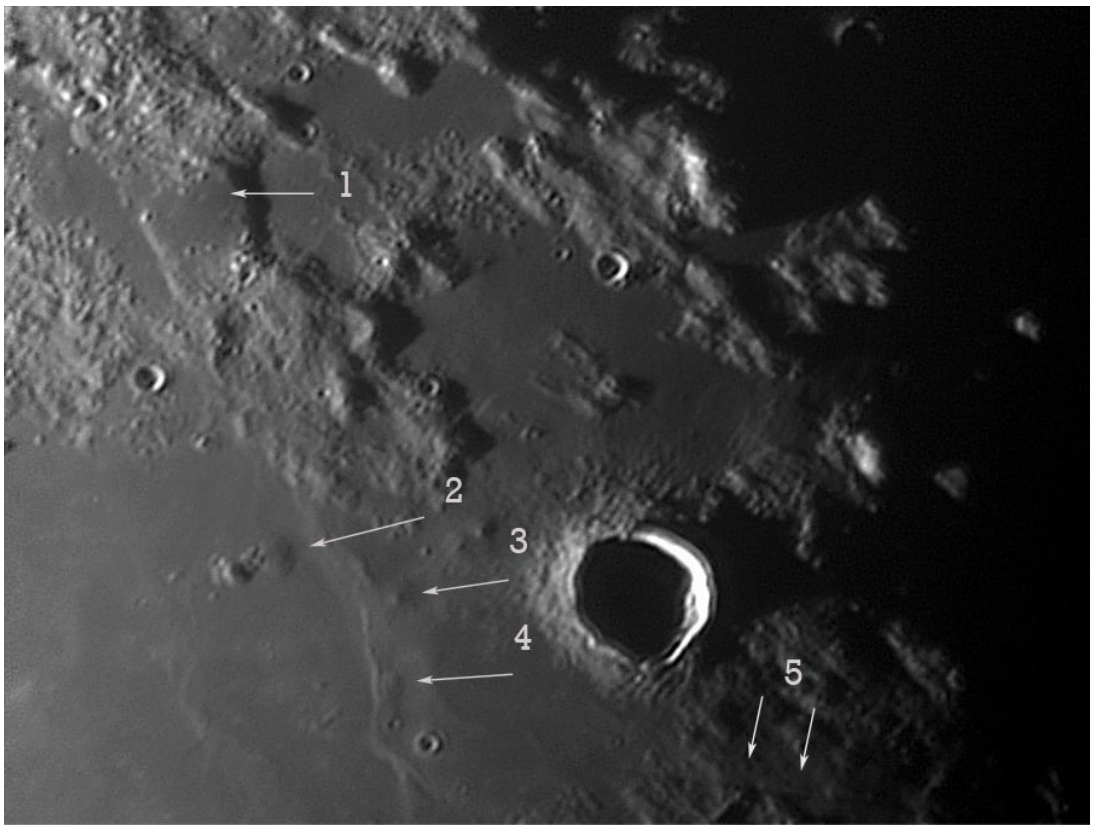

Figure 1

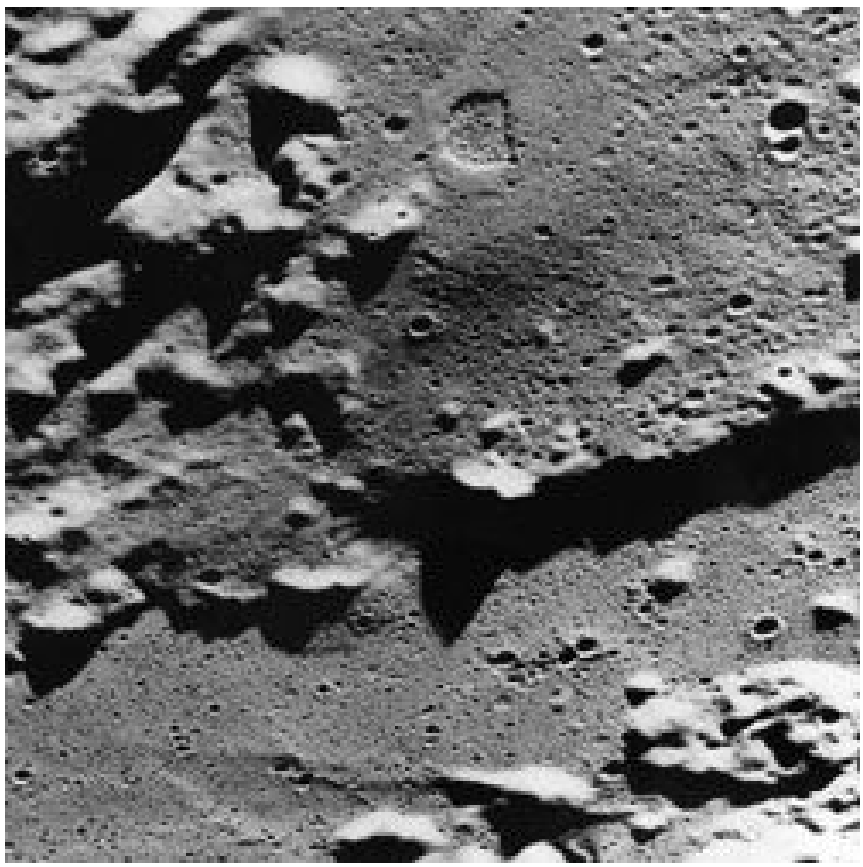

Figure 2

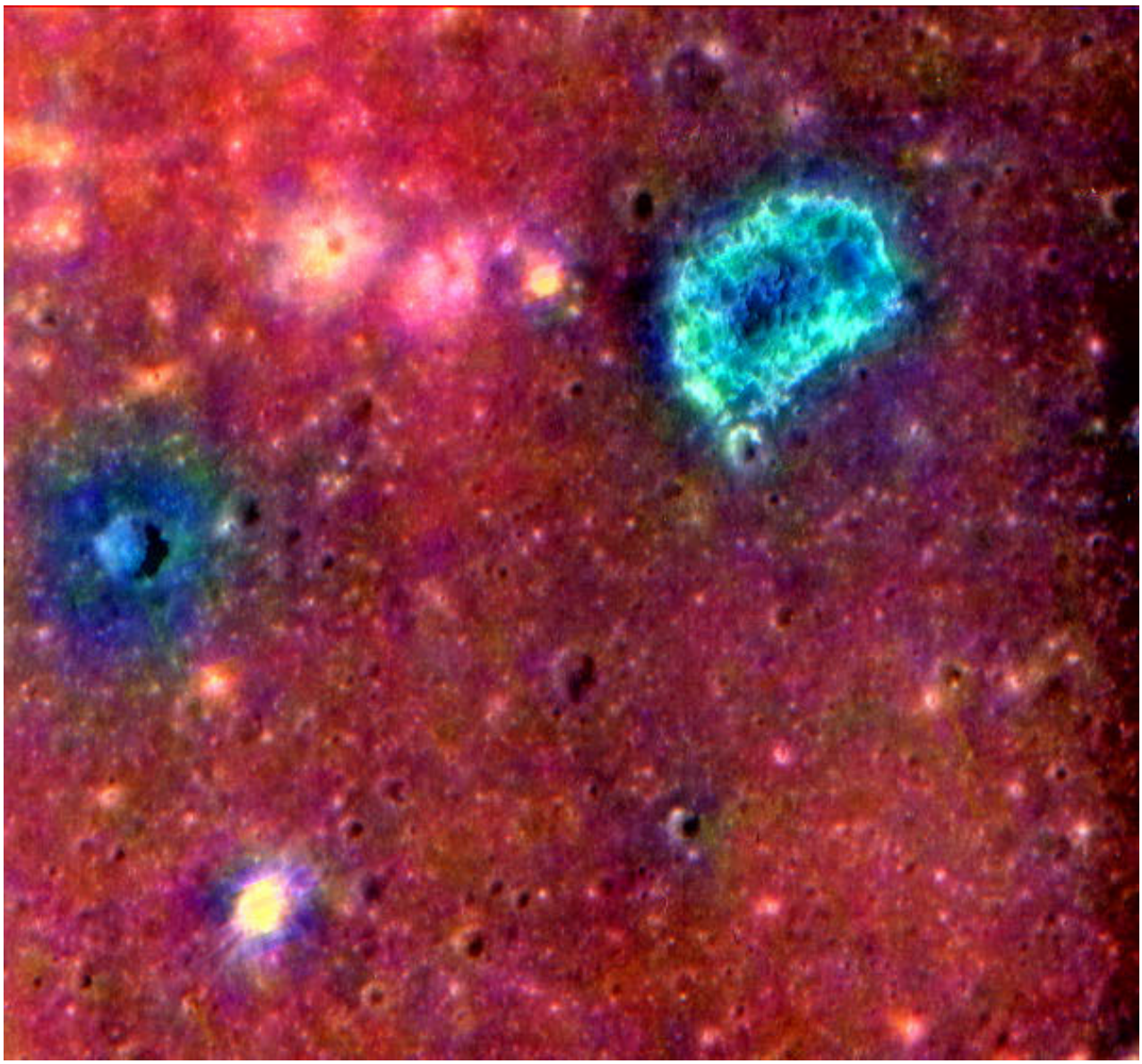

Figure 3

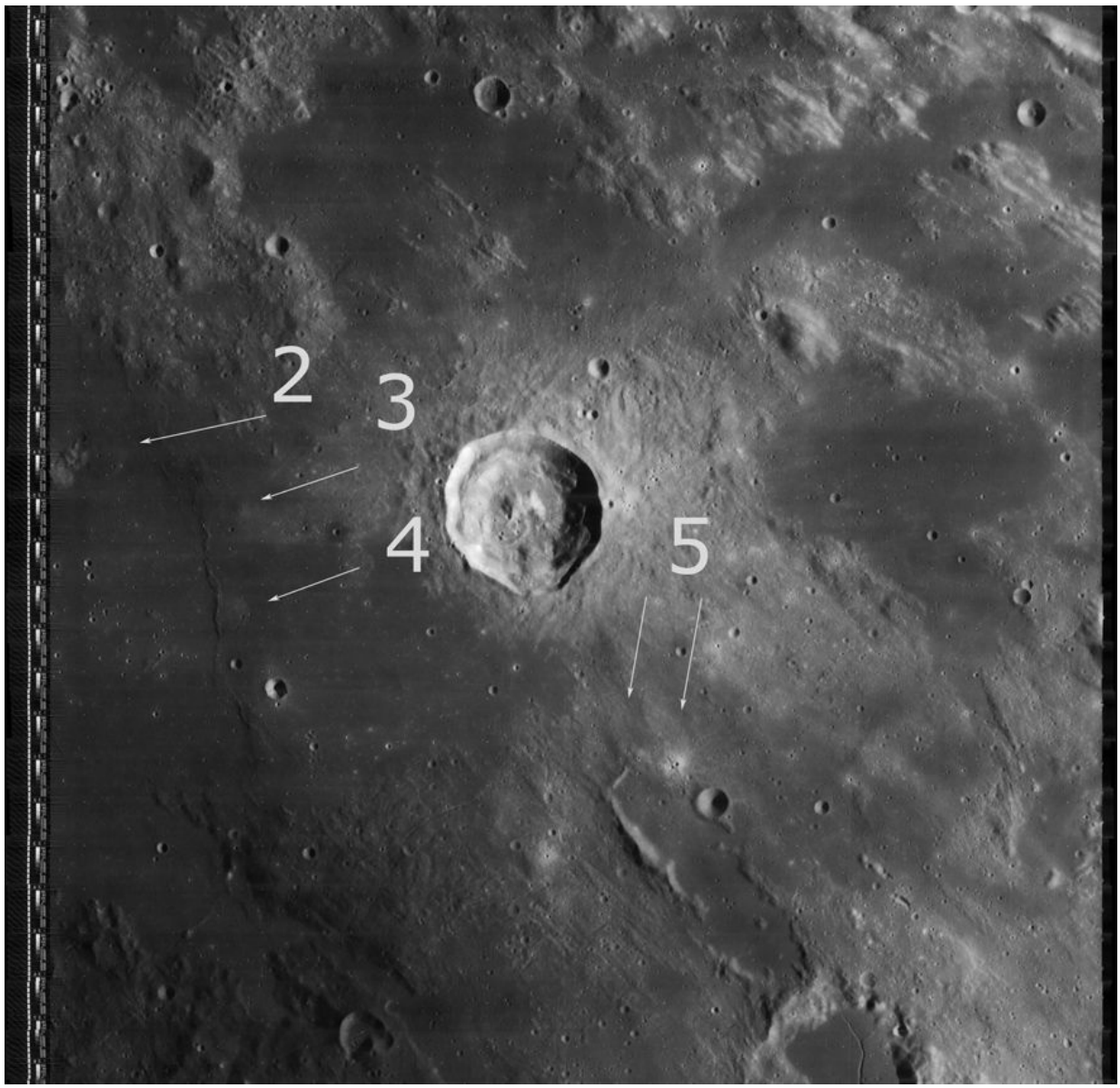

Figure 4